Chemical Science

ROYAL SOCIETY OF CHEMISTRY

REVIEW

View Article Online
View Journal

Cite this: DOI: 10.1039/d5sc08445h

Mechanisms, development, and applications of silicon-based anodes in solid state batteries

Feipan Liang,[a] Lichun Yang,*[a] Renzong Hu,[a] Bin Yuan,[a] Min Zhu[a] and Jun Liu*[ab]

This review focuses on the application of silicon-based materials in high-energy-density solid state batteries (SSBs), systematically organizing major research progress in SSBs centered on silicon-based anodes. The article reviews the technological development pathways in this field, analyzes the electrochemical processes, structural evolution behavior, and failure mechanisms of silicon-based anodes in solid-state batteries, and summarizes the research status of polymer solid electrolytes (PSEs), oxide solid state electrolytes (OSSEs), sulfide solid state electrolytes (SSSEs), halide solid state electrolytes (HSSEs), and composite solid electrolytes (CSEs) in silicon-based anode systems. It also proposes targeted potential future research directions. Finally, the commercial prospects of silicon-based anode solid-state batteries are discussed, aiming to provide insights for the strategic design of advanced silicon-based solid-state batteries and to offer clear theoretical and practical guidance for the development of high-performance lithium-ion batteries (LiBs).

Received 31st October 2025
Accepted 7th December 2025

DOI: 10.1039/d5sc08445h

rsc.li/chemical-science

1. Introduce

Since the commercialization of lithium-ion batteries (LiBs) in 1991, which have gradually impacted various aspects of daily life, the depletion of fossil fuels and the growing demand for sustainable energy alternatives have intensified the need for energy conversion and storage technologies that are lower-cost, ecologically benign, and higher-performing.[1–3] Currently, commercially mass-produced LiBs employ graphite anodes and liquid electrolytes, which increasingly fail to meet the rising demands in terms of safety, performance, and environmental impact.[4,5] Moreover, the energy density of liquid LiBs with graphite anodes has approached their theoretical limit of approximately 300 Wh kg^{-1}.[6,7] Therefore, it is imperative to accelerate the development of LiBs with higher energy density, longer cycle life, lower production costs, and improved safety.[8]

Solid state batteries (SSBs) represent a promising solution to address or mitigate these issues. Flammable organic

[a]South China University of Technology, School of Materials Science and Engineering, China. E-mail: mslcyang@scut.edu.cn; msjliu@scut.edu.cn
[b]China–Singpore International Joint Research Institute, Guangzhou, China

Feipan Liang

Feipan Liang is currently a PhD candidate under the supervision of Professor Lichun Yang and Professor Jun Liu at South China University of Technology. He graduated from Beijing University of Chemical Technology in 2022 with a Master of Engineering degree. His current research focuses on silicon-based anodes for lithium-ion batteries.

Lichun Yang

Lichun Yang is a professor at South China University of Technology, Guangzhou, China. She received her BSc degree in 2005 and her PhD degree in 2010 from Fudan University under the supervision of Prof. Yuping Wu. She carried out postdoctoral research in the Leibniz Institute for Solid State and Materials Research (Dresden) in Germany with Prof. Oliver G. Schmidt. Currently, She is mainly engaged in the research and development of electrode materials for lithium/sodium ion batteries and new electrochemical energy storage/conversion systems.

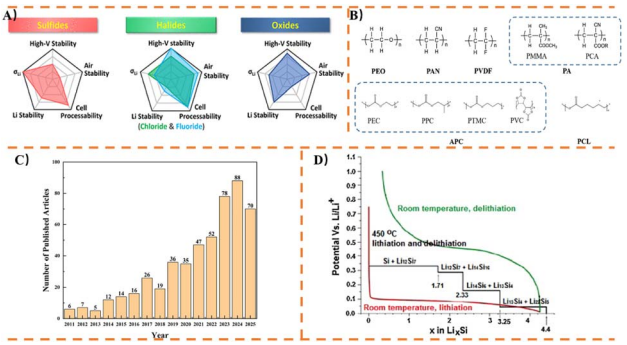

Fig. 1 (A) Spider plots comparing the key performances of three major inorganic SSEs: sulfides, halides, and oxides;[18] (B) chemical structure of common polymer matrix in solid composite electrolytes;[37,38] (C) annual distribution of publications on silicon-based anode solid-state batteries worldwide; (D) silicon electrochemical lithiation and delithiation curve at room temperature and high temperature.[39]

electrolytes are a primary cause of battery thermal failure; replacing them with thermally stable SSEs can reduce the risk of thermal runaway.[9] Meanwhile, mechanically rigid and non-flammable Solid state electrolytes (SSEs) membranes can effectively separate the cathode and anode while ensuring ion conduction. SSEs can be classified into inorganic solid electrolytes (ISEs), organic solid electrolytes (OSEs), and their composite solid electrolytes (CSEs).[10] In recent years, ISEs have been extensively studied, mainly including oxide solid state electrolytes (OSSEs), sulfide solid state electrolytes (SSSEs), and halide solid state electrolytes (HSSEs), as shown in Fig. 1A. OSSEs achieve an ionic conductivity on the order of 10^{-4} S cm^{-1} at room temperature, but their manufacturing process is complex, requiring high-temperature sintering and resulting in higher costs, which are insufficient to meet practical application requirements.[11] Additionally, due to their high hardness, OSSEs may exhibit poor mechanical properties, hindering ion transport at the electrolyte–electrode interface.[12] SSSEs, such as $Li_{10}GeP_2S_{12}$ (ref. 13) and $70Li_2S$-$30P_2S_5$,[14] have been reported to exhibit ultra-high ionic conductivities comparable to liquid electrolytes, reaching 12×10^{-3} S cm^{-1} and 3.2×10^{-3} S cm^{-1}, respectively. Owing to their highly deformable nature, SSSEs can provide favorable interparticle lithium conduction pathways and good mesoporous conduction routes between SSEs and electrode active materials.[12] However, these SSSEs are unstable and decompose in air upon exposure to H_2O, producing toxic H_2S; the presence of carbon materials in electrochemical environments can accelerate their decomposition.[15–17] HSSEs have attracted widespread scholarly attention in recent years due to their combination of some advantages of both OSSEs and SSSEs.[18] The composition of HSSEs varies but is generally represented as $Li_{3+a}M_{1+b}X_6$ (where M is a metal or rare-earth element: Y, In, Er, Sc, and Yb; X is a halogen: Cl, Br, and I).[19] This compositional diversity enables HSSEs to exhibit Young's moduli comparable to those of SSSEs. However, most HSSEs are moisture-sensitive and decompose in humid air.[20]

OSEs are mainly polymers, which are flexible and processable and can be made into films or Composites. So far, a large number of OSEs are mainly polymer solid electrolytes (PSEs). Compared to ISEs, PSEs offer several advantages: lower density, ease of processing, interfacial compatibility, and enhanced safety. PSEs facilitate Li^+ transport through the segment motion of polymer chains and can be prepared by dissolving lithium salts in a polymer matrix. Additionally, PSEs can compensate for volume changes in electrodes during charge and discharge cycles due to the inherent elastic and plastic deformation of polymers.[11] Generally, PSEs for LiBs can be classified into two main categories: Solvent-free Polymer Electrolytes (SPEs) and Gel Polymer Electrolytes (GPEs).[21,22] Among these, GPEs contain a small amount of liquid electrolyte, which can effectively enhance the lifespan and energy density of LiBs, making them the most promising alternative to liquid electrolytes.[23] Since the discovery of PEO-based PSEs in 1973,[24] researchers have explored various dielectric polymer hosts, including polyethers (*e.g.*, Polyethylene glycol (PEG),[25] Poly 1,3-dioxolane (PDOL)[26]), Polyacrylonitriles (*e.g.*, polyacrylonitrile (PAN)[27]), Polyesters (*e.g.*, Polymethyl Methacrylate (PMMA)[28]), Polycarbonates (*e.g.*, Poly(ethylene carbonate) (PEC[29]), Poly(propylene carbonate) (PPC[30]), Poly(Vinylene Carbonate) (PVC[31])), and polyfluorides (*e.g.*, Polyvinylidene difluoride (PVDF[6]), Poly(vinylidene fluoride-*co*-hexafluropropylene) (PVDF-HFP[32])), as illustrated in Fig. 1B. However, large-scale application of PSEs still faces three major challenges: low ionic conductivity, narrow electrochemical window, and the formation of lithium dendrites at the interface when paired with lithium anodes.[33] The room-temperature ionic conductivity of PSEs ranges from 10^{-8} to 10^{-5} S cm^{-1}, significantly lower than that of liquid electrolytes ($\sim 10 \times 10^{-3}$ S cm^{-1}).[34–36]

To achieve energy densities comparable to or even higher than those of current commercial LiBs, electrode materials must exhibit sufficiently high specific capacity and chemical/electrochemical compatibility with SSEs. The anode materials for SSBs primarily focus on graphite, Lithium (Li), Silicon (Si), Tin (Sn), Aluminum (Al), Antimony (Sb), Germanium (Ge), and Lithium Titanate Oxide (LTO). Although graphite anodes offer high conductivity, good reversibility, and relatively low cost,

Jun Liu

Jun Liu is a professor of materials science and engineering at South China University of Technology, PR China. He received his PhD in chemical engineering from Dalian University of Technology in 2010. From 2012 to 2015, he worked as a postdoctoral researcher at Deakin University and Max Planck Institute for Solid State Research. His current research interests mainly include the design of novel electrodes and electrolytes for rechargeable batteries, especially for Li-ion batteries, Zn–air batteries, and all-solid-state batteries.

their low specific capacity (372 mAh g^{-1}) limits their further application in power batteries.[40] In contrast, Li anodes have garnered significant attention due to their high specific capacity (3860 $mAhg^{-1}$), low density (0.534 g cm^{-3}), and the lowest redox potential (−3.04 V *vs.* standard hydrogen electrode).[41] However, they are prone to side reactions with electrolytes and the growth of lithium dendrites, which are the main causes of internal short circuits, posing risks of thermal runaway and explosion.[42,43] Therefore, the anticipated high areal capacity, high current density, and long cycle life of SSBs with Li anodes may be impractical. Additionally, limited Li reserves (only 0.0065% in the Earth's crust) and the air sensitivity of Li, leading to high industrial costs, further hinder its large-scale application. Compared to other alloy anodes (such as Sn, Al, Sb, and Ge), although Al has a crustal abundance of over 8%, its theoretical specific capacity (993 mAh g^{-1}) is relatively low. Moreover, its 100% volume expansion still leads to rapid cycle life decay, and its insufficient energy density advantage fails to attract substantial industrial investment to overcome the associated technical challenges. Sn, Ge, and Sb are rare metals with extremely low crustal abundance and undergo significant volume changes during lithiation. Although Ge, in particular, exhibits excellent performance (in terms of capacity and conductivity), its high cost restricts its application to extreme special fields such as aerospace, making it unsuitable for the mass consumer market. While LTO anodes demonstrate optimal safety and cycle life, their very low energy density cannot meet the basic endurance requirements of consumer electronics and electric vehicles. Si, with its high specific capacity (4200 mAh g^{-1}), relatively low discharge voltage (≤0.4 V), abundant reserves, non-toxicity, and good stability in air, qualifies for large-scale manufacturing and shows broad application prospects in SSBs.[44–46] SSBs paired with Si anodes exhibit minimal risk of lithium dendrite growth[47–50] and adverse interfacial side reactions,[41] as detailed in Table 1. However, the lithiation process, where Li atoms alloy with Si, is accompanied by significant volume expansion (300–400%),[51,52] inducing extreme stress–strain within Si particles and causing fracture and pulverization. Ultimately, the disconnection of active materials from conductive agents and current collectors results in electrical isolation, which further reduces the utilization of active materials and leads to rapid failure of Si-based anode electrodes.[53] Thus, for the large-scale commercial application of Si-based anode SSBs, simultaneous optimization of both SSEs and Si-based anodes is essential.

Herein, this review summarizes the application of Si-based materials in high-energy-density SSBs, retraces the general research pathways of SSBs utilizing Si-based anodes, and systematically outlines their electrochemical reaction processes, structural evolution, and failure mechanisms. It further reviews the developmental status of PSEs, OSSEs, SSSEs, and HSSEs applied to Si-based anodes, discusses the future commercialization prospects of Si-based all-solid-state batteries, and concludes with perspectives on constructing stable adaptive interfaces and developing scalable fabrication technologies to facilitate large-scale commercialization. This work aims to provide strategic insights for the design of advanced Si-based SSBs and hopes to offer clear guidance for the exploration of high-performance lithium batteries.

2. Development of Si-based anodes SSBs

At room temperature, although silicon-based anodes exhibit comparable specific capacity to lithium metal anodes, the suitable lithium insertion potential of silicon-based anodes effectively mitigates the issue of lithium dendrite growth. In recent years, they have attracted extensive attention from researchers as a promising alternative to lithium metal anodes before their full commercialization, and have become one of the key research directions in SSBs. A search conducted on Web of Science using the keywords “Silicon-based anode” and “Solid electrolyte” (as of August 30, 2025) revealed that, as shown in Fig. 1C, there were relatively few related studies before 2015. However, since 2020, the global number of publications in this field has entered a phase of rapid growth.

As early as the 1990s, extensive research was conducted on the lithiation mechanism of silicon materials, revealing that the lithium storage mechanism of silicon anodes is based on the alloying reaction between Li and Si, which can be specifically categorized into solid-solution reactions and addition reactions.[54] For crystalline silicon (c-Si), the lithiation process follows an addition reaction mechanism, forming a series of crystalline alloy phases. In contrast, for amorphous silicon (a-

Table 1 Comparison of anode materials

Anode materials	C	Si	Li	Sn	Al	Ge	Sb	LTO
Density (g cm^{-3})	2.25	2.33	0.53	7.31	2.7	5.32	6.70	3.42
Abundance (%)	0.027	26.3	0.0065	0.00022	8.13	0.00022	0.00002	0.66 (Ti)
Theory capacity (mAh g^{-1})	372	4200	3860	994	993	1384	660	175
Lithium structure	LiC_6	$Li_{22}Si_5$	—	$Li_{22}Si_5$	LiAl	$Li_{22}Si_5$	Li_3Sb	$Li_7Ti_5O_{12}$
Average potential (V)	0.1	0.35	—	0.5	0.4	0.35	0.9	∼1.55
Cost (Ind-scale) ($ per kg)	4.1–11	42–70	110–165	32–35	2.2–2.6	>1000	11.5–13	11–16.5
Expansion rate (%)	12	∼300	0	∼260	∼97	∼270	150	<1
Cycling life	>1500	500–800	100–200	400–600	100–200	500–800	500–800	>3000
ICE (%)	90–92	85–90	—	50–80	50–80	75–85	70–90	>97
Energy density (Wh kg^{-1})	250–300	300–400	350–500	220–280	230–290	280–350	150–200	80–120
Safety	★★★★	★★★	★	★★	★★	★★★	★★★	★★★★★

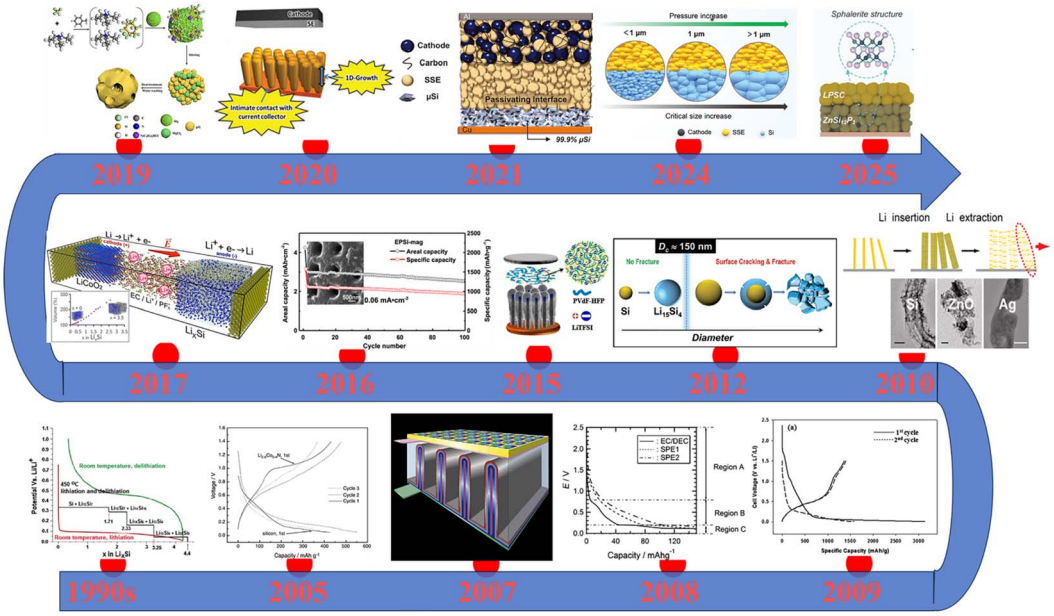

Fig. 2 Timeline of silicon anode development in SSBs.

Si), the process primarily involves a solid-solution reaction, exhibiting single-phase region behavior. At elevated temperatures, the lithiation of silicon undergoes multiple phase transformations, resulting in the formation of four distinct phases: Li_2Si_7 (0.332 V), Li_7Si_3 (0.288 V), $Li_{13}Si_4$ (0.158 V), and $Li_{22}Si_5$ (0.044 V), as illustrated in Fig. 1D. However, at room temperature, the lithiation reaction deviates from the equilibrium state. The first lithiation curve of silicon shows a plateau at approximately 0.1 V, where c-Si transforms into partially lithiated a-Li_xSi, resulting in the coexistence of c-Si and a-Li_xSi. When the voltage drops below 0.050 V, a-Li_xSi abruptly transforms into c-$Li_{3.75}Si$.[39,55,56]

Subsequently, in 2005, Liu[57] pioneered the study of the electrochemical behavior of composite electrodes containing $Li_{2.6}Co_{0.4}N$ and nanosized $SiO_{1.1}$ with solid PEO electrolytes at different temperatures, marking the inception of research on PSEs applications in Si-based anodes. In 2007, Notten *et al.* first explored SSBs utilizing a 3D thin-film silicon anode architecture with LiPON electrolyte.[58] By 2008, the integration of SiO/graphite anodes with SPEs led to the development of truly solid-state lithium-ion polymer batteries.[59] The use of silicon in SSSE-based ASSBs was initiated by Trevey[60] in 2009. In 2010, Choi[61] designed one-dimensional nanostructured silicon materials as anodes, offering new insights for developing novel nano-energy storage materials. In 2012, Liu[62] discovered that silicon particles with diameters below 150 nm do not pulverize during lithiation. Pandey[63] investigated the electrochemical performance of 3D nanostructured SiC anodes in GPE electrolytes, representing the first application of SiC anodes in solid-state batteries. In 2016, Li[64] proposed an improved magnesiothermic reduction method to fabricate silicon anodes with stable nanoporous structures, enabling low-cost production of bulk silicon anode materials. Through molecular dynamics simulations, the formation of the $Li_{15}Si_4$ alloy during the initial lithiation of silicon anodes and its mechanism leading to 281% volume expansion were revealed in 2017.[65] Later, Wang[66] introduced a solution-based synthesis method for porous silicon particles, providing a new approach for large-scale preparation of silicon-based anodes. In 2020, Cangaz[67] found that the inherent porosity of columnar structures and external pressure compensation could mitigate volume changes during silicon lithiation. In 2021, Tan[68] first resolved the issue of capacity fading of Si in solid-state systems, achieving an average coulombic efficiency of 99.95% after 500 cycles with a 99.9% micron silicon (mSi) anode in a sulfide electrolyte. Li[69] revealed the size effect and pile pressure dependence of Si anodes in SSBs, finding that the critical size threshold (*i.e.*, the minimum size leading to particle rupture) is significantly affected by pile pressure in SSBs, with higher pile pressure resulting in a larger critical size threshold in 2024. Recently, Shen[70] developed a $ZnSi_{12}P_3$ silicon-based anode to alleviate volume expansion through reversible phase transitions ($Li_{15}Si_4$/LiZn/Li_3P) during lithiation/delithiation. Fig. 2 summarizes the development timeline of Si-based anode SSBs.

Si-based anodes SSBs have become a core area of global battery technology competition due to their high specific capacity, low voltage platform, and synergistic advantages with solid electrolytes. Despite facing challenges such as material costs, process complexity, and interface stability, commercial breakthroughs are expected through structural optimization, interface engineering, and domestic process development.

3. Failure principle

SSBs are promising alternatives to existing liquid LiBs. However, unlike liquid LiBs, SSBs do not achieve direct atomic-level contact between electrodes and electrolytes. As shown in Fig. 3A, SSBs face unique challenges such as high-resistance

solid–solid interfaces, sluggish kinetics, and a tendency to form interfacial voids. These challenges must be overcome for their widespread adoption. Particularly when using Si-based active materials as anodes, the significant volume expansion during lithiation exerts compressive stress on the SSEs and leads to interfacial voids. Therefore, studying the failure mechanisms of SSBs is crucial for providing theoretical guidance for subsequent SSBs design. Given that OSSEs and SSSEs correspond to the two most fundamental and typical scientific challenges—"mechanical contact failure" and "chemical interfacial side reactions"—respectively, overcoming these issues holds foundational guiding significance. Consequently, current research on failure mechanisms in Si-based SSBs primarily focuses on OSSEs and SSSEs.

3.1 Failure principle of OSSEs in Si

Although OSSEs exhibit excellent electrochemical stability and non-flammability, their intrinsic brittleness can easily lead to microcracks at the interface, resulting in loss of interfacial contact, localized potential concentration, lithium dendrite growth, and even internal short circuits and structural failure. However, failure mechanisms of OSSEs in Si-based anodes primarily focus on Li^+ transport mechanisms, that is, mechanical contact failure. A rate-dependent study by Jouybari[71] using linear sweep voltammetry on magnetron-sputtered all-solid-state Si|LiPON|Li cells (as shown in Fig. 3B) revealed that: (1) two distinct Li^+ transport mechanisms exist in Si electrodes at different scan rates: a diffusion-controlled mechanism at high scan rates and a uniform Li concentration distribution at very low scan rates; (2) the effective activation energy for Li^+ migration in Si at 165 °C was 0.1 eV, significantly lower than the 0.55 eV observed at room temperature, confirming the absence of side reactions or microstructural changes at elevated temperatures. Basak[72] utilized *in situ* transmission electron microscopy to visualize the solid–solid electrode–electrolyte interface between Si particles and lithium OSSEs in a model system (Fig. 3C), and found that: (1) lithiation and delithiation do not require all particles to be in direct contact with the electrolyte at the hundreds-of-nanometers length scale; (2) redistribution of Li occurs among interconnected active particles, indicating that Li is not necessarily isolated within individual particles due to loss of direct contact; (3) the rate of chemical lithiation depends solely on the ionic conductivity of the particles, as it does not involve applied current. Vadhva[73] developed a two-dimensional electrochemomechanical model and validated it experimentally using steady-state, transient, and pulsed electrochemical techniques (Fig. 3D). During the first cycle formation, a thin Li_ySi layer forms at the a-Si|LiPON interface. The a-Si electrode exhibits two polarization processes: one at the Li_ySi alloy layer on the a-Si|LiPON interface and another at the additional interface between this layer and the non-lithiated a-Si in the electrode bulk. Subsequent modeling correlated chemical and mechanical material properties with electrochemical responses to explore the evolution of stress at the solid–solid electrolyte interface.[74] In thin-layer solid-state batteries with a-Si anodes, expansion due to Si lithiation imposes compressive stress on the solid electrolyte: (1) slow Li diffusion in Si creates Li concentration gradients, leading to localized stress; (2) interface stress at 100% state of charge (SOC) is rate-independent but increases with applied stack pressure; (3) tensile stress occurs at the end of discharge, potentially causing void formation at the electrode interface; (4) battery capacity is strongly influenced by rate but only minimally by applied pressure, indicating that slow Li^+ diffusion in Si is the key driver for localized concentration gradients.

In liquid LiBs, the fluidity of the electrolyte ensures sufficient contact between Li^+ and active materials. In contrast, SSBs replace solid–liquid interfaces with solid–solid interfaces, where Li^+ transport relies entirely on the SSEs itself and its physical contact with electrode materials. For anode materials like silicon, which undergo significant volume changes (>300%) during cycling, maintaining stable and efficient Li^+ transport channels becomes extremely challenging. Applying appropriate external pressure in SSBs is the simplest and most effective engineering approach to maintain solid–solid interfacial contact. This mechanically "clamps" the interfaces that may separate due to expansion, ensuring uninterrupted Li^+ transport pathways.

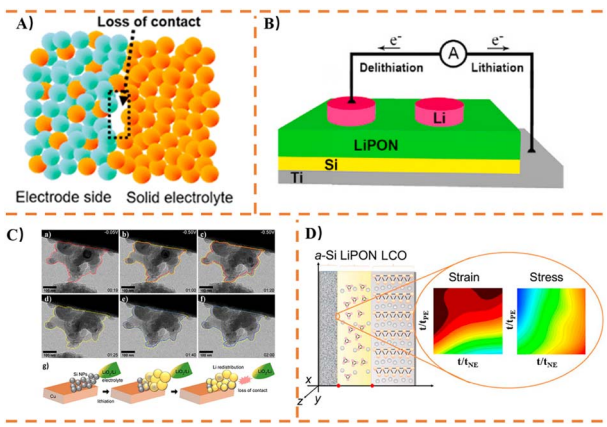

Fig. 3 (A) Solid–solid interface in SSBs; (B) schematic presentation of the solid-state battery; (C) SEM and schematic of lithium redistribution during lithium particle shrinkage; (D) 2D electrochemical mechanical model of thin film SSBs schematic.

3.2 Failure principle of SSSEs in Si

While significant volume expansion of Si in SSSEs can also lead to poor electrode–electrolyte contact, capacity decay, and eventual battery failure, the chemical instability at the SSSE/Si interface represents another extreme and critical scientific challenge. During cycling, chemical/electrochemical reactions occur between Si particles and SSSEs at the interface, exacerbating both physical and chemical instability, ultimately resulting in battery failure.

3.2.1 Formation of voids leads to battery failure. Otoyama[75] conducted the first *in situ* observation of digital image correlation (DIC) analysis for sulfide-based all-solid-state batteries, visualizing the local strain distribution and providing insights into how and where cracks form, as shown in Fig. 4A. Higher

strain variations in the *Y*-direction were observed at relatively large Si particles, leading to crack formation during the initial stages of lithiation. Meanwhile, Okuno[43] combined electrochemical impedance spectroscopy (EIS) with cross-sectional observations using field emission scanning electron microscopy (FE-SEM) and energy-dispersive X-ray spectroscopy (EDX) to study the electrochemical behavior and microstructure of nanoporous Si composite anodes, as shown in Fig. 4B. It was found that microcracks formed within the SSSE rather than at the Si-SSSE interface during cycling. Huo[49] separated the effects of chemical degradation and mechanical cracking to better understand the failure mechanisms of SSBs based on Si anodes, as shown in Fig. 4C. Chlorine-rich $Li_{5.5}PS_{4.5}Cl_{1.5}$ pairing with Si could suppress interfacial chemical degradation, while fine-grained Li_6PS_5Cl led to a 4.3-fold increase in interfacial resistance due to the large Si|Li_6PS_5Cl contact area. Fine-grained Li_6PS_5Cl improved the microstructural homogeneity of electrode composites, effectively alleviating stress accumulation caused by Si particle expansion/contraction. This minimized macrocracks in Li_6PS_5Cl during lithiation and reduced interfacial void formation during delithiation. Sakka[76] conducted *in situ* X-ray computed tomography on an ASSBs composed of silicon active material and the $Li_{10}GeP_2S_{12}$, accompanied by charge/discharge tests and EIS measurements. The plastic SSSE responded to the volume expansion of silicon but not to its contraction, resulting in the formation of shell-like voids around the active material. These shell-like voids increased the tortuosity of Li^+ conduction pathways within the composite anode and raised the interfacial resistance due to severe loss of the Si/SSSE interface. The degradation of the Si/SSSE interface, caused by the plasticity of the SSSE, significantly limited the electrochemical performance of the ASSBs with a silicon anode, leading to incomplete delithiation reactions and low coulombic efficiency.

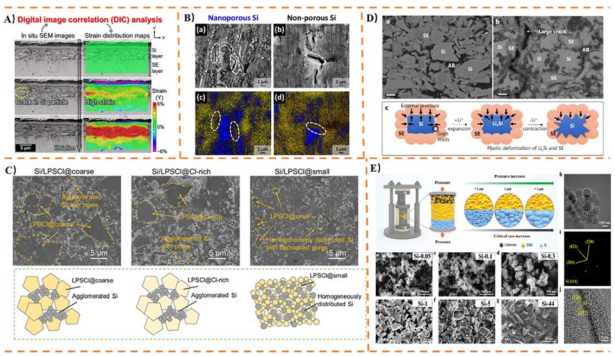

Fig. 4 (A) Visualizing local strain distributions through DIC analysis of *operando/in situ* images of all-solid-state batteries can provide insights into how and where cracks form; (B) CrosS-SSEctional SEM images and EDX mapping images of nanoporous and non-porous Si composite anodes, respectively; (C) microstructures and related ion/electron transport in different Si|LPSCl composites; (D) CrosS-SSEctional back-scattered electron images of the Si-composite electrode in the Si/NMC full-cells under a compressive pressure of 75 MPa; (E) schematic of battery assembly and morphology characterization of the pristine samples.

Guan[77] developed a flexible thin-film ASSBs composed of an NMC811 cathode, SiC anode, and LGPS solid electrolyte. Using numerical solutions, they established an interfacial contact model and a coupled electrochemical–mechanical model for the ASSBs under bending effects. The results demonstrated that bending effects can alleviate interfacial stress generated during lithiation; curvature primarily influences the electrolyte potential, while the contact coefficient mainly affects the overpotential. Nelson[78] employed *in situ* X-ray computed microtomography to investigate the chemomechanical degradation process of silicon anodes in SSBs across micro- to macro-scales. *In situ* EIS revealed that the increase in impedance during delithiation in silicon-anode SSBs may be related to the formation of large crack networks throughout the Si electrode. The study identified three crack formation mechanisms in silicon-anode SSBs: (1) vertical paste-layer-type channel cracks propagating along the thickness of the Si electrode; (2) interfacial fracture induced by delithiation; (3) interfacial fracture caused by relithiation. Mechanisms 2 and 3 were observed predominantly in relatively thick silicon electrodes. Han[79] investigated the evolution of stress (stacking pressure) in composite anode batteries containing active materials such as Si, Sn, and Sb with sulfide electrolytes. The study revealed that in liquid LiBs, relatively high applied stacking pressures (approximately 3–5 MPa) significantly accelerate capacity decay due to increased interphase growth, which contrasts with SSBs. SSBs generally exhibit improved cycling stability under higher stacking pressures within the range of 5–30 MPa. Yamamoto[80] conducted a detailed investigation into silicon anode batteries under different stacking pressures (75 MPa and 50 MPa), focusing on cycling stability, rate capability, internal resistance, and microstructure, as shown in Fig. 4D. The study revealed that applied pressure helps prevent crack formation in silicon particles, repairs fine cracks, and promotes intimate contact between the SSSEs and Li_xSi through plastic deformation. Over-extended cycling, pressure induces the formation of numerous vertical cracks. The repeated occurrence and repair of cracks at the same locations effectively mitigate stress generated by silicon volume changes, thereby enabling stable cycling. Li[69] systematically studied the size effect of silicon anodes in sulfide-based ASSBs and their structural evolution during cycling using silicon particles ranging from tens of nanometers to tens of micrometers (Fig. 4E). The results confirmed that the size effect persists in sulfide-based ASSBs. Applying a stacking pressure of 330 MPa proved crucial for enhancing interfacial contact and charge transfer within ASSBs, raising the critical size threshold of silicon particles from 150 nm in conventional liquid electrolyte LiBs to the micrometer scale in ASSBs. Wang[81] conducted an in-depth investigation into the failure mechanisms of Si|Li_6PS_5Cl composite anodes at temperatures above 80 °C from the perspectives of interfacial stability and (electro) chemomechanical effects. Excessive volume expansion and localized stress induced by silicon lithiation at elevated temperatures disrupt the mechanical structure of the Si|Li_6PS_5Cl composite anode. Electrochemical analysis revealed that the differences in performance at various temperatures are attributed to interfacial reactions and mechanical failure within

the Si/Li_6PS_5Cl anode, leading to a sharp capacity decay above 80 °C. Results from *ex situ* XPS, ToF-SIMS, and computational studies confirmed the presence of semiconducting silicon and/or Si–P compounds at the $Li_xSi|Li_6PS_5Cl$ interface. This causes the interface to become non-passivating at high temperatures.

The formation of voids is one of the most typical and critical failure modes in Si-based anodes coupled with SSSEs. Its fundamental impact lies in disrupting the continuous pathways for Li^+ transport, thereby triggering a chain of adverse reactions that ultimately lead to battery failure. Common mitigation strategies include applying external pressure to mechanically compensate for volume changes and maintain interfacial contact, or designing composite anodes that blend silicon with flexible electrolytes (such as PSEs) or buffering materials to internally accommodate stress.

3.2.2 Side reactions lead to failure. With the development of highly conductive SSEs, the performance limitations of ASSBs are no longer primarily governed by Li^+ diffusion within the electrolyte, but rather by low coulombic efficiency (CE) and short cycle life. These issues result from side reactions at the electrode/electrolyte interface that form highly resistive layers. The high chemical/electrochemical reactivity of silicon anodes further exacerbates the physical and chemical instability at these interfaces.

Sun[82] employed ultrasonic transmission technology to investigate the chemomechanical and morphological dynamics of silicon electrodes in c-Si|Li_6PS_5Cl|$Li_{0.5}$ batteries. The study revealed that stress evolution within the Si electrode is a nonlinear function of the state of charge and depends on metastable Li_xSi phases. Brow[48] conducted a detailed analysis of cobalt-free NMA|Li_6PS_5Cl|Si batteries, and found that electrolyte degradation closely resembled that observed with other nickel-rich transition metal oxide cathode materials, demonstrating that NMA does not cause additional electrolyte degradation. However, the NMA cathode exhibited significant fracture after applying a pressure of 350 MPa. In contrast, Nagata[83] investigated the impact of mechanochemical reactions between various solid electrolytes and silicon on battery performance. The results indicated that reactions between silicon and SSSEs increase resistance, thereby reducing electronic conductivity.

Cao[15] systematically investigated the electrochemical and mechanical evolution of nano-silicon (nSi) composite anodes in SSSEs ASSBs using *in situ* synchrotron X-ray absorption near-edge structure (XANES), *in situ* scanning electron microscopy (SEM), and *in situ* synchrotron X-ray nanotomography (XnT), as illustrated in Fig. 5A. The study revealed that the SSSEs undergo electrochemical decomposition during the initial lithiation of the silicon anode, a process accelerated by the addition of carbon. The decomposition products, however, stabilize in subsequent cycles. *In situ* SEM and *in situ* XnT confirmed that incorporating both SSSEs and carbon into the silicon anode enhances mechanical structural stability. The addition of solid electrolyte and carbon to the nano-silicon anode improves reaction kinetics, increases silicon utilization, and promotes mechanical structural integrity. Asano[84] analyzed the interface between high-density silicon thin films with roughness <1 nm and Li_3PS_4 electrolyte, as shown in Fig. 5B. It was found that

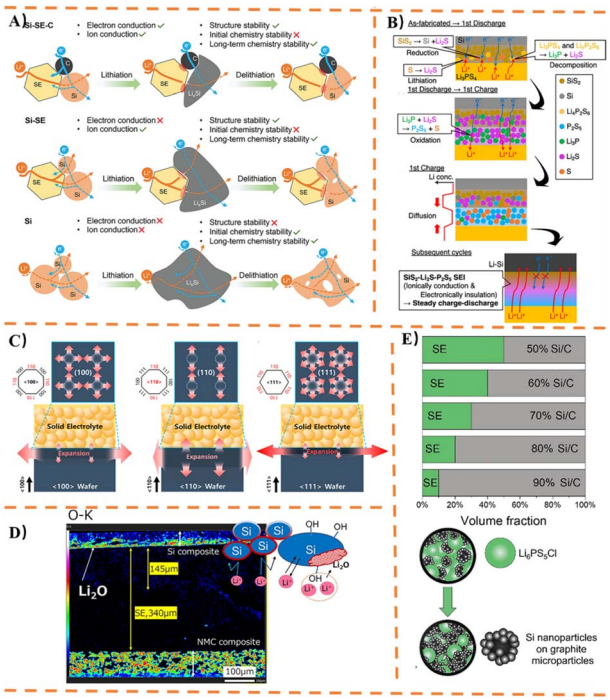

Fig. 5 (A) Schematic illustrating the chemistry and structure evolution of Si-SSE-C, Si-SSE, and Si anodes in ASSBs; (B) schematics of the structural changes at the Si/Li_3PS_4 interface; (C) cracks evolved along [110] direction due to anisotropic volume expansion of wafers; (D) elemental mapping of the cross section of ASSB-argyro using SEM-EDS; (E) the variation of the volume fraction of the SE and the active material allows influencing the cell performance based on anode composition.

during the first cycle, lithiation and delithiation scarcely occurred at the interface; however, reduction or oxidation of interfacial components or the Li_3PS_4 electrolyte took place in the initial cycle, while side reactions primarily emerged in subsequent cycles. Huo[47] elucidated the chemomechanical failure mechanisms of composite Si|Li_6PS_5Cl anodes and solid-electrolyte-free silicon anodes by combining structural/chemical characterization with theoretical modeling. The study revealed that the SEI layer formed at the Si|Li_6PS_5Cl interface significantly increased the resistance of the composite anode, accelerating capacity decay. In contrast, SSE-free silicon electrodes enabled a 2D planar Si|LPSCl interface, where SEI formation had a minor impact on overall cell resistance. It was also confirmed that chloride-rich $Li_{5.5}PS_{4.5}Cl_{1.5}$ effectively suppresses interfacial chemical degradation when paired with silicon.[49] Na[85] demonstrated that lithiation initiation at the beginning of charging triggers vertical expansion of the interface and drives solid electrolyte movement along the ⟨110⟩ direction, resulting in tighter interfacial contact (Fig. 5C). The monolithic silicon structure facilitates rapid Li^+ transport across the electrode thickness, while surface modifications enhance interfacial stability and cycling retention.

Matsuda[86] prepared all-solid-state anodes using two different sulfide electrolytes—$Li_{5.5}PS_{4.5}Cl_{1.5}$ and Li_2S-P_2S_5-LiI—with silicon material, and discovered that Li_2O formed in the

anodes of both electrolyte systems after 50 cycles, as shown in Fig. 5D. In a full cell system, the consumption of a limited amount of Li^+ to generate Li_2O leads to reduced battery capacity due to Li^+ depletion and increased irreversible capacity. Moreover, coating Si particles in the anode with Li_2O increases resistance because Li_2O has lower ionic conductivity than the SSSEs. Rudel[87] systematically varied the ratio of the solid electrolyte Li_6PS_5Cl to the Si/C active material and investigated the electrochemical behavior through rate capability and long-term cycling tests. The study demonstrated the influence of effective ionic conductivity on the electrochemical performance of Si/C-based composite anodes. It was found that the effective ionic conductivity of the electrode composite increases exponentially with higher solid electrolyte content, which in turn leads to increased specific capacity of the composite at various rates, as illustrated in Fig. 5E. So[88] proposed a simulation framework using the discrete element method (DEM) for the fabrication and lithiation of silicon anodes in ASSBs. During charging, lithium insertion causes silicon particles to expand, increasing electrode height. Furthermore, the void space increases significantly throughout the charging cycle. Due to diffusion-limited reactions, expansion within the silicon particles is non-uniform. Steep lithium concentration gradients cause adjacent particles to expand at different rates, generating stress in the binder bonds that hold the particles together. If the stress exceeds the material's hardness, the bonded contacts will be damaged. The amount of void space decreases significantly with increasing stack pressure, owing to the elastic response of the electrode structure to the applied stress. In addition, the content of silicon and carbon leads to increased porosity. A higher silicon content results in a stiffer and less deformable electrode because silicon is a hard and brittle material. The contact area is primarily controlled by stack pressure due to the elastic response of the materials. Since the reaction is limited by lithium diffusion transport, increasing the C-rate amplifies the lithium concentration gradient within the silicon particles. This concentration gradient causes stress accumulation, leading to damage in the silicon particles. Fragmentation of silicon particles is mainly controlled by the charge rate and is also influenced by the silicon fraction, as it determines both the contact area and the concentration gradient. In contrast, stack pressure has no significant impact on particle fragmentation. Although local stress near the contact points increases under higher pressure, the reduction in concentration gradient due to the increased surface area has a more dominant effect.

Unlike the physical failure mechanism caused by voids, side reactions lead to a chemical failure. This stems from the thermodynamic instability between the silicon anode and the SSSEs, resulting in continuous chemical reactions at the interface that eventually poison the interface and block Li^+ transport pathways. To address this, an ultra-thin protective layer that is ionically conductive, electronically insulating, and chemically stable (such as LiPON, Li_3N, or LiSiON) can be constructed between the silicon particles and the SSSEs. This layer prevents direct contact between Si and the SSSEs while allowing smooth Li^+ passage. Alternatively, blending nSi with more stable ionic conductors (*e.g.*, PSEs) can reduce the direct contact area between Si and the SSSEs, thereby improving interfacial instability. In summary, side reactions impair the Li^+ transport function of the interface through "chemical poisoning." Although the failure process is less abrupt than void formation, it is equally detrimental and often irreversible. Overcoming this challenge is essential for building long-life silicon-based SSBs.

4. Polymer solid electrolytes (PSEs)

In rechargeable LiBs, PSEs are situated between the positive and negative electrodes, serving dual roles as both electrolyte and separator. Therefore, polymers suitable for PSEs must possess the following properties: (1) solubility: they should contain polar groups, such as –O–, C═O, and C≡N, to dissolve lithium salts and form polymer-salt complexes; (2) electrochemical stability: they should exhibit a wide voltage window, with a significant difference between the onset potentials of oxidative and reductive decomposition; (3) high ionic conductivity, high ion transference number, and electrical insulation: these properties are essential to maintain expected performance and minimize self-discharge processes, thereby extending storage life; (4) chemical and thermal stability: they should not undergo chemical reactions during battery operation; (5) mechanical strength: adequate mechanical stability is necessary to ensure processability and effective isolation of the positive and negative electrodes. Although numerous types of PSEs have been studied, polyethers are predominantly used for Si-based anodes.

4.1 Polyether-based PSEs

Polyethers are characterized by an ether bond (–R–O–R–) in their main chain, which facilitates the dissociation and complexation of lithium salts. Currently, polyether-based PSEs primarily include PEO,[89] PEG,[25] PDOL,[90] and polyethylene glycol diacrylate (PEGDA).[91,92] Among these, PEG shares the same chemical structure as PEO but has a lower molecular weight (<20 000). Shorter polymer chains exhibit better molecular mobility but inferior mechanical strength. Therefore, PEG is typically used as a polymerization precursor or as a modifier for inorganic fillers to enhance dispersion, rather than serving as the main component of PSEs.

Wang[93] utilized the retarding effect of $LiNO_3$ to control the low-rate ring-opening polymerization of 1,3-dioxolane (DOL), constructing a 2D SEI film on the surface of the Si anode and developing a high-concentration polymer electrolyte. Batteries employing this PSE delivered a high capacity of 1765 mAh g^{-1} at 2C and maintained a high capacity of 2000 mAh g^{-1} after 100 cycles at 0.2C. Wang[45] prepared a GPE *via in situ* thermal polymerization of ethoxylated trimethylolpropane triacrylate (ETPTA) and polyethylene glycol dimethacrylate (PEGDMA) monomers, as shown in Fig. 6A, which is suitable for SiO_x anodes and achieves long-term cycling stability. The GPE-based batteries alleviate the volume expansion of SiO_x anodes by guiding a unique lithiation/delithiation mechanism that favors formation and delithiation with reduced volume changes, thereby mitigating electrode damage and cracking and

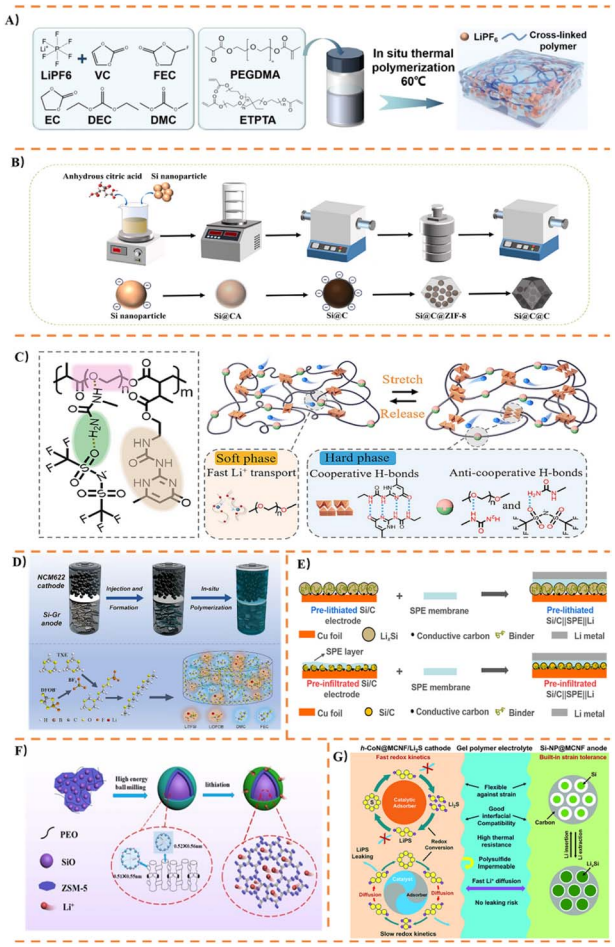

Fig. 6 (A) Schematic diagram of the preparation process of GPE; (B) schematic illustrations of Si@C@C composites and PDOL polymer electrolyte synthesis; (C) molecular structure of the meticulously constructed SHDSE and demonstration of the mechanical properties; (D) schematic illustration of preparing the full cell with the *in situ* generated quasi-solid-state electrolyte and mechanism of the polymerization from TXE to polymer skeleton; (E) cell configuration of solid-state lithium batteries using prelithiated and preinfiltrated Si/C electrodes; (F) schematic diagram of the preparation process of electrode material SZP; (G) schematic illustration of the configuration and merits of quasi-solid-state h-CoN@MCNF|Li_2S|Si-NP@MCNF full cells.

significantly enhancing cycling performance. Qiu[94] co-designed an all-solid-state lithium-ion battery with high stability and excellent coulombic efficiency through a triple strategy involving double-layer carbon coating, chemical pre-lithiation, and *in situ* polymerization techniques. $LiPF_6$ was utilized to initiate the *in situ* ring-opening polymerization of DOL with the addition of succinonitrile (SN) to enhance the ionic conductivity of the resulting *in situ* polymer electrolyte and improve the stability of the high-voltage cathode, as illustrated in Fig. 6B. Rui[95] proposed a novel method for preparing practical quasi-solid-state batteries (QSSBs) by combining a high-safety ethylene carbonate-free liquid electrolyte with an *in situ* polymerization process involving HLE, MMA monomer, and cross-linker EGDMA. The *in situ* polymerization suppressed exothermic reactions between the electrolyte and the anode, delayed oxygen release from the cathode, and prevented violent redox reactions through improved electrode contact. He[96] designed a self-healing dynamic supramolecular elastomer electrolyte (SHDSE) using dynamic bonds, which also functions as a binder for silicon anodes with enhanced adhesion capabilities, as depicted in Fig. 6C. The SHDSE-based Si|Li battery establishes electrolyte–electrode interfacial contact at the molecular level, providing continuous and stable Li^+ transport pathways, reducing Si particle displacement, and mitigating electrode volume expansion, thereby further improving cycling stability.

Zhao[97] employed *in situ* polymerization using 1,3,5-trioxane (TXE) as the monomer, with LiDFOB inducing the ring-opening polymerization of TXE (Fig. 6D). The resulting quasi-solid electrolyte exhibited a high ionic conductivity of up to 2.16×10^{-3} S cm^{-1} and a high Li^+ transference number of 0.61. Moreover, due to the dense solid electrolyte interphase (SEI) film formed by the preferential decomposition of LiDFOB, the contact and reaction between $TFSI^-$ and the anode were suppressed. This effectively inhibited the volume expansion of the Si/C anode after 300 cycles to 26.7%, significantly lower than the 60.7% observed with conventional liquid electrolytes. Göttlinger[98] prepared a hybrid polymer electrolyte (HPE) using two ether-based materials with siloxane end groups. In Si|HPE|Li cells, the HPE system—containing LiTFSI as the conductive salt and no ionic liquid—achieved a high capacity of approximately 1300 mAh g^{-1} at 0.1C. Dong[99] utilized micron-sized porous Si/C electrodes in combination with PEO-LiTFSI electrolyte. The pre-lithiated and pre-soaked Si/C electrodes exhibited higher specific capacity compared to the pristine electrode, owing to the continuous lithium-ion conduction pathways formed within these pre-treated electrodes, as shown in Fig. 6E. Li[100] selected ZSM-5, which possesses unique channel and pore structures, and combined it with PEO to enhance ion transport kinetics and reduce interfacial resistance (Fig. 6F). Through variable-temperature impedance tests and CV analysis, it was demonstrated that this electrolyte effectively reduces the activation energy of SiO and mitigates its volume expansion. Zhang[101] grew vertical graphene sheets on silicon nanoparticles (Si@VG) *via* thermal chemical vapor deposition for application in PEO-based ASSBs. The flexible vertical graphene sheets not only form a 3D conductive network that enhances the electrical connectivity across the electrode but also improve contact with the solid polymer electrolyte, thereby reducing interfacial impedance.

Polyether-based PSEs offer the following advantages: flexibility to accommodate the volume changes of Si, ensuring good interfacial contact; high chemical stability with moderate side reactions and relatively low interfacial impedance; excellent processability for facile composite electrode fabrication and low cost. As such, polyether-based PSEs represent one of the most compatible and promising solid electrolyte systems for Si anodes in the near term.

4.2 Other PSEs

Wu[102] employed thermal-initiated polymerization with $LiPF_6$ to prepare a GPE. This GPE effectively passivates both the NCM811

Table 2 Application of PSEs in silicon-based anode electrodes

Si anode	PSEs	Ionic conductivity (S cm^{-1})	Current density	Capacity (mAh g^{-1})	Retention/ cycle number	Ref.
nSi@VG	PEO	8.06×10^{-5}	0.5 A g^{-1}	1756.9	25.3%/200	101
			1 A g^{-1}	955	32.6%/200	101
nSi	PEI	2.0×10^{-4}	0.3 A g^{-1}	606	64.0%/100	106
nSi	QS-SCN	1.5×10^{-4}	0.02C	>2000		104
Si/C	PEO	7.72×10^{-6}	0.8 A g^{-1}	>2000	~50%/100	99
Si	PDOL	0.38×10^{-3}	0.2C	~3600	~55.5%/100	93
Gr@SiO	PEGMA				84.6%/250	102
Si@C@C	PDOL-SN	1.51×10^{-4}	0.3 A g^{-1}	1228.4	75.4%/10	94
Si-Gr	TXE	2.16×10^{-3}	0.5C		58.32%/300	97
SiO_x	PEGDMA	1.0551×10^{-3}	0.5 A g^{-1}	1129.10	61.4%/450	45
nSi	PEO-PDOL		0.2C	827	67.7%/100	103
Si	PEGDA	3.54×10^{-4}	1 A g^{-1}	2603.1	68.1%/500	96
SiO	PEO	3.74×10^{-4}	5 A g^{-1}	1489.37	13.9%/300	100
Si	TPU	9.31×10^{-4}	0.3 A g^{-1}	~1050	67.8%/60	107
nSi	HPE	0.2×10^{-3}	0.1C	1507	74%/100	98

cathode and the Gr@SiO anode by forming stable inorganic-rich electrode–electrolyte interphases, thereby ensuring excellent electrochemical performance and a high safety runaway threshold. Meng[103] fabricated a GPE with favorable interfacial contact and ionic conductivity *via* electrospinning using PAN and PMMA for quasi-solid-state batteries with lithium-metal-free redox chemistry (Li_2S cathode and Si anode), as illustrated in Fig. 6G. The assembled solid-state battery delivered an initial discharge capacity of up to 827 mAh g^{-1} at 0.2C, achieving a high initial coulombic efficiency (ICE) of 94.2%. Bintang[104] utilized the unique phase transition behavior of a quasi-solid succinonitrile-based electrolyte (QS-SCN) to infiltrate the silicon electrode with liquid electrolyte above its melting point, followed by a simple cooling process to form a quasi-solid Li–Si battery. Furthermore, a pre-cycling process induced the formation of a stable and rigid SEI, maintaining intimate contact between the QS-SCN and Si particles. The soft QS-SCN acted as a buffer during large volume expansion while preserving favorable interfacial contact. The formed SEI layer facilitated reversible lithiation and delithiation in the Si particles. Ueda[105] investigated the influence of Li^+-containing organic ionic plastic crystals (OIPCs) as solid electrolytes on the electrochemical performance of electrodes. Various Si-OIPC composite electrodes were prepared using four different methods. Among them, the Si-OIPC composite electrode containing *N*-ethyl-*N*-methylpyrrolidinium bis(fluorosulfonyl)imide ([C_2mpyr][FSI]) with 50 mol% LiFSI exhibited the highest initial coulombic efficiency and cycling stability. Chae[106] proposed a simple aqueous chemical method for synthesizing electrostatically assembled nanostructured Si–C composites. Negatively charged graphene oxide (GO) and Si nanoparticles (Si-NPs) were internally stacked in an aqueous medium using the cationic polyelectrolyte poly(ethyleneimine). Subsequently, a conductive internal pathway was established by incorporating water-dispersed amine-functionalized multi-walled carbon nanotubes (NH_2-MWNTs). ASSBs were fabricated using the internally interconnected Si-RGO/MWNT composite electrode and a semi-interpenetrating network SPEs. Finally, Table 2 summarizes the applications of PSEs in silicon-based anode electrodes.

4.3 Summary of PSEs

Research on PSEs applied to Si-based anodes has primarily focused on constructing functional SEI films on Si particle surfaces to enhance cycling stability, designing PSEs *via in situ* polymerization, and improving the ionic conductivity or transference number of PSEs. However, these efforts have shown limited effectiveness in improving the cycling performance of Si-based anodes. As summarized in Table 2, most Si anodes exhibit capacity retention below 60% after fewer than 200 cycles. The fundamental challenge in applying PSEs to Si-based anodes lies in the conflict between the large volume changes of Si and the relatively weak mechanical/chemical stability of polymers.

To address this, "network" or "block" copolymers can be designed, where one segment provides high ionic conductivity (flexible chains) and the other offers high mechanical strength (rigid chains), achieving synergistic performance. Alternatively, a gradient interlayer with a composition/modulus transition from the Si anode to the PSEs can be engineered to enable gradual stress distribution. Another promising approach involves incorporating dynamic reversible bonds—such as hydrogen bonds, ionic bonds, or dynamic covalent bonds—into the polymer network. When localized stress from Si expansion becomes excessive, these bonds can reversibly break and reform, enabling "self-healing" at the interface to maintain contact and thereby extend the cycling life of Si-based anodes.

5. Oxide solid state electrolytes (OSSEs)

In contrast to PSSEs, which suffer from poor oxidation stability and low Li^+ transference numbers, many OSSEs exhibit an ultra-high Li^+ transference number approaching.[108] The development of OSSEs began in 1976 when Goodenough *et al.*[109] synthesized the sodium superionic conductor (NASICON)-type solid electrolyte $Na_3Zr_2PSi_2O_{12}$ *via* high-temperature solid-state reaction. Subsequently, in 1990, Aono *et al.* produced the layered

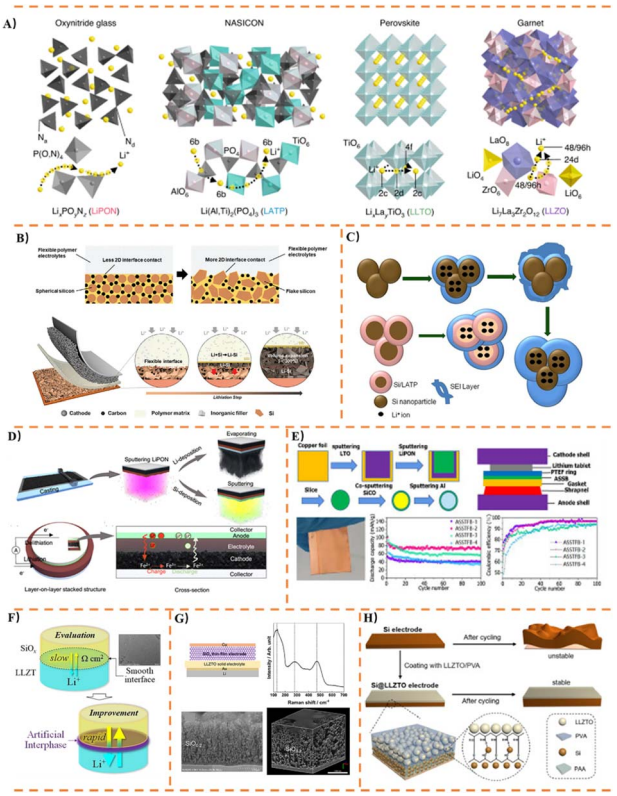

Fig. 7 (A) Structures, local bonding units and network for convenient Li-ion migration paths of oxide-based Li-ion conductors, including amorphous LiPON, NASICON-type LATP, perovskite-type LLTO and garnet-type LLZO; (B) schematic diagram of spherical and flaky Si anode with CSEs; (C) schematic illustration of the structural changes, like SEI layer formation for Si and LATP-Si during cycling; (D) schematic illustration of the fabrication processes of tape-casting electrodes, LiPON sputtering deposition, and evaporating Li or sputtering Si as anodes. The schematic diagram of layer-on-layer stacked structure and electron/ion transport mechanism of LFP|LiPON|Li (or Si) all-solid-state thin-film microbatteries; (E) the preparation process, multi-layer structure, atomic configurations; (F) Li^+ transfer resistivity at a solid/solid interface was quantitatively evaluated with a flat and smooth $Li_{6.6}La_3Zr_{1.6}Ta_{0.4}O_{12}$ electrolyte and a SiO_x thin-film electrode; (G) schematic of a SiO_x|LLZTO|Li-Au cell, Raman spectrum, crosS-SSEctional SEM image, and FIB-SEM image of porous $SiO_{0.2}$ films; (H) schematic illustration of Si@LLZTO composite electrode preparation process.

$Li_{1.3}Al_{0.3}Ti_{1.7}(PO_4)_3$ (LATP)[110] electrolyte through sintering, which demonstrated an ionic conductivity of 7×10^{-4} S cm^{-1} at room temperature. In 1992, they further sintered $Li_{1.5}Al_{0.5}Ge_{1.5}(PO_4)_3$ (LAGP)[111] electrolyte with a room-temperature ionic conductivity of 2.4×10^{-4} S cm^{-1}. Also in 1992, the research team of Bates[112] in the United States successfully developed lithium phosphorous oxynitride (LiPON), a new type of amorphous glassy OSSE. Inaguma *et al.*[113] discovered in 1993 that polycrystalline lithium lanthanum titanate ($Li_{0.34(1)}La_{0.51(1)}TiO_{2.94(2)}$, LLTO) exhibited an ionic conductivity exceeding 2×10^{-5} S cm^{-1} at room temperature. The Werner team first identified in 2003 that garnet-like structured $Li_5La_3M_2O_{12}$ (M = Ta, Nb)[114] possessed high ionic conductivity and a wide electrochemical window. Later, in 2007, they synthesized $Li_7La_3Zr_2O_{12}$ (LLZO),[115] a typical garnet-structured OSSE with a room-temperature lithium-ion conductivity of approximately 10^{-4} S cm^{-1}.

To date, OSSEs widely studied by researchers mainly include NASICON-type (*e.g.*, LATP), perovskite-type (*e.g.*, LLTO), lithium phosphorus oxynitride-type (*e.g.*, LiPON), and garnet-type (*e.g.*, LLZO) structures, as illustrated in Fig. 7A. However, the ionic conductivity of perovskite-type LLTO is predominantly limited by its internal grain boundary resistance, reducing its lithium-ion conductivity to below 10^{-5} S cm^{-1} at 25 °C. Furthermore, in the presence of graphite at the anode, Ti^{4+} in crystalline LLTO can be reduced to Ti^{3+}, significantly increasing electronic conductivity and potentially causing short circuits in all-solid-state battery systems. Currently, OSSEs applied in Si-based anodes are mainly NASICON-type, LiPON-type, and Garnet-type electrolytes. Finally, Table 3 summarizes the applications of OSSEs in silicon-based anode electrodes.

5.1 NASICON-type

The NASICON-structured LATP offers advantages such as high ionic conductivity, low cost, and excellent air stability. However, its application in ASSBs is significantly limited by high interfacial impedance and severe interfacial side reactions with electrodes.[128–131] For instance, the Si|LATP interface undergoes pronounced interdiffusion and alloying during cycling, leading to rapid degradation of the interfacial properties between the Si-based anode and the LATP electrolyte. To address this, Liu[132] applied a graphene coating on the LATP surface to improve the interface. The graphene film effectively prevents the diffusion of Si atoms into LATP, and the graphene-modified full cell achieved an initial discharge specific capacity of 150 mAh g^{-1}. To address the issues of high interfacial resistance at the OSSEs Si/LATP interface and the poor ionic conductivity of polymer electrolytes—both of which are exacerbated by the volume expansion of Si—Liu[50] directly dispersed LATP into a PVDF-HFP and PEO matrix to prepare a composite electrolyte, as shown in Fig. 7B. This electrolyte enhances the amorphous degree of the polymer through chemical interactions among PVDF-HFP, PEO, and LATP, thereby accelerating Li^+ transport. Meanwhile, the highly stretchable solid film restrains electrode structural degradation and suppresses continuous interfacial growth, resulting in the formation of a stable 2D SEI layer. In a separate approach, Augustine[133] coated LATP powder onto Si nanoparticles as an artificial SEI layer. This layer selectively conducts Li^+ ions while preventing the formation of a thick native SEI, thereby improving cycling stability (Fig. 7C). The composite electrode delivered a specific discharge capacity of 1789 mAh g^{-1} at 0.1C and maintained over 75% capacity retention after 500 cycles.

Another NASICON-type solid electrolyte is LAGP, which exhibits a high ionic conductivity exceeding 10^{-4} S cm^{-1} at room temperature.[134–136] Sau[122] synthesized a Si-doped LAGP electrolyte, $Li_{1.6}Al_{0.5}Ge_{1.5}P_{2.9}Si_{0.1}O_{12}$ (LAGPS). After coating Si nanoparticles with a uniform Si/C layer of less than 10 nm, the half-cell assembled with LAGPS demonstrated a high discharge capacity of 2077 mAh g^{-1} and excellent cycling stability.

NASICON represents a typical class of OSSEs with the general formula $Li_{1+x}A_xB_{2-x}(PO_4)_3$, among which LATP and LAGP are

Table 3 Application of OSSEs in silicon-based anode electrodes

Si anode	OSSEs	Current density	Capacity (mAh g^{-1})	Retention/cycle number	Ref.
$SiO_{0.2}$	$Li_{6.6}La_3Zr_{1.6}Ta_{0.4}O_{12}$	0.1C	1349	77.8%/100	116
Si	$42Li_2SO_4$-$28Li_2CO_3$-30LiI	0.064 mA cm^{-2}	2250		12
$SiO_{0.4}$	$Li_7La_3Zr_2O_{12}$			50%/100	117
SiC	$Li_{6.75}La_3Zr_{1.75}Ta_{0.25}O_{12}$	0.1C	155	89%/100	118
Si	$Li_7La_3Zr_2O_{12}$	7.5 mA g^{-1}	2685		119
nSi	LiPON	2 μA cm^{-2}	6.1 (μAh cm^{-2})	74.5%/100	120
nSi	$Li_{6.4}La_3Zr_{1.4}Ta_{0.6}O_{12}$	800 mA g^{-1}	2503	70%/320	121
nSi	$Li_{1.5}Al_{0.5}Ge_{1.5}P_3O_{12}$	0.8 A g^{-1}	2077	71.21%/300	122
SiO_x-C	LiCPON		511.5		123
Si	$45Li_2SO_4$-$30LiCO_3$-25LiBr	0.13 mA cm^{-2}		89%/50	124
SiCO	LiPON	0.1C	104.15	73.29%/40	125
Si/SiCO	LiAlPON		190.1		126
nSi	$Li_{6.4}La_3Zr_{1.4}Ta_{0.6}O_{12}$	1 A g^{-1}		60%/200	53
nSi	$Li_7La_3Zr_2O_{12}$	C/18	2702	~44.4%/100	127

the most common representatives. They are renowned for their high ionic conductivity and exceptional stability in air, yet they face severe challenges when paired with Si-based anodes. Specifically, issues such as chemical incompatibility with Si and their inherent rigidity as ceramics hinder their ability to accommodate the volume changes of Si, leading to interfacial gaps and cracking. To enable their application in high-capacity Si-based anodes, highly sophisticated interfacial engineering design is essential, which remains one of the most significant challenges in the field.

5.2 LiPON-type

LiPON is an amorphous lithium-ion solid electrolyte, specifically a type of glassy material used as an electrolyte in thin-film flexible batteries.[137] Its ionic conductivity at room temperature is approximately 2×10^{-6} S cm^{-1}, significantly lower than that of other types of solid electrolytes, which severely restricts its application.[138] For silicon-based anodes, the sheet-type pouch cells configuration is more compatible with LiPON thin films. This structure provides a more controllable and uniform mechanical environment, enabling continuous and dense LiPON films to fully leverage their interfacial passivation advantages. In contrast, the random stresses and point contacts inherent in powder-pressed pellet-type cells are detrimental to any brittle protective coating. This also explains why the industry predominantly adopts pouch or similar stacked structures in the development of solid-state batteries. The specific microstructural evolution pathways are as follows: in pouch cells, interface layer failure is dominated by macroscopic mechanical issues, ultimately leading to localized short circuits or interfacial delamination; whereas in powder-pressed pellet-type cells, localized failures at the particle scale accumulate and propagate into systemic global failure.

Ke[120] deposited an approximately 3 μm-thick LiPON thin-film electrolyte *via* radio-frequency reactive magnetron sputtering (Fig. 7D) and seamlessly integrated it with a 70 nm-thick Si anode. The resulting cell exhibited a capacity retention of 74.5% after 100 cycles. Qiao[123] developed a prelithiation method based on lithium solid-state corrosion. Using carbon-doped lithium phosphorus oxynitride (LiCPON) OSSEs, they avoided various side reactions associated with lithium and achieved a perfect interface with a SiO_x-C composite anode through decomposition products derived from LiCPON. Feng[139] evaluated the influence of oxygen content in silicon oxides on the interfacial stability with LiPON. Computational results on thermal stability and electronic properties indicated that the $SiO_{0.5}$|LiPON interface constitutes the most stable system. Further optimization of the $SiO_{0.5}$|LiPON interface was carried out *via Ab Initio* Molecular Dynamics (AIMD) simulations combined with doping LiPON with Si, B, and C elements. Doping with Si significantly enhanced both interfacial stability and ionic conductivity. Owing to the tetrahedral silicon structure in SiCO and improved wettability at the electrolyte interface, Feng[125] fabricated a novel silicon carbon oxynitride/lithium metal composite anode *via* magnetron sputtering and integrated it with a LiPON-based all-solid-state thin-film microbattery, as illustrated in Fig. 7E. The battery demonstrated an initial discharge capacity of 104.15 mAh g^{-1}. Raman spectroscopy revealed the presence of both sp^3 amorphous carbon and sp^2 graphitic carbon in the magnetron-sputtered SiCO layer. Using first-principles calculations, Xu[126] evaluated and engineered the interface between LiPON doped with various elements (Al, Si, C, Sn, Y, Ta) and SiCO. Their study revealed that Al-doped LiPON exhibits a higher interfacial formation energy, which helps eliminate the space charge layer and enhances lithium-ion transport capability. This improvement is attributed to Al doping primarily acting as a network former, enhancing structural stability and significantly increasing lithium-ion conductivity through the introduction of lithium vacancies, while also demonstrating stronger interface passivation capability. In contrast, Si doping serves as an isovalent network former, slightly modifying the glass network structure and lithium-ion migration barriers. While it offers limited improvement in conductivity, it enhances densification and interfacial contact. On the other hand, C doping functions as a network terminator, disrupting the long-range P–O/N network and forming strong covalent C=O/N bonds. This typically leads to a significant

reduction in ionic conductivity, though it may improve interfacial stability against lithium metal.

LiPON is primarily utilized as a functional protective layer in Si-based anodes, yet its preparation involves extremely high costs. The synthesis of LiPON heavily relies on vacuum sputtering technology—a process characterized by expensive equipment, very low deposition rates, high energy consumption, and difficulties in scaling up production. As a result, its application in thick electrodes (>100 μm) and large-format cells is not economically viable.

5.3 Garnet-type

Garnet-type electrolytes, such as LLZO and its derivatives, exhibit high ionic conductivity at room temperature, a wide electrochemical stability window, a high Li^+ transference number, and good stability against lithium metal anodes. However, their practical application is hindered by issues such as lithium dendrite growth, poor interfacial contact, and inherent brittleness.[140,141] Doping has proven to be an effective strategy for enhancing the performance of LLZO-based electrolytes.

Doping with Al can induce lithium vacancies, thereby enhancing the ionic conductivity of LLZO and improving interfacial compatibility, which collectively contribute to better cycling and rate performance. When investigating the interfacial and nanomechanical evolution of Si anodes in solid-state batteries, Ping[119] found that LLZAO ($Li_7La_3Zr_2O_{12}$ with 3 wt% Al_2O_3) forms good contact with the Si anode and maintains structural integrity during lithium insertion and extraction. Ta doping can further enhance the electrochemical performance of LLZO and improve its phase stability. Sugimoto[117] quantitatively evaluated and optimized the Li^+ transfer across the interface between SiO_x electrodes and Ta-doped garnet-type LLZO ($Li_{6.6}La_3Zr_{1.6}Ta_{0.4}O_{12}$) electrolyte, as shown in Fig. 7F. Although Li^+ transfer at the solid/solid interface is slower than that at solid/liquid interfaces with liquid electrolytes, introducing an artificial SEI at the SiO_x/LLZTO contact interface effectively reduces interfacial resistance. Marumoto[116] fabricated ultra-porous $SiO_{0.2}$ electrodes with distinct porous architectures on LLZTO *via* radio-frequency magnetron sputtering to enhance interfacial contact, as illustrated in Fig. 7G. The interconnected open-pore structure with nanoscale porosity effectively acts as a buffer, mitigating both internal and interfacial stresses during Si expansion (lithiation) and contraction (delithiation). In a separate approach, Zeng[53] utilized chemical bonding between the PVA binder in the LLZTO coating and the PAA binder in the Si-based electrode to establish a stable interface between the electrode and electrolyte, as shown in Fig. 7H.

Compared to NASICON-type electrolytes (*e.g.*, LATP), LLZO exhibits significantly improved compatibility with Si anodes due to its superior reduction stability. However, physical contact failure caused by its inherent rigidity remains the major obstacle to achieving long-term cycling stability. Future advancements will depend not on breakthroughs in LLZO itself, but rather on innovations in interfacial engineering, particularly in: (1) developing efficient, low-cost, and scalable interfacial buffer layer technologies; (2) designing advanced composite Si anode architectures.

The LLZO-Si system represents a critical pathway toward high-energy-density ASSBs, yet its successful commercialization hinges on effectively addressing the aforementioned challenges in mechanical and chemical interfacial stability.

5.4 Others-type

Nagata[12] reported a highly deformable and ion-conductive oxide-glass solid electrolyte. The glassy state was achieved in the $(1-x)Li_2SO_4$-xLi_2CO_3 system within the range of $x = 30$ to 70 *via* ball milling, exhibiting excellent deformability. Furthermore, the $(1-y)(0.6Li_2SO_4$-$0.4Li_2CO_3)$-$yLiX$ (X = Cl, Br, I) system demonstrated enhanced deformability and improved ionic conductivity with increasing atomic number of X. All-solid-state full cells employing a Li_2S cathode and Si anode with $(1-y)(0.6Li_2SO_4$-$0.4Li_2CO_3)$-$yLiX$ delivered a relatively high discharge capacity of 740 mAh g^{-1} at 45 °C. After compositional optimization, Nagata[124] synthesized a $0.45Li_2SO_4$-$0.30Li_2CO_3$-0.25LiBr (LSCB) oxide electrolyte, which showed high electrochemical stability between 0 and 4.5 V (*vs.* Li). The assembled all-solid-state NCM-Si cell exhibited a specific energy density of 205 Wh kg^{-1} at 0.064 mA cm^{-2} and 25 °C. Subsequently, Nagata[142] found that a one-step mechanical ball milling process—used to prepare cathode/anode composites from Li_2S or Si with conductive carbon and Li_2SO_4-Li_2CO_3-LiX—narrowed the potential distribution gap between the cathode and anode, significantly enhancing battery performance.

OSSEs have attracted significant attention due to their high ionic conductivity, excellent mechanical strength, and wide electrochemical windows. However, when paired with Si-based anodes—which exhibit extremely high theoretical capacity—they introduce a series of interfacial challenges that are more severe than those encountered in polymer-based systems. The core issue at the OSSEs|Si interface lies in the fundamental incompatibility between rigid contact and significant volume expansion. To address this critical challenge of rigid interfacial contact, modification strategies primarily focus on introducing flexible mediators and structural design, including: (1) *in situ* formed/artificial SEI layers: ultra-thin, dense, and ion-conductive interlayers—such as LiPON—are fabricated on OSSE or Si surfaces using precision techniques like magnetron sputtering, pulsed laser deposition (PLD), and atomic layer deposition (ALD). (2) Flexible interfacial buffer layers: an intermediate layer is introduced between OSSEs and Si that not only conducts lithium ions but also buffers mechanical stress and suppresses side reactions. (3) Optimization of OSSEs' bulk properties: doping modifications are applied to OSSEs to improve electrode contact and reduce bulk impedance.

5.5 Summary of OSSEs

OSSEs are renowned for their excellent thermal stability and high bulk ionic conductivity. However, when paired with silicon anodes, the fundamental challenge lies in the irreconcilable mechanical conflict between two brittle and rigid materials undergoing dynamic volume changes. This represents the most

critical issue: OSSEs are hard and brittle ceramics lacking elasticity, while silicon undergoes ~300% volume expansion and contraction during cycling, generating immense repetitive stress at the rigid interface. This leads to: (1) separation and void formation at the interface when silicon particles contract, disrupting ion transport pathways; (2) microcracks or even macroscopic fracture in the OSSEs themselves when silicon expands.

To address this, a promising strategy is to avoid direct contact between the silicon anode and dense OSSEs, instead incorporating OSSEs as fillers or scaffolds within a polymer matrix. Specific approaches include: dispersing OSSE nanoparticles in a polymer matrix, where the polymer provides flexibility to maintain continuous contact with the silicon particles; fabricating OSSE nanofibers *via* electrospinning to form a three-dimensional porous scaffold, which is then infused with polymer to provide continuous ion channels and macroscopic flexibility; or introducing a soft, stable, and lithium-conductive interlayer between Si and OSSEs, such as a thin coating of elastic polymer on the silicon surface or an *in situ* formed interfacial layer, to effectively mitigate cyclic stress.

6. Sulfide solid state electrolytes (SSSEs)

OSSEs are hard and brittle, typical of ceramics, and exhibit poor solid–solid contact with electrodes, requiring extremely high sintering temperatures or pressures to achieve adequate interfacial contact. In contrast, SSSEs are relatively softer, possessing certain plasticity and deformability. Under moderate pressure, they can form intimate conformal contact with electrode materials, enabling theoretically lower interfacial impedance. Since the development of glassy SSSEs based on Li_2S-P_2S_5 (ref. 143) in the 1980s, SSSEs have attracted extensive attention from researchers. Subsequently, in 2001, the first crystalline SSSEs, $Li_{3.25}Ge_{0.25}P_{0.7}S_4$, was discovered by Kanno's group at the Tokyo Institute of Technology.[144] In 2005, Professor Tatsumisago's team synthesized the glass-ceramic electrolyte $Li_7P_3S_{11}$ and investigated its fundamental properties.[145–149] In 2008, Deiseroth identified the crystalline argyrodite-type Li_6PS_5X (X = Cl, Br, I).[150] In 2011, Professor Kanno's group at the Tokyo Institute of Technology synthesized $Li_{10}GeP_2S_{12}$ (LGPS), which exhibited an ionic conductivity of 1.2×10^{-2} S cm^{-1}—a value comparable to that of organic liquid electrolytes.[13] Later, in 2016 and 2023, the ionic conductivity of LGPS was further improved to 2.5×10^{-2} S cm^{-1} with $Li_{9.54}Si_{1.74}P_{1.44}S_{11.7}Cl_{0.3}$ (LSiPSCl), which shares the same crystal structure as LGPS,[151] and subsequently to 3.2×10^{-2} S cm^{-1}.[152] Fig. 8A summarizes the general timeline of SSSEs' development, and Table 4 provides an overview of the applications of SSSEs in silicon-based anode electrodes.

6.1 Glassy state SSSEs

Among glassy SSSEs, systems such as Li_2S-P_2S_5 and Li_2S-SiS_2 are prominent, which can be prepared by melt-quenching or mechanical ball milling. The Li_2S-P_2S_5 system has been extensively studied for Si-based anodes. Its amorphous structure

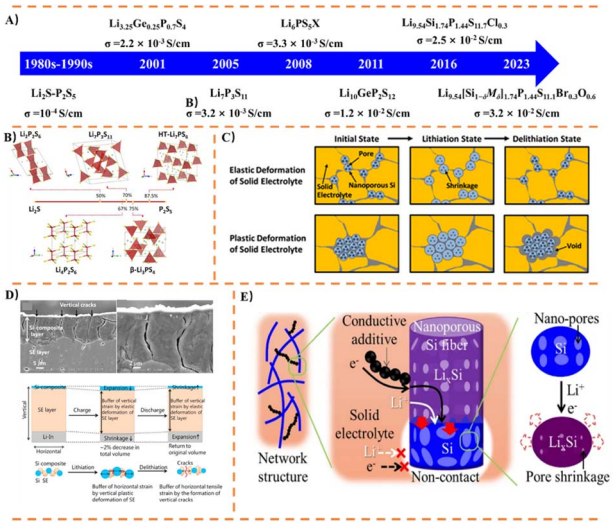

Fig. 8 (A) Development schedule of SSSEs; (B) some of the crystal structures observed in materials. Formed within the Li_2S-P_2S_5 binary system;[186] (C) microstructural behavior of mechanically milled and hand-milled nanoporous Si composite anodes; (D) CrosS-SSEsctional SEM image and corresponding magnified image of binder-free mSi half-cell with configuration of electrode-sheet/r-LPS/Li-In after 350 cycles and schematic diagram of half-cell (consisting of Si-composite layer, SSEs layer, and Li-In counter electrode) during charge and discharge; (E) schematic of the strategy for achieving stable cycling performance.

consists of $[PS_4]^{3-}$ tetrahedra and $[P_2S_7]^{4-}$ ditetrahedral units. Li_2S-P_2S_5 exhibits multiple structural forms, as illustrated in Fig. 8B. Notably, the $70Li_2S$-$30P_2S_5$ composition can form a glass-ceramic state under specific processing conditions.

Dunlap,[153] using a $77.5Li_2S$-$22.5P_2S_5$ electrolyte, discovered that silicon nanoparticles in Si-based anodes retain small tetrahedrally coordinated clusters during cycling. Moderate lithiation helps maintain this local tetrahedral atomic structure, thereby enhancing the cycling stability of the Si anode. Okuno[170] first prepared nanopororous Si composite anodes with different degrees of dispersion to compare their electrochemical performance in ASSBs with Li_3PS_4. The ball-milled anode with higher dispersion maintained 80% capacity retention after 150 cycles at 70 MPa. Subsequently, porous silicon was employed as an anode material in ASSBs to accommodate volume expansion,[184] demonstrating high capacity retention exceeding 90% after 100 cycles under 70 MPa pressure. The electrochemical properties of composite anodes consisting of nanoporous silicon particles and Li_3PS_4 were then systematically studied[154] (Fig. 8C). Key findings include: (1) the large volume expansion of Si is buffered by pore contraction; (2) the elasticity of Li_3PS_4 mitigates the strain induced by expanding Si particles; (3) these effects are enhanced when Si particles are highly dispersed within the Li_3PS_4 matrix. In further work, Okuno[162] analyzed the electrochemical performance of porous Si, conducting the first study on the influence of conductive agents in Li_3PS_4 solid electrolytes on the electrochemical performance of Si anodes in all-solid-state lithium-ion batteries. The study concluded that: (1) both electrical conductivity and

Table 4 Application of SSSE in silicon-based anode electrodes

Si anode	SSSEs	Pressure	Current density	Capacity (mAh g^{-1})	Retention/cycle number	Ref.
Si-C	$Li_{5.4}PS_{4.4}Cl_{1.6}$	150 MPa	0.5 mA cm^{-2}	2037	55.8%/50	15
nSi	$77.5Li_2S$-$22.5P_2S_5$	10 MPa	0.1C	2074	77.4%/200	153
mSi	Li_6PS_5Cl	460 MPa	1C	162 (NMC/Si)	57%/500	69
nSi	LPS	75 MPa	0.3 mA cm^{-2}	1532	80%/150	154
mSi	LiI-Li_3PS_4	3 Nm	0.05C	1350	~88.9%/50	155
SiS_2	Li_6PS_5Cl		0.1 A g^{-1}	1610	86.0%/800	156
nSi : mSi = 7 : 3	Li_2S-P_2S_5	4 Nm	0.12 A g^{-1}	1708	72%/200	157
Si/CNF	Li_6PS_5Cl	10 MPa	0.5C	1172	84.3%/50	158
Si/CNTs/C	Li_6PS_5Cl	20 MPa	0.05 A g^{-1}	1695	72.3%/200	
			0.2 A g^{-1}	882	44.8%/200	159
SiO-C	$75Li_2S$-$25P_2S_5$		0.064 mA cm^{-2}	1340	94.5%/10	160
P-nSi	$80Li_2S$-$20P_2S_5$		0.1 mA cm^{-2}	3128	93%/100	161
P-nSi	Li_3PS_4		0.3 mA cm^{-2}	2071	91%/50	162
P-mSi@C	Li_6PS_5Cl		0.2 mA cm^{-2}	2679.65	~37%/100	163
mSi	Li_6PS_5Cl	3.5 Nm	0.15 mA cm^{-2}		79.1%/50	164
Si-NWs	Li_6PS_5Cl	82 MPa	0.05C	2500	~20%/35	165
mSi-SLMP	Li_6PS_5Cl	75 MPa	5 mA cm^{-2}		73.8/1000	166
Si/C fibers	Li_2S-P_2S_5	20 MPa	0.1C		~70%/70	167
P-nSi$Mg_{5.0}$	$75Li_2S$-$25P_2S_5$	111 MPa	0.1 mA cm^{-2}	1734	85%/40	168
Si@$LiAlO_2$	Li_6PS_5Cl		0.33C	2045	56.9%/150	169
P-nSi	Li3PS4	70 MPa	0.3 mA cm^{-2}	1240	80%/150	170
Si-NWs	$Li_{10}SnP_2S_{12}$		0.1C	2125	20%/50	
	Li_6PS_5Cl		0.1C	2125	20%/50	171
Si	Li_6PS_5Cl	50 MPa	0.5 mA cm^{-2}	2067	65.1%/200	172
Si	$Li_7P_3S_{11}$		50 mA g^{-1}	1053	86.2%/35	173
mSi	$Li_7P_3S_{11}$ + SiS_2	100 MPa	0.1C	2208.7	15.4%/100	174
Si-Ag@PAP	Li_6PS_5Cl	5 MPa	4.4 mA cm^{-2}	1906.9	53.9%/500	175
Si/C	Li_6PS_5Cl	70 MPa	0.1C	515	67%/50	87
Micro–nano Si	Li_6PS_5Cl	30 MPa	0.2C	3169.7	84.1%/50	81
Si	Li_6PS_5Cl	120 MPa	0.5C	162.6 (NMC/Si)	51.7%/300	176
C/Si	$Li_{5.5}PS_{4.5}Cl_{1.5}$		0.5C	195.1 (LNTO/Si)	80.8%/200	177
mSi	$75Li_2S$-$25P_2S_5$	20 MPa	0.1C	853	58.86%/100	178
nSi + $Li_{4.4}Si$	Li_6PS_5Cl	70–80 MPa	0.5C	~120 (NMC/Si)	70.03%/400	179
P-nSi	Li_3PS_4	75 MPa	0.3 mA cm^{-2}	1674	89%/50	43
Si-HC	Li_6PS_5Cl	120 MPa	1C	123.6 (NMC/Si)	61.5%/5000	42
Si-C	Li_6PS_5Cl	75 MPa	0.5C	~1060	~75%/150	180
mSi	Li_6PS_5Cl	5 MPa	0.1C	173.6 NMC/Si	83.6%/100	181
col-Si	Li_6PS_5Cl	20 MPa	0.08C	203 (NMC/Si)	58.1%/100	67
mSi	$75Li_2S$-$25P_2S_5$	75 MPa	0.3 mA cm^{-2}	3412	64%/500	67
		50 MPa	0.3 mA cm^{-2}	2849	39%/500	80
mSi	Li_6PS_5Cl	50 MPa	0.1C	2800	45.1%/100	49
mSi	Li_6PS_5Cl	81 MPa	0.2C	~3100	50%/50	182
Si	Li_6PS_5Cl	10 MPa	0.05C	210 (NMA/Si)		182
			0.25C	178 (NMA/Si)		48
mSi	Li_6PS_5Cl	50 MPa	0.1C		29.6%/100	47
Li_2SiO_x	Li_6PS_5Cl	50 MPa	C/3	107 (NMA/Si)	75.7%/30	183

charge capacity increase proportionally with conductive agent content; (2) an optimal amount of conductive agent exists, which improves the discharge capacity and capacity retention after cycling. It was demonstrated that adding a conductive agent to the nanoporous Si composite anode facilitates the formation of new conductive pathways. Yamamoto[185] proposed a slurry mixing method for preparing uniformly distributed composite anodes containing mSi particles and Li_3PS_4, as shown in Fig. 8D. The silicon composite anode exhibited a high initial coulombic efficiency of 95% and maintained a reversible specific capacity of 2300 mAh g^{-1} after 100 cycles. Cracks formed perpendicular to the Si composite layer during cycling buffered the internal strain caused by volume changes in Si, contributing to excellent cycling stability. To address the issue of severe volume changes in Si during cycling—which leads to loss of electronic/ionic conduction pathways and rapid capacity decay—Yamamoto[168] fabricated nanoporous Si fibers *via* electrospinning (Fig. 8E). The total pore volume within the fibers allowed pore contraction to compensate for the volume expansion of $Li_{12}Si_7$, thereby suppressing outward expansion and preserving the Si-solid electrolyte ($75Li_2S$-$25P_2S_5$) interface.

Branchi[155] prepared a Si-based anode by simple manual grinding, comprising mSi, graphite, LiI-Li_3PS_4 solid electrolyte (LPSI), and carbon nanofibers. It was found that LPSI not only

acts as an ionic conductor within the electrode but also helps reduce Si aggregation and improves electrode homogeneity. Furthermore, the proportion of LPSI used had the most significant impact on the available specific capacity for lithiation/delithiation reactions and the effective utilization of Si. Sakabe[161] achieved enhanced cycling performance using a nSi thin film and an $80Li_2S$-$20P_2S_5$ electrolyte, as shown in Fig. 9A. The study demonstrated that an amorphous porous silicon thin film (~3 μm) could maintain high capacity after cycling. To investigate the correlation between fiber dimensions and electrochemical performance, Kim[167] fabricated Si/C fibers with different diameters for use as anodes. It was found that Si/C fibers with a diameter of ~0.1 μm and Si particle size of ~50 nm were most effective in mitigating the increase in internal resistance and the imbalance in lithium concentration formed during subsequent cycling tests. To study the chemomechanical failure mechanisms of Li_3PS_4-based ASSBs, Oh[187] assembled a bulk-type ASSBs cell consisting of a Li_3PS_4 electrolyte, a sulfur-composite cathode, and a Li–Si alloy anode. Cycling tests were conducted under two different cutoff voltage conditions. The results revealed that oxidation decomposition of Li_3PS_4 occurred at around 3.7 V state of charge, and significant decomposition of Li_3PS_4 at the cathode side induced lithium dendrite growth, leading to micro-short circuits through the SSSEs. Jeong[178] applied a very thin Al_2O_3 coating *via* radio-frequency (RF) plasma as an artificial SEI layer on Si-PAN anodes. An appropriate Al_2O_3 coating reduces interfacial resistance, effectively suppresses electrolyte decomposition, inhibits the formation of additional SEI layers, thereby decreasing Li^+ consumption and improving cycling performance. Particle size significantly influences electrochemical properties: mSi particles exhibit excellent initial discharge capacity but suffer from poor capacity retention and rapid decay. nSi particles show lower initial discharge capacity but superior capacity retention, exceeding the capacity of mSi particles after 50 cycles. To address this, Chiku[157] fabricated a hybrid electrode combining mSi and nSi (Fig. 9B), integrating the advantages of both. An electrode with an nSi : mSi ratio of 7 : 3 achieved the optimal balance between maximum discharge capacity and capacity retention when paired with a Li_2S-P_2S_5 electrolyte. The redox activity of Li_3PS_4 is a major cause of its chemomechanical failure. Kim[17] designed two types of Li–Si alloy anodes to mitigate such failure in Li_3PS_4. The study demonstrated that LPS-based batteries can undergo reversible cycling with LPS redox activity under high cut-off voltage conditions, provided that inhomogeneous alloying and lithium dendrite growth in the anode are avoided (Fig. 9C).

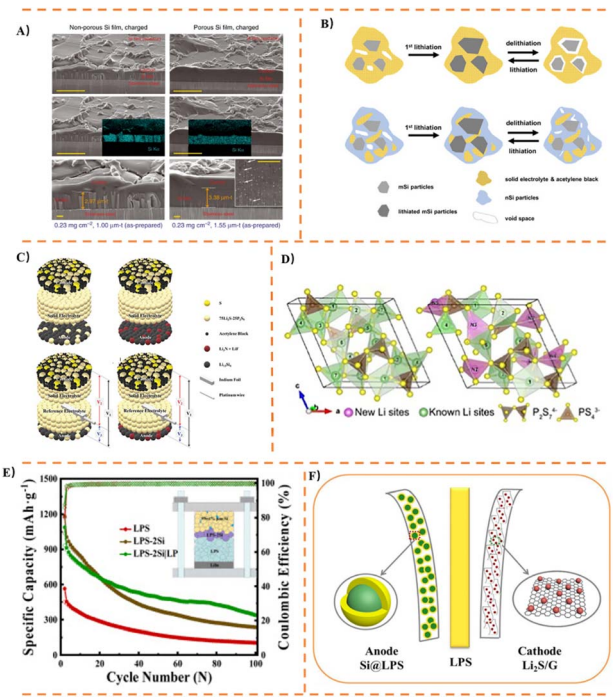

Fig. 9 (A) Microscopy images of fully charged amorphous Si anode films; (B) schematic image of cycling degradation with micro-sized silicon particles and schematic image of the after-cycling with mixed micro-sized and nano-sized silicon particles; (C) schematics of the fabricated two-electrode (standard) T1 and T2 cells and three-electrode T1 and T2 cells; (D) the schematic crystal structures of the reported ground state and new ground state;[189] (E) schematic diagram of Si|LPS (LPS-2Si, LPS-2Si|LPS)|Li-In cells and cycling test; (F) schematic of the structure of the all-solid-state Li_2S|Si battery with LPS solid electrolyte; the cathode consists of Li_2S and graphene, and the anode contains silicon coated with LPS solid electrolyte layer.

Due to its relatively small volume variation, Ishii[160] prepared carbon-coated SiO (SiO-C) as a binder-free material and granulated electrodes incorporating solid electrolyte for use as anode materials in Li_3PS_4-based all-solid-state batteries. The SiO-C granulated electrodes delivered high capacity in all-solid-state batteries employing lithium-ion-conductive sulfide-based solid electrolytes at room temperature. SiO-C granulated electrodes containing Li_3PS_4 exhibited superior cycling stability compared to those without the solid electrolyte. Ohta[188] found that as the oxygen content in silicon active materials increases, the initial coulombic efficiency decreases due to the formation of oxygen-related irreversible phases (such as lithium oxides or lithium silicates). Batteries composed of silicon nanoparticles (<150 nm) with low oxygen content (SiO_x, $x < 0.1$) and $70Li_2S$-$30P_2S_5$ electrolyte demonstrated stable cycling performance, maintaining a high capacity of 2600 mAh g^{-1} over 50 cycles.

Glassy-state SSSEs are regarded as one of the most promising candidates for achieving high-power and long-life Si-based SSBs, owing to their exceptionally high ionic conductivity and excellent flexibility. They effectively address the physical contact failure issues commonly encountered with OSSEs. However, their extremely poor chemical stability remains a major obstacle on the path to commercialization. Future advancements will almost entirely depend on breakthroughs in interfacial engineering, particularly in the development of efficient, low-cost, and scalable coating technologies for silicon particles.

6.2 Glass-ceramic state SSSEs

A typical representative of glass-ceramic SSSEs is $Li_7P_3S_{11}$, which possesses a metastable crystal structure and is typically composed of 70%Li_2S-30%P_2S_5. Its crystalline structure is illustrated in Fig. 9D. Ionic conduction is based on two

fundamental structural units within the crystal: $[PS_4]^{3-}$ tetrahedra and $[P_2S_7]^{4-}$ ditetrahedra.[190]

The incompatible interface between sulfide electrolytes and silicon anodes remains a major cause of poor cycling performance. To address this, Chen[174] introduced a SiS_2-doped $Li_7P_3S_{11}$ (LPS-*x*Si) interlayer sandwiched between the $Li_7P_3S_{11}$ electrolyte and the Si electrode, forming a bilayer sulfide electrolyte configuration (LPS-*x*Si|LPS). This design improves contact with the silicon anode, facilitates the formation of a Li–Si alloy at the interface, suppresses detrimental side reactions, and enhances interfacial Li^+ transport, as illustrated in Fig. 9E. Fan[191] utilized the oxidation pathway of lithium phenylselenolate during initial charging to effectively activate the Li_2S cathode. In a full cell employing $Li_7P_3S_{11}$ electrolyte and a silicon anode, an average discharge capacity of 524 mAh g^{-1} was achieved at a current density of 0.1 A g^{-1}. Xu[173] reported an all-solid-state full cell composed of a $Li_7P_3S_{11}$-coated silicon anode, a Li_2S/graphene composite cathode, and a $Li_7P_3S_{11}$ solid electrolyte layer, as shown in Fig. 9F. The silicon nanoparticles were coated with $Li_7P_3S_{11}$, which provides intimate interfacial contact, suppresses volume expansion of silicon, and facilitates Li^+ diffusion during cycling.

Glass-ceramic SSSEs represent the pursuit of extreme ionic conductivity and serve as important benchmarks in fundamental research. However, their rigid structure and inherent thermodynamic instability make them one of the least compatible sulfide electrolytes with silicon anodes, which undergo significant volume expansion. Although their theoretical performance is intriguing, the practical application of glass-ceramic sulfide electrolytes in silicon-based ASSBs appears highly challenging. In contrast, crystalline sulfides (such as Li_6PS_5Cl) combine high ionic conductivity with better flexibility and more achievable interfacial stability, making them a far more practical and engineerable choice compared to their glass-ceramic counterparts.

6.3 Crystalline state SSSEs

Crystalline SSSEs primarily include Li_6PS_5X and LGPS electrolytes, both exhibiting high ionic conductivity exceeding 10^{-3} S cm^{-1}. Among them, Li_6PS_5X electrolytes can achieve ionic conductivities over 10^{-2} S cm^{-1}, offering advantages such as good electrochemical stability and low cost. However, they suffer from poor air stability and relatively high interfacial resistance. In contrast, LGPS electrolytes demonstrate ionic conductivity comparable to liquid electrolytes due to collective ion migration induced by strong coulombic interactions among Li^+ ions within one-dimensional diffusion channels.[192] Further improvements in ionic conductivity have been achieved by adjusting Li, Ge, and P compositions, such as substituting Ge with Si and partially replacing S with Cl.[151,152]

To address the poor interfacial performance between crystalline SSSEs and active materials, extensive research has been conducted by scholars. Cangaz[67] fabricated columnar silicon anodes *via* a scalable physical vapor deposition process and integrated them into all-solid-state batteries based on Li_6PS_5Cl electrolyte and NCM9055 cathode, as shown in Fig. 10A. Under applied pressures of 20 MPa and 25 MPa, the batteries exhibited capacity retention rates of 83% and 95%, respectively, after 50 cycles. Poetke[193] designed a Si/C anode with a void-containing structure. Leveraging the close contact between the carbon shell and nSi, the void structure enables effective lithiation and stable cycling of silicon while compensating for its volume changes, as illustrated in Fig. 10B. In the assembled solid-state battery, Li_6PS_5Cl did not penetrate the void structure of the Si/C anode, which reduced side reactions and improved the initial coulombic efficiency. Sun[163] utilized amino acids as sources of carbon, nitrogen, and sulfur to form an amorphous carbon layer on the surface of porous mSi through a facile sintering process. This layer not only provides high mechanical strength to buffer mechanical stress during cycling but also facilitates Li^+ transport from the sulfide electrolyte to the porous mSi. Additionally, it enhances both ionic and electronic conductivity while mitigating electrolyte degradation caused by interfacial side reactions due to the presence of the amorphous carbon, as depicted in Fig. 10C. The porous mSi@C/LPSCl composite anode with the amorphous carbon layer maintained a high discharge-specific capacity of 2679.65 mAh g^{-1} and a high ICE of 84%. Kim[158] reported a composite electrode (Si/CNF@LPSCl) consisting of carbon nanofibers (CNFs) as the shell with embedded silicon nanoparticles, coated with Li_6PS_5Cl, for use as an anode

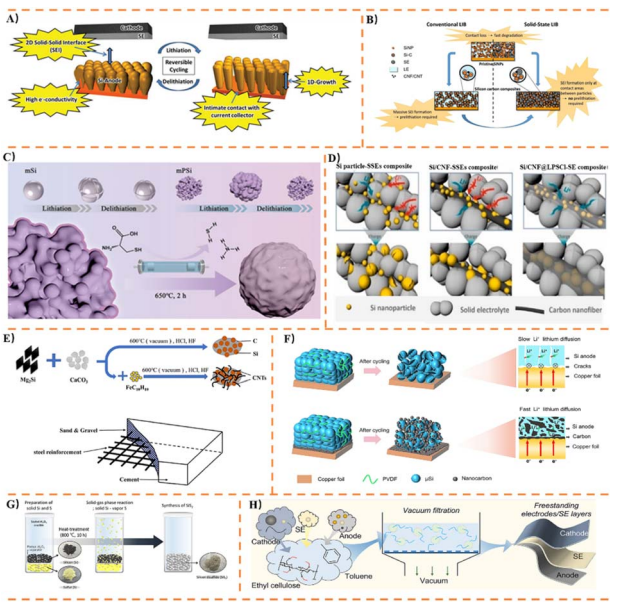

Fig. 10 (A) Reversible volume changes of columnar silicon anode systems upon (de-)lithiation under ASSBs cell configuration; (B) schematic representation of SiNP (top) and Si–C (bottom) anode in liquid (left) and solid electrolyte (right) Li-ion battery systems; (C) schematic diagram of the preparation of p-mSi@C; (D) schematic illustration of the active material and solid electrolyte composite electrode; (E) schematic of the synthesis process of Si/C and Si/CNTs/C composites and schematic of the reinforced concrete structure; (F) schematic illustration of degradation mechanisms for mSi, and *in situ* formation of the nanocarbon layer on mSi in ASSBs; (G) schematic of the solid–gas phase reaction for synthesizing SiS_2; (H) the fabrication process of the freestanding cathode, SE, and anode layers *via* vacuum filtration.

material to achieve high energy density and stable cycling performance in all-solid-state batteries (Fig. 10D). By embedding Si within CNFs, more favorable strain release and robust electron pathways were achieved. Coating the surface of the Si/CNF composite with solid electrolyte enhanced the interfacial stability between the active material and the solid electrolyte, thereby improving electrochemical performance by suppressing contact loss.

Hu[159] synthesized a Si/CNTs/C anode with a "reinforced concrete"-like structure, in which carbon nanotubes act as "steel bars" to provide a mechanically stable scaffold for silicon particles, as shown in Fig. 10E. This structure not only maintains good interfacial contact between silicon and the Li_6PS_5Cl component but also mitigates the volume expansion of silicon and prevents disruption of the lithium-ion pathways in Li_6PS_5Cl. Huang[177] developed a high-performance $Li_{5.5}PS_{4.5}Cl_{1.5}$-based ASSBs by simply coating nano-carbon onto mSi and drying to form the electrode, as illustrated in Fig. 10F. During *in situ* electrochemical charging/discharging, the nano-carbon penetrates the silicon, forming an active carbon-coated silicon anode. When combined with moderately flexible PVDF, a 3D conformal network for rapid Li^+ and electron conduction is created, improving electrode kinetics and mechanical stability within the μSi anode. The conductive nano-carbon layer retained at the interface during cycling acts as a buffer, suppresses silicon volume expansion, and maintains electron transport between silicon and the current collector. Nam[156] adopted an alternative approach by synthesizing layered SiS_2 *via* a solid–gas phase reaction method for use as an anode material. The SiS_2, composed of ultrafine nanocrystallites (2–4 nm), undergoes repeated electrochemical conversion/recombination reactions during cycling. This process induces a continuous mechano-electrochemically stable nano-anchoring effect, where SiS_2 nanocrystallites become embedded within an amorphous carbon matrix, as illustrated in Fig. 10G. Sulfide-based electrolytes exhibit high ionic conductivity, and their ductility enables easy processing without high-temperature sintering. In sulfide-based ASSBs, polymer binders play a critical role in maintaining strong interfacial contact within composite electrodes during cycling, which is essential for achieving good cycling performance. To address this, Cao[183] utilized amphiphilic ethyl cellulose as a dispersant (Fig. 10H), which also functions as a binder in freestanding electrodes. This stacking design reduces the proportion of inactive materials in the cell.

Jo[180] fabricated composite Si/C anodes for ASSBs applications using a nitrile rubber binder and investigated the effect of binder content on mechanical and electrochemical properties. The study concluded that: (1) increasing binder content enhanced the bonding performance of the composite electrode in terms of both adhesion and cohesion; (2) higher binder content increased cell resistance due to reduced active surface area of the active material, leading to disrupted Li^+ ion and electron transport pathways. Additionally, excessive binder induced residual lithium ions in the composite anode after delithiation. Wang[175] designed a binder with hard segments of PAA and soft segments of PEGMA, modified by *in situ* reduction of silver nanoparticles. This effectively suppressed silicon volume expansion and mitigated crack formation. The ether groups in the binder formed conductive pathways for lithium ions, increasing the Li^+ conductivity of the binder, as illustrated in Fig. 11A. An[182] compared the effects of aqueous and non-aqueous binders on all-solid-state mSi anodes with Li_6PS_5Cl electrolyte. It was found that anodes with PVDF exhibited faster capacity decay as binder content increased compared to those with PAA. However, Si electrodes containing 0.5 wt% of either PAA or PVDF binder showed similar performance. Neumann[194] investigated the use of PAA as a binder, highlighting its promise due to its ability to form strong adhesive bonds with silicon particles, especially in Si-dominant anodes. Based on electrochemical evaluations and cycling stability results, PAA-based anodes (using ethanol as solvent) were identified as a promising approach for designing solid-electrolyte-free anodes in ASSBs, as shown in Fig. 11B. Coating layers also serve as an effective method to improve interfacial issues. Xu[169] introduced a Li^+-conductive $LiAlO_2$ coating on the surface of silicon particles and investigated its effects on the electrochemical performance and morphological evolution of Si electrodes. Owing to

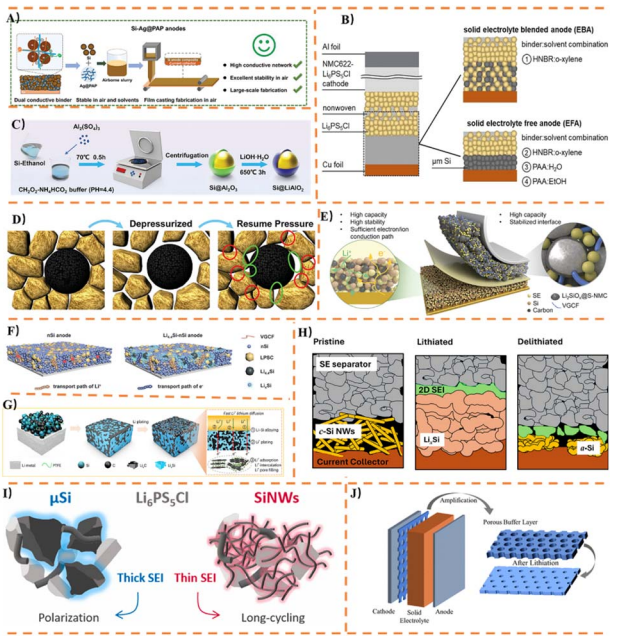

Fig. 11 (A) Diagram of Si-Ag@PAP anodes; (B) schematic overview of solid electrolyte blended, and solid electrolyte free anode designs evaluated within the scope; (C) schematic diagrams of the preparation process of Si@$LiAlO_2$; (D) schematic of the microstructure evolution between SSE and cathode when insufficient pressure is applied and the inability to restore to their original state even after the pressure returns to the initial value; (E) schematic representations of high-energy ASSBs based on a Si composite anode and Li_2SiO_x@S-NMC composite cathode; (F) schematic of nSi anode compared with $Li_{4.4}Si$-nSi anode design; (G) HC provides the graphene layer, pores and surface to accommodate excessive lithium and suppress lithium dendrite growth; (H) schematic representation of the microstructural evolution of the Si NWs electrodes over (de)lithiation in which the drastic shrinkage of the electrode over delithtaion and formation of cracks result in electrode capacity fading; (I) study the compatibility between LPSCl and micron-sized silicon-based anode; (J) schematic diagram with the buffer layer coated at the cathode/SE interface.

the high mechanical strength and ionic conductivity of the $LiAlO_2$ layer, which effectively mitigates the large volume expansion of silicon and facilitates Li^+ diffusion, the electrochemical performance was significantly enhanced, as shown in Fig. 11C. Chen[181] developed a pressurization system capable of achieving uniform and precise pressure control. By utilizing compressed air to apply more evenly distributed pressure compared to systems with rigid metal surfaces or flexible rubber gaskets, the $LiNi_{0.8}Co_{0.1}Mn_{0.1}O_2|Li_6PS_5Cl|Si$ pouch cell demonstrated stable cycling even at a low pressure of 2 MPa and a rate of 1C. As illustrated in Fig. 11D, the cell delivered an initial specific capacity of 135.4 mAh g^{-1}.

To mitigate side reactions between NMC and SSSEs and facilitate the fabrication of high-performance full cells with silicon-based anodes, Brow[48] pioneered a cobalt-free NMA cathode paired with a high-loading 99 wt% silicon anode (~5 mAh cm^{-2}) in a LiPSCl-based all-solid-state pellet cell. The extent of electrolyte degradation was found to be highly similar to that observed with other nickel-rich transition metal oxide cathode materials, confirming that NMA does not induce additional electrolyte decomposition. Cao[172] adopted a scalable interfacial stabilization strategy for NMC by applying a thin lithium silicate (Li_2SiO_x) coating to alleviate side reactions with SSSEs, as illustrated in Fig. 11E. Using a composite anode comprising nSi, Li_6PS_5Cl, and conductive carbon, the silicon-based composite anode demonstrated superior cycling stability compared to lithium metal. However, slight decomposition of Li_2S by SSSEs was observed, leading to a gradual decline in ionic conductivity during cycling. In contrast, lithium metal anodes exhibited severe chemical and electrochemical instability when coupled with SSSEs. Furthermore, additional noteworthy studies have been conducted focusing on LPSCl electrolytes in combination with silicon-based anodes. To address the issue of rapid capacity decay in nSi anodes during cycling, Jing[179] developed a bifunctional $Li_{4.4}Si$-modified nSi anode sheet. In this design, $Li_{4.4}Si$ plays a dual role: it not only provides additional lithium ions, but also stabilizes the anode structure with its low Young's modulus during cycling, as shown in Fig. 11F. Yan[42] opted to use hard carbon to stabilize the Li–Si alloy anode, achieving long-term cycling under high loading and high current density while suppressing lithium dendrite growth, as illustrated in Fig. 11G. The low ICE of silicon anodes, caused by irreversible capacity loss in the first cycle, limits energy density. To overcome this, Ham[166] employed a prelithiation strategy using stabilized lithium to improve the ICE and conductivity of the anode. A full cell using $Li_{15}Si_4$ and LCO as the anode and cathode, respectively, with Li_6PS_5Cl as the electrolyte, demonstrated an ICE exceeding 95%. Fan[176] implemented a unique *in situ* prelithiation method for an electrolyte-free silicon anode using an ultrathin lithium foil to enhance the ICE of ASSBs. The full cell with the prelithiated silicon anode and an NCM811 cathode delivered an energy density of 402 Wh kg^{-1} at 0.1C. Poetke[164] evaluated the practical application of mSi as an industrially scalable anode material for SSBs. The study revealed that: half-cell measurements against lithium demonstrated that mSi composite electrodes achieved stable cycling with a capacity limit of 800 mAh g_{Si}^{-1}, compared to full lithiation; partially lithiated mSi particles in full cells exhibited reasonable electrochemical performance, delivering energy density up to 28% higher than conventional graphite anodes. Sánchez-Ahijón[165] reported the first integration of silicon nanowires (Si NWs) with Li_6PS_5Cl electrolyte (Fig. 11H). By monitoring the morphological evolution (*e.g.*, porosity) of Si NWs during cell stacking and continuous (de)lithiation processes, it was observed that: (1) Si NWs remained structurally intact throughout cycling; (2) electrode porosity effectively accommodated expansion during the first lithiation; (3) electrode contraction during delithiation led to crack formation at the electrode/electrolyte interface and micro-scale vertical cracks within the electrode layer, which were identified as the primary causes of electrode polarization and capacity decay.

Grandjean[171] selected LPSCl to investigate the influence of silicon size and morphology using two distinct silicon materials (mSi powder and Si NWs), as shown in Fig. 11I. EDX mapping analysis of the composite powders highlighted the superior dispersibility of SiNWs, which resulted in improved contact among all components within the composite electrode. The Si NWs exhibited a high initial specific delithiation capacity of 2600 mAh g^{-1}, while mSi showed a slightly higher initial lithiation capacity of 2700 mAh g^{-1}. However, although Si NWs limited electrode polarization and maintained relatively stable lithiation behavior during galvanostatic cycling at C/20, mSi demonstrated more rapid capacity fade. At a cycling rate of C/10, cells with Si NWs also exhibited better stability than those with mSi, with silicon remaining active after 100 cycles. Chen[195] investigated ASSBs with an NMC811|LGPS|SiC configuration using theoretical contact mechanics and EIS. A porous polymer interlayer was applied at the interface between the cathode and solid electrolyte to buffer volume changes during lithium-ion cycling, as illustrated in Fig. 11J.

Crystalline SSSEs represent one of the most promising solutions for constructing high-power, high-energy-density silicon-based ASSBs, thanks to their unparalleled ionic conductivity and excellent flexibility. They effectively address the issue of contact failure inherent in rigid electrolytes from a physical perspective. However, their inherent thermodynamic instability remains an obstacle that must be overcome on the path to commercialization. The future success of this technology hinges entirely on breakthroughs in interfacial engineering, with the core challenge being the development of ultrathin, dense, and stable coating technologies for silicon particles that are scalable and low-cost.

6.4 Summary of SSSEs

SSSEs exhibit the highest ionic conductivity among all SSEs—even comparable to liquid electrolytes—yet their interface with silicon-based anodes presents one of the most chemically unstable and challenging scenarios in all-solid-state systems. The core issues stem from intrinsic thermodynamic instability and the large volume changes of silicon. Strategies addressing the SSSEs|Si interface must simultaneously suppress chemical side reactions and buffer mechanical stress. Nearly all strategies primarily revolve around constructing a stable artificial interlayer:

Constructing an artificial interlayer: this involves pre-coating silicon particles with a dense, stable, and ion-conductive "protective shell" to fundamentally prevent direct contact between Si and SSSEs, with carbon coating being the most common approach.

Composite anode and structural design: this method involves mixing nSi with SSSEs powder and conductive agents to form a composite anode, or designing gradient interfaces to smooth abrupt changes in mechanical and chemical properties, alleviate stress concentration, and stabilize the interface.

Applying external pressure: for relatively soft sulfide electrolytes, applying appropriate pressure helps maintain physical contact at the interface and reduces void formation caused by volume changes, making it an essential measure in laboratory testing.

In contrast to the physical contact failure in PSEs and mechanical contact failure in OSSEs, the challenges at the SSSE-Si anode interface are predominantly centered on chemical and electrochemical instability. When the silicon anode (with its low chemical potential, ~0.4 V *vs.* Li/Li^+) comes into contact with SSSEs (which have low reduction potentials, ~1.5–2.0 V *vs.* Li/Li^+), spontaneous and severe chemical reactions and electrochemical reduction occur.

To address this issue, the core strategy is to abandon reliance on *in situ* formed interphase layers and instead proactively construct an artificial interlayer that is thermodynamically stable and kinetically slow. For instance, ALD can be employed to deposit oxide protective layers such as Li_2O–ZrO_2 (LZO), Al_2O_3, or LiPON at the interface. Alternatively, vapor deposition or sputtering techniques can be used to prepare thin film layers of nitrides, such as Li_3N. Explore element doping (*e.g.*, Al, Si) to enhance the reduction stability of the electrolyte. Construct multi-layer interface structures to simultaneously block electron leakage and facilitate Li^+ transport.

7. Halide solid state electrolytes (HSSEs) and other solid state electrolytes

The earliest application of halogens in SSEs can be traced back to $LiAlCl_4$ in 1923, but it was not until 1977 that its ionic conductivity (10^{-6} S cm^{-1}) was systematically studied.[196] Subsequently, various Li_aMCl_6 and Li_aMBr_6 compounds (where M is a transition metal) were developed to enhance ionic conductivity. The transport kinetics of HSSEs are closely related to their structural characteristics. In a cubic close-packed (ccp) sublattice, Li^+ diffuses through a three-dimensional isotropic network, hopping between intermediate tetrahedral sites and adjacent octahedral sites.[197] These fast-transport pathways are susceptible to blockage by defects such as vacancies,[198] as illustrated in Fig. 12A. Many researchers have successfully improved ionic conductivity by tuning the degree of disorder within the HSSEs crystal structure and adjusting cation/anion compositions. For example, Li_3YCl_6 and Li_3YBr_6 (ref. 199 and 200) exhibit lithium-ion conductivities exceeding 10^{-3} S cm^{-1} at room temperature. HSSEs represent a promising class of battery materials due to their high ionic conductivity and favorable stability, though challenges remain in terms of thermal stability and interfacial issues.

Li[201] evaluated the electrochemical performance of all-solid-state batteries using mSi, submicron Si, and nSi anodes with the halide electrolyte Li_3InCl_6. It was found that the Li–Si alloy formed during silicon lithiation can react with Li_3InCl_6. This reaction reduces In^{3+} to metallic indium, which further consumes Li_3InCl_6 and degrades the battery structure. Submicron silicon, owing to its moderate tap density and expansion rate, facilitates the fabrication of densely packed electrodes and promotes ion transport. This property also contributes to a more uniform delithiation process, preventing crack formation and large voids, thereby ensuring electrode structural stability and delivering a high ICE of 78.37%.

Lithium borohydride ($LiBH_4$) electrolyte exhibits a soft texture with good ductility and adaptability, enabling intimate contact with silicon anodes through cold pressing and providing a certain degree of buffering against silicon's volume changes. The combination of $LiBH_4$ and silicon anodes represents a "flexibility-over-rigidity" strategy. Miyazaki[202] first reported a hydride material with high Li^+ conductivity by doping $LiBH_4$ with NaI. To prevent the migration of externally introduced Li^+ ions in a heterogeneous lattice, the 15 NaI·$LiBH_4$ solid electrolyte achieved a conductivity of 5×10^{-6} S cm^{-1}. When paired with an aSi anode in a half-cell, it maintained a capacity of approximately 1300 mAh g^{-1} at a current density of 12.7 μA cm^{-2}. Sharma[203] replaced the silicon anode with Si_3N_4 and employed $LiBH_4$ as the solid electrolyte to mitigate lithiation-induced expansion in silicon-based anodes. Subsequent galvanostatic charge–discharge tests and XRD analysis revealed thermochemical reactions between $LiBH_4$ and Si_3N_4 during cycling. The electrochemical delithiation products (Si or Si_3N_4) were converted into Li–Si and Li–N alloys.[204] Huang[205] compared the electrochemical stability of silicon with various SSEs and found that the $3LiBH_4$-LiI (LBHI) electrolyte composite with a silicon anode demonstrated greater electrochemical and chemical stability than SSSEs.

HSSEs exhibit outstanding ionic conductivity and stability against high-voltage cathodes, making them promising for pairing with high-capacity silicon-based anodes to construct all-

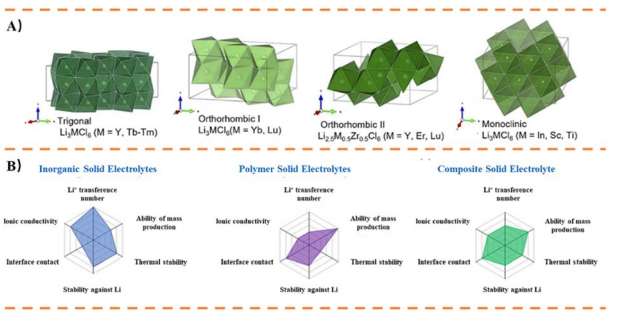

Fig. 12 (A) Crystal structure and ion transport dynamics of HSSEs;[197] (B) comparison of the advantages and disadvantages of three types of SSEs.

solid-state batteries with higher energy density and improved safety. However, publicly available literature and detailed studies on the direct combination of HSSEs with silicon anodes remain relatively limited. The soft nature of $LiBH_4$ offers an advantage over rigid OSSEs, as it can better accommodate the expansion and contraction of silicon particles without fracturing. For systems targeting ultra-high energy density, the $LiBH_4$-Si configuration may ultimately need to be coupled with a lithium metal anode rather than relying on the lithiated state of silicon itself—i.e., forming an all-solid-state battery with the structure $LiBH_4$-Si|$LiBH_4$|Li. This approach, however, introduces new challenges such as lithium dendrite growth. At present, this remains a valuable yet frontier research direction still in the exploratory stage.

8. Composite solid electrolytes (CSEs)

Compared to liquid electrolytes, SSEs offer higher safety, stability, and non-flammability, thereby improving both the safety and efficiency of batteries. However, different types of SSEs have their own advantages and limitations:

OSSEs exhibit high ionic conductivity at room temperature and excellent chemical/electrochemical stability, but they suffer from a complex manufacturing process, high cost, and high brittleness.

SSSEs possess ionic conductivity comparable to liquid electrolytes and high deformability, yet they are inherently unstable when exposed to moisture and air.

PSEs are notable for their mechanical flexibility and low cost, but they generally show relatively low ionic conductivity and inconsistent conduction performance.

CSEs, which consist of two or more different SSEs, can combine the advantages of multiple electrolyte types. CSEs that integrate the benefits of inorganic and polymer electrolytes are currently regarded as one of the most suitable options for commercial production. The advantages and disadvantages of these three types of SSEs are compared in Fig. 12B.

8.1 Composite of polymer and oxide

OSSEs exhibit excellent ionic conductivity and electrochemical stability, but they are limited by high brittleness and elevated costs. Although PSSEs can compensate for electrode volume changes during charge/discharge cycles through the inherent elasticity and plastic deformation of polymers, their relatively low ionic conductivity makes it difficult to meet the requirements for practical battery applications. CSEs formed by combining PSSEs and OSSEs integrate the high ionic conductivity of OSSEs with the mechanical flexibility of PSSEs, resulting in superior overall ionic conduction performance. Currently, PSSE-OSSE composite electrolytes compatible with silicon-based anodes primarily focus on OSSEs such as LATP and LLZO.

Li[206] prepared a micro-silicon/carbon (mSi/C) anode by calcining PAN-coated mSi and assembled a half-cell with a PVDF-HFP/LATP composite electrolyte. Without any external pressure and under a high current density of 1 A g^{-1}, the mSi/C anode delivered a specific capacity of 2131 mAh g^{-1}. To address the volume expansion of silicon anodes and related interfacial stability issues, Han[207–209] conducted extensive research. In one approach, Han decorated porous mSi with Ag nanoparticles and N-doped thin carbon (Fig. 13A) and combined it with PVDF-HFP/LATP to form a composite anode.[207] The highly porous structure alleviates volume changes during silicon lithiation, effectively suppressing mechanical stress at the interface and thereby improving interfacial stability. The Ag nanoparticles can react with Li^+ to form a solid-solution-based Li–Ag alloy, which subsequently infiltrates the pores of the mSi. This phenomenon not only restores short- and long-range electron pathways but also reduces the energy barrier for Li^+ transport from the Li–Ag alloy to Si, ultimately enhancing charge transfer kinetics. Additionally, leveraging the low fluidity of the PVDF-HFP/LATP SSEs, a dual-layer polymer-crystalline LiF organic–inorganic SEI with good flexibility and ductility was formed, contributing to high Li^+ reversibility and interfacial stability. Subsequently, a monolithic electrode structure with a carbon network embedded with MgO-coated mSi was

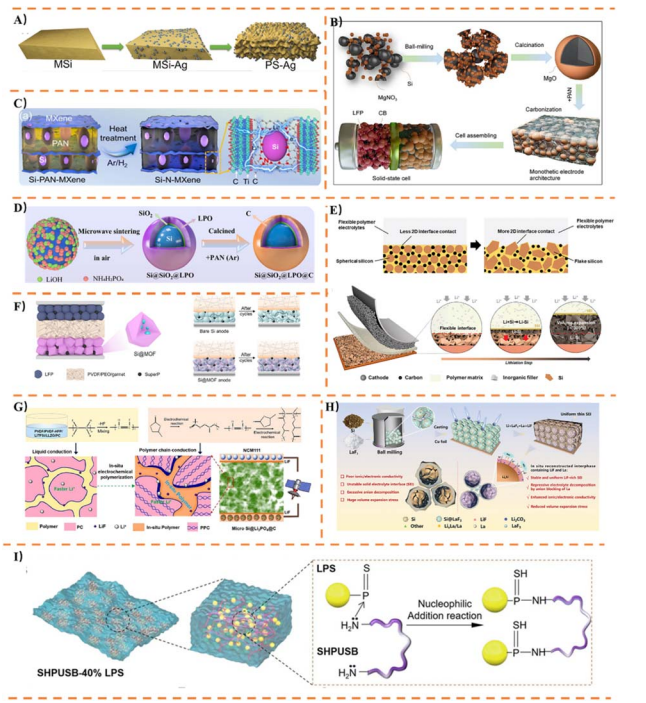

Fig. 13 (A) The schematic illustration of the synthesis process of PS-Ag particles *via* an Ag assisted wet chemical etching method; (B) schematic illustration of synthesis process and potential advantages; (C) the synthesis process and schematic of the interfacial nitrogen layer between Si and MXene; (D) the synthesis processes of Si@SiO_2@-LPO@C material; (E) schematic diagram of spherical and flaky Si anode with CSEs and schematic diagram of the ASSBs full cell and lithiation process of Si electrode and CSEs; (F) schematic illustration of the ASSBs composed of LFP|PVDF/PEO/garnet (PPG)|Si@MOF and interfacial evolution between PPG and bare Si or the Si@MOF anode; (G) design and properties of 3D-PPLLP-CPEs; (H) illustration of the preparation process of Si@LaF_3 and stabilization mechanism derived from *in situ* reconstruction and anion-blocking interphase strategy on silicon anodes; (I) chemical grafting reaction between $Li_7P_3S_{11}$ and SHPUSB.

designed.[208] The conductive carbon network not only facilitates rapid electron transport throughout the electrode but also improves charge transfer kinetics at the interface between mSi and the solid-state electrolyte, as shown in Fig. 13B. The ceramic MgO coating helps to release mechanical stress generated in silicon particles during lithiation and delithiation, thereby enhancing particle integrity. The composite anode assembled with PEO/LATP/NCF electrolyte exhibited a high specific capacity of 3224.6 mAh g^{-1}. Han[209] also designed a Si–N-MXene composite anode, where a nitrogen-intercalated bonding layer between silicon and MXene enhances mechanical adhesion and structural integrity of the anode. Simultaneously, the nitrogen-doped MXene promotes Li^+ transport with a low energy barrier of 0.15 eV, as illustrated in Fig. 13C. In a composite anode coupled with PEO/LATP electrolyte, a specific capacity of 880 mAh g^{-1} was retained after 100 cycles. Gu[210] also used PEO/LATP as the electrolyte and designed a novel ion-conductive SiO_2/Li_3PO_4 layer with a carbon coating on the surface of mSi to address the severe volume changes of silicon anodes during cycling, as shown in Fig. 13D. This approach tackles the issues of poor structural and interfacial stability, which lead to significant capacity decay over cycles and hinder practical application. Liu[50] focused on the challenges of high interfacial resistance at rigid ceramic electrolyte/electrode interfaces and the poor ionic conductivity of polymer electrolytes—both exacerbated by silicon's volume expansion. They designed a composite electrolyte by dispersing LATP into a PVDF-HFP and PEO matrix, achieving high ionic conductivity, high tensile strength, and flexibility, as illustrated in Fig. 13E. This electrolyte leverages chemical interactions between PVDF-HFP, PEO, and LATP to increase polymer amorphousness, accelerating Li^+ transfer. Meanwhile, the highly tensile solid membrane restricts electrode structural degradation and eliminates continuous interfacial growth, resulting in a stable 2D SEI film and cycling performance superior to that of liquid electrolytes.

In addition to NASICON-type LATP OSSEs, there has also been extensive research on composites involving garnet-type LLZO electrolytes and PSSEs. Zhang[211] developed a high-capacity ASSBs using a metal–organic framework-derived carbon-supported silicon (Si@MOF) anode and a PVDF-fiber-reinforced PEO/garnet CSEs, as shown in Fig. 13F. The MOF-derived carbon host effectively suppresses the repeated deformation of silicon nanoparticles, significantly enhancing interfacial stability with the CSEs. This endows the Si@MOF anode with excellent reversibility and high lithiation/delithiation capability. Huo[212] constructed a flexible interface between a silicon anode and a CSEs composed of PPC and garnet powder. This design effectively alleviates the significant stress induced by volume changes in the silicon anode and maintains good contact between the silicon anode and the SPEs.

PSEs offer advantages in terms of interfacial contact but face challenges due to their low ionic conductivity. Pan[213] prepared a 3D porous CSEs based on PVDF, PVDF-HFP, LiTFSI, LLZO, and PC. Compared to traditional gel electrolytes, this CSEs demonstrated optimal interfacial stability, as shown in Fig. 13G. During the initial discharge cycle, electrochemical polymerization occurred between PC and PVDF/PVDF-HFP, which enhanced the safety of the CSEs without compromising their mechanical strength or ionic conductivity. Tian[214] utilized an *in situ* reconstructed LaF_3 layer on the surface of prelithiated nSi to form an interface containing LiF and La. The LiF interface promotes the uniform formation of a LiF-rich SEI, while La grains help prevent anion penetration from the electrolyte into the electrode, thereby inducing a stable and thin SEI on the silicon-based anode, as illustrated in Fig. 13H. This approach significantly enhances the interfacial compatibility between the anode and the PEO/LLZTO solid electrolyte.

Polymer/oxide CSEs skillfully combine the excellent flexibility and interfacial adaptability of polymers with the high mechanical strength and thermal stability of oxides, offering an effective solution to bottleneck issues such as volume expansion and interfacial instability in silicon-based anodes. They demonstrate significant potential in enhancing battery energy density, cycle life, and safety. Although challenges remain in areas such as ionic conductivity, interface optimization, material dispersion, and cost control, continuous advancements in material technology, refined interface engineering, and ongoing optimization of manufacturing processes are expected to enable polymer/oxide CSEs to play a vital role in the technological evolution and industrialization of solid-state batteries—particularly in application scenarios demanding high energy density and safety.

8.2 Polymer and sulfide compound

CSEs based on PSEs and SSSEs combine the high ionic conductivity of SSSEs with the excellent interfacial flexibility of PSEs. This approach offers a strategy to mitigate issues such as the large volume changes and interfacial instability of silicon anodes, thereby contributing to improved battery energy density and safety. However, this system still requires in-depth research to address challenges, including the inherent chemical instability of SSSEs (air sensitivity, interfacial side reactions, and sensitivity to polar solvents), long-term cycling stability at the interface, as well as cost and process control. Wang[215] developed a self-healing poly(urethane disulfide urea) polymer (SHPUSB)-$Li_7P_3S_{11}$ (LPS) composite SSEs, which integrates seamlessly with silicon-based anodes to achieve high-performance silicon-based SSBs, as shown in Fig. 13I. Due to P–N bond interactions between LPS and SHPUSB, the synthesized SHPUSB-40%LPS exhibits rapid Li^+ transport kinetics and a stable electrochemical window reaching 5.1 V.

9. Commercial development of Si-based anode SSBs

The development of silicon-based anode solid-state batteries globally has followed a trajectory evolving from "basic research" to "route exploration," then achieving technological implementation through a "semi-solid-state transition," and finally advancing toward the overarching goal of "all-solid-state batteries", as illustrated in Fig. 14. In this process, China has gained a first-mover advantage in market application by leveraging semi-solid-state batteries, while Japan and the United States have accumulated substantial advantages in

fundamental technologies and innovations related to all-solid-state solutions.

The current status of mass production development for silicon-based anode SSBs worldwide can be summarized as follows: the technology is in a critical transitional phase from laboratory research to early-stage industrialization, yet significant differences exist in technical routes, progress speed, and commercialization strategies. At present, strictly defined ASSBs using silicon as the primary anode material have not yet achieved large-scale mass production. However, closely related semi-solid-state batteries have taken the lead in small-batch production and vehicle application, some of which incorporate silicon-based anodes.

Currently, the pure combination of "silicon-based anodes and all-solid-state batteries" has not yet achieved large-scale mass production. The industry has adopted a pragmatic and incremental strategy:

Semi-solid/solid–liquid hybrid batteries: these contain a significant amount of liquid electrolyte (typically 5–20%) to infiltrate the solid–solid interfaces, substantially reducing interfacial impedance. This approach can accommodate high-energy-density anodes (like silicon-based anodes) while maintaining relatively high compatibility with existing liquid battery production lines, resulting in lower mass-production difficulty. This is the primary form currently being commercialized.

Condensed-state batteries: proposed by CATL, this technology can be viewed as a special type of semi-solid battery. It utilizes high-kinetics biomimetic electrolytes and rheology modulation technology to place the battery in a "condensed state", achieving both high energy density and high safety. It has begun initial commercialization, initially targeting high-end markets like aviation.

All-solid-state batteries: these contain almost no liquid electrolyte. They are currently in the stages of engineering prototype development, testing, and sampling, representing the ultimate goal in the technology roadmaps of major manufacturers.

From the current commercialization perspective, silicon-based anodes are progressing ahead of solid-state batteries. Silicon-carbon/silicon monoxide anodes have been widely adopted in high-end liquid lithium-ion batteries, accumulating valuable data and experience for their application in solid-state systems. Semi-solid batteries serve as the current "bridgehead" for commercialization, balancing performance, safety, and manufacturing costs while providing a relatively "friendly" initial application platform for silicon-based anodes. All-solid-state batteries are universally recognized as the ultimate goal, yet they face significant challenges, with interfacial impedance, cost, and mass-production processes being the three major obstacles. It is anticipated that the first vehicle models equipped with mass-produced all-solid-state batteries will emerge around 2027–2030, while widespread adoption may require a longer timeframe.

Fig. 14 Milestone events and critical turning points in the transition of silicon-based anodes from laboratory to industrial competition.

10. Summary and outlook

10.1 Summary

This article first systematically reviews the major research advances in SSBs centered on silicon-based anodes. Subsequently, it provides an in-depth analysis of the electrochemical reaction mechanisms, significant volume change characteristics, and complex interfacial failure modes (such as physical contact loss and chemical side reactions) of silicon-based anodes within solid-state systems. These mechanistic insights form the foundation for designing compatible SSEs. The review then comprehensively examines the application and development of various types of SSEs—including PSEs, OSSEs, SSSEs, HSSEs, and CSEs—in conjunction with silicon-based anodes. For each electrolyte type, the discussion focuses on their interfacial characteristics, modification strategies (*e.g.*, interfacial buffer layers, structural design, electrolyte compositing), and recent research progress, summarizing their unique advantages and challenges in addressing interfacial contact and stability issues. Furthermore, the article offers perspectives on future research directions, highlighting that constructing stable self-adaptive interfaces and developing scalable integrated manufacturing processes are essential pathways toward the commercial application of silicon-based SSBs. Finally, it briefly introduces the current state of commercialization and the policy support provided by various countries for the R&D and industrialization of silicon-based anode SSBs. This review aims to provide strategic insights for the design of practical high-energy-density silicon-based SSBs.

SSEs are the key to unlocking the full potential of silicon-based anodes and realizing high-energy-density SSBs. This review systematically addresses the critical scientific issues at the interface between SSEs and silicon-based anodes, aiming to provide clear guidance for the development of high-performance silicon-based SSBs. Integrating silicon-based anodes with SSEs represents one of the core pathways to break through the current energy density and safety limits of LiBs. The underlying rationale lies in utilizing the unique properties of SSEs to address the inherent challenges of silicon-based anodes. The extremely high theoretical specific capacity of silicon is counteracted by its large volume expansion (>300%), which leads to particle pulverization, repeated rupture and reformation of the SEI film, continuous consumption of active lithium, and rapid capacity decay. In contrast, SSEs offer advantages such as high mechanical strength, intrinsic safety (non-flammability), and a wide electrochemical window. These characteristics directly counter the weaknesses of silicon. By leveraging the physical constraints of SSEs to suppress silicon's

expansion and utilizing their solid-state nature to construct more stable interfaces, it becomes possible to harness the ultra-high capacity potential of silicon anodes and build next-generation battery systems with high energy density and safety. However, the commercialization of silicon-based anode SSBs still faces challenges such as high electrolyte costs, solid–solid interface issues, and low production yield.

The large-scale industrialization of silicon-based all-solid-state batteries faces severe challenges in three key areas: cost, manufacturing processes, and supply chain, which constitute the major bottlenecks on its commercialization path. The synthesis of industrial-grade nano-silicon (*e.g.*, silicon nanowires, porous silicon) involves complex processes, high energy consumption, and low yield, leading to costs significantly higher than traditional graphite anode materials. SSSEs raw materials are inherently expensive and require extremely high purity. The entire production process must be conducted in an ultra-dry environment (*e.g.*, glove boxes), resulting in substantial construction and operational costs for the facilities. OSSEs typically require high-temperature sintering to achieve densification, which is highly energy-intensive. While the PSEs itself is not expensive, high-performance lithium salts (*e.g.*, LiTFSI) and functional fillers contribute significantly to the cost. Both high-performance silicon materials and SSEs lack mature, large-scale industrial supply chains. The market is often characterized by materials being "quoted but unavailable" or supplied only at the kilogram scale, which is insufficient to support GWh-level battery production.

A major engineering hurdle of Solid–Solid Interface Manufacturing is ensuring atomic-level intimate and uniform contact between each layer of electrode and electrolyte on high-speed production lines (operating at hundreds of meters per minute). While techniques like ALD can create perfect protective layers in the lab, ALD is too slow and expensive for continuous battery manufacturing. Developing high-speed, low-cost alternatives (*e.g.*, solution-based methods, spray deposition) is essential, but their effectiveness and uniformity require further validation.

Production speed and yield as bottlenecks. All-solid-state batteries are essentially precise stacks of multiple brittle thin layers (cathode–electrolyte–anode). Achieving high-speed, damage-free, and precisely aligned lamination of these thin layers is a significant bottleneck for commercialization. The winding process commonly used for conventional liquid electrolyte batteries is largely unsuitable for all-solid-state structures.

Enterprises need to address these problems gradually through technological innovation, scaled production, and industrial chain collaboration to reduce manufacturing costs. Simultaneously, governments should continue to strengthen policy support, promote the establishment and refinement of SSBs standards, and create a favorable environment for commercialization. In the long term, silicon-based anode SSBs are expected to become a mainstream technology in the battery industry, reshaping the global battery landscape.

10.2 Outlook

The integration of SSEs with silicon-based anodes aims to combine their respective advantages—high energy density and enhanced safety—while synergistically addressing their key limitations. Previous research has primarily focused on enabling SSEs to "tolerate" the volume expansion of silicon anodes. Future academic prospects lie in designing the two as a unified "composite system" to achieve a synergistic effect where $1 + 1 > 2$.

Constructing stable self-adaptive interfaces can be constructed through the following approaches:

Multi-dimensional, multi-scale composite structural design: construct a three-dimensional continuous porous SSE scaffold and *in situ* fill silicon nanoparticles into the pores. The 3D skeleton provides predefined space to accommodate silicon expansion, disperses stress throughout the network structure, and prevents local failure. The continuous SSE framework ensures ultra-fast ion transport, overcoming the issue of long ion diffusion paths in traditional composite electrodes. This design maximizes and stabilizes the contact area between silicon and SSEs.

Gradient/multi-layered ultrathin interfacial engineering: utilize techniques such as atomic/molecular layer deposition to design ultrathin interfacial layers with gradient compositions or multilayer structures. For example, a tough Li_3N layer adjacent to silicon can buffer stress, while an outer stable LZO layer blocks chemical side reactions. Achieving large-scale, low-cost fabrication of such ultrathin interlayers represents a key academic challenge in transitioning this technology from the laboratory to industrialization.

Dynamically adaptive interface design: inspired by muscle contraction and expansion, design polymer interlayers incorporating dynamic reversible bonds (*e.g.*, hydrogen bonds, coordination bonds, disulfide bonds). When silicon expansion causes interfacial rupture, these bonds can spontaneously reassemble, enabling "self-healing" of the interface to maintain optimal contact and stability throughout cycling.

Scalable integrated manufacturing processes is the most critical and challenging step in transitioning silicon-based all-solid-state batteries from the laboratory to industrialization. The core solution lies in developing manufacturing technologies that are compatible with existing industrial chains, high-speed, and low-cost.

Integrated "one-step" formation of cathode–electrolyte–anode: solution/slurry coating integration: this involves sequentially coating and drying the cathode slurry, solid electrolyte slurry, and anode slurry in a sandwich structure on a single production line using continuous coating techniques. This method is highly compatible with existing liquid battery coating processes and holds the greatest potential for scalability. However, it requires ensuring tight contact between layers after drying, preventing interlayer penetration (especially preventing cathode and anode particles from crossing the electrolyte layer), and necessitates developing binder and solvent systems suitable for tape casting.

"Pre-composite" strategy for silicon anode and electrolyte: this strategy abandons the pursuit of a perfect, separate electrolyte layer and instead incorporates the electrolyte as part of the anode itself. During the preparation of the silicon-based anode, SSE powder is directly mixed with silicon nanoparticles, conductive agents, and binders to form a slurry for coating. This process is simple and compatible with existing anode production lines. Furthermore, the SSE particles provide fast ion transport pathways within the anode and offer some mechanical buffering. Key challenges include ensuring the continuity of the ionic conduction network and optimizing the ratio of SSEs to silicon.

Impregnation of porous electrolyte scaffolds: this method first prepares a porous, rigid electrolyte scaffold (*e.g.*, porous LLZO), then fills the pores with silicon anode material or a polymer electrolyte *via* solution infiltration or vacuum injection. It leverages the 3D structure to provide excellent mechanical support and ion channels. Ensuring the uniformity and completeness of the filling is the critical challenge for this technology.

Author contributions

Feipan Liang: conceptualization, draft preparation, reviewing & editing, visualization. Renzong Hu, Bin Yuan, Min Zhu: reviewing. Lichun Yang and Jun Liu: funding, supervision, reviewing.

Conflicts of interest

There are no conflicts to declare.

Abbreviations

LiBs	Lithium-ion batteries
SSBs	Solid state batteries
QSSBs	Quasi-solid-state batteries
QS-SCN	Quasi-solid succinonitrile-based electrolyte
ASSBs	All-solid-state batteries
SSEs	Solid state electrolytes
ISEs	Inorganic solid electrolytes
OSEs	Organic solid electrolytes
CSEs	Composite solid electrolytes
OSSEs	Oxide solid state electrolytes
SSSEs	Sulfide solid state electrolytes
HSSEs	Halide solid state electrolytes
PSEs	Polymer solid electrolytes
SPEs	Solvent-free polymer electrolytes
GPEs	Gel polymer electrolytes
HPE	Hybrid polymer electrolyte
PEG	Polyethylene glycol
DOL	1,3-Dioxolane
PDOL	Poly 1,3-dioxolane
PAN	Polyacrylonitrile
PMMA	Polymethyl methacrylate
PEC	Poly(ethylene carbonate)
PPC	Poly(propylene carbonate)
PVC	Poly(vinylene carbonate)
PVDF	Polyvinylidene difluoride
PVDF-HFP	Poly(vinylidene fluoride-*co*-hexafluropropylene)
PAA	Polyacrylic acid
SN	Succinonitrile
ETPTA	Ethoxylated trimethylolpropane triacrylate
PEGDMA	Polyethylene glycol dimethacrylate
c-Si	Crystalline silicon
a-Si	Amorphous silicon
mSi, μSi	Micron silicon
nSi	Nano-silicon
Si-NPs	Si nanoparticles
SOC	State of charge
EIS	Electrochemical impedance spectroscopy
FE-SEM	Field emission scanning electron microscopy
EDX	Energy-dispersive X-ray spectroscopy
CE	Coulombic efficiency
ICE	Initial coulombic efficiency
XANES	X-ray absorption near-edge structure
SEM	Scanning electron microscopy
XnT	X-ray nanotomography
DEM	Discrete element method
SEI	Solid electrolyte interphase
GO	Graphene oxide
AIMD	*Ab initio* molecular dynamics
ALD	Atomic layer deposition
PLD	Pulsed laser deposition
LiDFOB	Lithium difluoro(oxalato)borate
LiTFSI	Lithium bis((trifluoromethyl)sulfonyl)azanide

Data availability

This review does not include any primary research results, software, or code, and no new data were created.

Acknowledgements

This work was financially supported by the National Key Research and Development Program of China (No. 2022YFB2502000), and the National Natural Science Foundation of China (No. 22479051, U21A20332).

References

1 M. Winter, B. Barnett and K. Xu, Before Li Ion Batteries, *Chem. Rev.*, 2018, **118**, 11433–11456.
2 H. Xie, J. Feng and H. Zhao, Lithium metal batteries with all-solid/full-liquid configurations, *Energy Storage Mater.*, 2023, **61**, 102918.
3 Z. Wang, L. Kong, Z. Guo, X. Zhang, X. Wang and X. Zhang, Bamboo-like SiO/C nanotubes with carbon coating as a durable and high-performance anode for lithium-ion battery, *Chem. Eng. J.*, 2022, **428**, 131060.
4 T. Zhu, X. Hao, Y. Cao, T. Li, Y. Li and W. Wang, Ultraviolet-cured heat-resistant and stretchable gel polymer electrolytes for flexible and safe semi-solid lithium-ion batteries, *J. Power Sources*, 2024, **613**, 234944.

5 T. Zhou, R. Xu, X. Cao, J. Zhang, J. Wang, R. Huang, X. Ping, P. Bai, Z. Sun, M. Liu and X. Wang, Bio-inspired rigid-soft coupling gel polymer electrolyte for stable lithium batteries, *Sci. China Mater.*, 2024, **67**, 2256–2265.
6 Y. Wu, Y. Li, Y. Wang, Q. Liu, Q. Chen and M. Chen, Advances and prospects of PVDF based polymer electrolytes, *J. Energy Chem.*, 2022, **64**, 62–84.
7 S. Tang, W. Guo and Y. Fu, Advances in Composite Polymer Electrolytes for Lithium Batteries and Beyond, *Adv. Energy Mater.*, 2020, **11**, 2000802.
8 S. Zhou, X. Wang, Z. Xu, T. Guan, D. Mo and K. Deng, Rapid self-healing, highly conductive and near-single-ion conducting gel polymer electrolytes based on dynamic boronic ester bonds for high-safety lithium metal batteries, *J. Energy Storage*, 2024, **75**, 109712.
9 A. Song, W. Zhang, H. Guo, L. Dong, T. Jin, C. Shen and K. Xie, A Review on the Features and Progress of Silicon Anodes-Based Solid-State Batteries, *Adv. Energy Mater.*, 2023, **13**, 2301464.
10 Z. Zhang, L. Gao, X. Sun, N. Deng, Y. Zhao and W. Kang, Matching strategy between sulfide solid electrolyte and various anodes: electrolyte modification, interface engineering and electrode structure design, *Energy Storage Mater.*, 2024, **69**, 103422.
11 Q. Zhang, K. Liu, F. Ding and X. Liu, Recent advances in solid polymer electrolytes for lithium batteries, *Nano Res.*, 2017, **10**, 4139–4174.
12 H. Nagata and J. Akimoto, Excellent Deformable Oxide Glass Electrolytes and Oxide-Type All-Solid-State Li2S–Si Batteries Employing These Electrolytes, *ACS Appl. Mater. Interfaces*, 2021, **13**, 35785–35794.
13 N. Kamaya, K. Homma, Y. Yamakawa, M. Hirayama, R. Kanno, M. Yonemura, T. Kamiyama, Y. Kato, S. Hama, K. Kawamoto and A. Mitsui, A lithium superionic conductor, *Nat. Mater.*, 2011, **10**, 682–686.
14 F. Mizuno, A. Hayashi, K. Tadanaga and M. Tatsumisago, New, Highly Ion-Conductive Crystals Precipitated from Li2S–P2S5 Glasses, *Adv. Mater.*, 2005, **17**, 918–921.
15 D. Cao, T. Ji, A. Singh, S. Bak, Y. Du, X. Xiao, H. Xu, J. Zhu and H. Zhu, Unveiling the Mechanical and Electrochemical Evolution of Nanosilicon Composite Anodes in Sulfide-Based All-Solid-State Batteries, *Adv. Energy Mater.*, 2023, **13**, 2203969.
16 D. H. S. Tan, E. A. Wu, H. Nguyen, Z. Chen, M. A. T. Marple, J.-M. Doux, X. Wang, H. Yang, A. Banerjee and Y. S. Meng, Elucidating Reversible Electrochemical Redox of Li6PS5Cl Solid Electrolyte, *ACS Energy Lett.*, 2019, **4**, 2418–2427.
17 M. Kim, M. J. Kim, Y. S. Oh, S. Kang, T. H. Shin and H. T. Lim, Design Strategies of Li–Si Alloy Anode for Mitigating Chemo-Mechanical Degradation in Sulfide-Based All-Solid-State Batteries, *Adv. Sci.*, 2023, **10**, 2301381.
18 H. Kwak, S. Wang, J. Park, Y. Liu, K. T. Kim, Y. Choi, Y. Mo and Y. S. Jung, Emerging Halide Superionic Conductors for All-Solid-State Batteries: Design, Synthesis, and Practical Applications, *ACS Energy Lett.*, 2022, **7**, 1776–1805.
19 J. Liang, X. Li, S. Wang, K. R. Adair, W. Li, Y. Zhao, C. Wang, Y. Hu, L. Zhang, S. Zhao, S. Lu, H. Huang, R. Li, Y. Mo and X. Sun, Site-Occupation-Tuned Superionic LixScCl3+xHalide Solid Electrolytes for All-Solid-State Batteries, *J. Am. Chem. Soc.*, 2020, **142**, 7012–7022.
20 F. Shen, M. McGahan, J. D. Pietras, M. M. Doeff, V. S. Battaglia and M. C. Tucker, Optimization of catholyte for halide-based all-solid-state batteries, *J. Power Sources*, 2025, **640**, 236709.
21 D. Zhou, D. Shanmukaraj, A. Tkacheva, M. Armand and G. Wang, Polymer Electrolytes for Lithium-Based Batteries: Advances and Prospects, *Chem*, 2019, **5**, 2326–2352.
22 B. Jin, Y. Zhao, D. Ye, X. Jiang, X. Ye and C. Li, Mechanically robust and highly electrochemical performance of polyethylene oxide gel polymer electrolyte, *J. Appl. Polym. Sci.*, 2024, e55176, DOI: 10.1002/app.55176.
23 L. Zhang, M. Bai, X. Wang, Z. Huang, B. Hong and Y. Lai, A strong nucleophilic fluorination agent to achieve highly stable in-situ 3D cross-linked gel polymer electrolyte for lithium-ion batteries, *Chem. Eng. J.*, 2024, **481**, 148579.
24 D. E. Fenton, J. M. Parker and P. V. Wright, Complexes of alkali metal ions with poly(ethylene oxide), *Polymer*, 1973, **14**, 589.
25 Y. G. Choi, J. C. Shin, A. Park, Y. M. Jeon, J. I. Kim, S. Kim, S. Kim, W. B. Lee, M. Lee and J. H. Park, Pyrrolidinium-PEG Ionic Copolyester: Li-Ion Accelerator in Polymer Network Solid-State Electrolytes, *Adv. Energy Mater.*, 2021, **11**, 2102660.
26 M. Xin, Y. Zhang, Z. Liu, Y. Zhang, Y. Zhai, H. Xie and Y. Liu, In Situ-Initiated Poly-1,3-dioxolane Gel Electrolyte for High-Voltage Lithium Metal Batteries, *Molecules*, 2024, **29**, 2454.
27 J. Liu, H. Lin, H. Li, D. Zhao, W. Liu and X. Tao, In Situ Polymerization Derived from PAN-Based Porous Membrane Realizing Double-Stabilized Interface and High Ionic Conductivity for Lithium-Metal Batteries, *ACS Appl. Mater. Interfaces*, 2024, **16**, 21264–21272.
28 S. Qin, M. Wu, H. Zhao, J. Li, M. Yan, Y. Ren and Y. Qi, An in-situ cross-linked network PMMA-based gel polymer electrolyte with excellent lithium storage performance, *J. Mater. Sci. Technol.*, 2024, **199**, 197–205.
29 Z. He and L. Fan, Poly(ethylene carbonate)-based electrolytes with high concentration Li salt for all-solid-state lithium batteries, *Rare Met.*, 2018, **37**, 488–496.
30 Z. Zhang, Y. Ren, J. Liang, M. Xiao, S. Wang, S. Huang, D. Han and Y. Meng, Rationally designed poly(propylene carbonate)-based electrolyte for dendrite-free all solid-state lithium metal batteries, *Energy Storage Mater.*, 2024, **71**, 103667.
31 J. Chai, Z. Liu, J. Ma, J. Wang, X. Liu, H. Liu, J. Zhang, G. Cui and L. Chen, In Situ Generation of Poly (Vinylene Carbonate) Based Solid Electrolyte with Interfacial Stability for LiCoO2 Lithium Batteries, *Adv. Sci.*, 2016, **4**, 1600377.
32 H. Peng, Y. Zhu, C. Liu, X. Fang, Q. Zhou, Y. Li and Y. Yang, Fabrication of mesoporous SiO2/P(VDF-HFP) composite membrane for high-performance lithium-ion batteries, *Mater. Lett.*, 2024, **355**, 135483.

33 J. Tan, L. Guo, J. Hu and S. Liu, Recent Advances in Poly(ethylene oxide)-Based Solid-State Electrolytes for Lithium-Ion Batteries, *J. Phys. Chem. C*, 2024, **128**, 17197–17218.
34 Z. Xue, D. He and X. Xie, Poly(ethylene oxide)-based electrolytes for lithium-ion batteries, *J. Mater. Chem. A*, 2015, **3**, 19218–19253.
35 P. Shi, J. Ma, M. Liu, S. Guo, Y. Huang, S. Wang, L. Zhang, L. Chen, K. Yang, X. Liu, Y. Li, X. An, D. Zhang, X. Cheng, Q. Li, W. Lv, G. Zhong, Y.-B. He and F. Kang, A dielectric electrolyte composite with high lithium-ion conductivity for high-voltage solid-state lithium metal batteries, *Nat. Nanotechnol.*, 2023, **18**, 602–610.
36 Z. Zhang, X. Wang, X. Li, J. Zhao, G. Liu, W. Yu, X. Dong and J. Wang, Review on composite solid electrolytes for solid-state lithium-ion batteries, *Mater. Today Sustain.*, 2023, **21**, 100316.
37 M. Dirican, C. Yan, P. Zhu and X. Zhang, Composite solid electrolytes for all-solid-state lithium batteries, *Mater. Sci. Eng., R*, 2019, **136**, 27–46.
38 G. Xi, M. Xiao, S. Wang, D. Han, Y. Li and Y. Meng, Polymer-Based Solid Electrolytes: Material Selection, Design, and Application, *Adv. Funct. Mater.*, 2020, **31**, 2007598.
39 H. Wu and Y. Cui, Designing nanostructured Si anodes for high energy lithium ion batteries, *Nano Today*, 2012, **7**, 414–429.
40 H. Liu, Q. Sun, H. Zhang, J. Cheng, Y. Li, Z. Zeng, S. Zhang, X. Xu, F. Ji, D. Li, J. Lu and L. Ci, The application road of silicon-based anode in lithium-ion batteries: From liquid electrolyte to solid-state electrolyte, *Energy Storage Mater.*, 2023, **55**, 244–263.
41 W. Liang, K. Zhao, L. Ouyang, M. Zhu and J. Liu, A review of functional group selection and design strategies for gel polymer electrolytes for metal batteries, *Mater. Sci. Eng., R*, 2025, **164**, 100973.
42 W. Yan, Z. Mu, Z. Wang, Y. Huang, D. Wu, P. Lu, J. Lu, J. Xu, Y. Wu, T. Ma, M. Yang, X. Zhu, Y. Xia, S. Shi, L. Chen, H. Li and F. Wu, Hard-carbon-stabilized Li–Si anodes for high-performance all-solid-state Li-ion batteries, *Nat. Energy*, 2023, **8**, 800–813.
43 R. Okuno, M. Yamamoto, A. Kato and M. Takahashi, High Cycle Stability of Nanoporous Si Composites in All-solid-state Lithium-ion Batteries, *J. Electrochem. Soc.*, 2022, **169**, 080502.
44 D. Zhang, Y. Ouyang, Y. Wang, L. Liu, H. Wang, J. Cui, M. Wang, N. Li, H. Zhao and S. Ding, A gradient-distributed binder with high energy dissipation for stable silicon anode, *J. Colloid Interface Sci.*, 2024, **673**, 312–320.
45 R. Wang, Y. Wu, Y. Niu, Q. Yang, H. Li, T. Chen, Y. Song, B. Zhong and Z. Wu, Favored Amorphous LixSi Process with Restrained Volume Change Enabling Long Cycling Quasi-Solid-State SiOx anode, *ChemSusChem*, 2024, **18**, e202400168.
46 Q. Liu, Y. Feng, J. Liu, Y. Liu, X. Cui, Y.-J. He, Y. Nuli, J. Wang and J. Yang, In Situ Integration of a Flame Retardant Quasisolid Gel Polymer Electrolyte with a Si-Based Anode for High-Energy Li-Ion Batteries, *ACS Nano*, 2024, **18**, 13384–13396.
47 H. Huo, M. Jiang, Y. Bai, S. Ahmed, K. Volz, H. Hartmann, A. Henss, C. V. Singh, D. Raabe and J. Janek, Chemo-mechanical failure mechanisms of the silicon anode in solid-state batteries, *Nat. Mater.*, 2024, **23**, 543–551.
48 R. Brow, Z. Berquist, S. Lee, T. Martin, L. Meyer, M. Schulze, A. Singh, R. Tancin, G. Teeter, G. Veith, B. J. Tremolet de Villers, A. Colclasure and A. Manthiram, Cobalt-free cathodes and silicon thin-film anodes towards high-capacity solid-state batteries, *J. Energy Storage*, 2024, **99**, 113329–113342.
49 H. Huo, Y. Bai, S. L. Benz, T. Weintraut, S. Wang, A. Henss, D. Raabe and J. Janek, Decoupling the Effects of Interface Chemical Degradation and Mechanical Cracking in Solid-State Batteries with Silicon Electrode, *Adv. Mater.*, 2024, **37**, 2415006.
50 X. Liu, D. Wang, X. Wang, D. Wang, Y. Li, J. Fu, R. Zhang, Z. Liu, Y. Zhou and G. Wen, Designing Compatible Ceramic/Polymer Composite Solid-State Electrolyte for Stable Silicon Nanosheet Anodes, *Small*, 2024, **20**, 2309724.
51 X. Wang, K. Wang, Z. Zheng, Z. Wan, J. Zhao, H. Li, W. Jiang, Z. Wu, B. Chen, Y. Tan, M. Ling, M. Sun and C. Liang, Advanced inorganic lithium metasilicate binder for high-performance silicon anode, *J. Colloid Interface Sci.*, 2023, **652**, 971–978.
52 X. Li, K. Qian, Y.-B. He, C. Liu, D. An, Y. Li, D. Zhou, Z. Lin, B. Li, Q.-H. Yang and F. Kang, A dual-functional gel-polymer electrolyte for lithium ion batteries with superior rate and safety performances, *J. Mater. Chem. A*, 2017, **5**, 18888–18895.
53 B. Zeng, Q. Gu, Y. Zhang, M. Wang, J. Gao, C. Fan and W. Tang, Engineering electrode–electrolyte interface for ultrastable Si-based solid-state batteries, *Surf. Interfaces*, 2024, **44**, 103687.
54 K. Amezawa, N. Yamamoto, Y. Tomii and Y. Ito, Single-Electrode Peltier Heats of Li-Si Alloy Electrodes in LiCl-KCl Eutectic Melt, *J. Electrochem. Soc.*, 1998, **145**, 1986.
55 Z. Chang, J. Wang, W. Li, Z. Wu and S. Lu, Research progress on interface reaction of silicon-based anode for lithium-ion battery, *J. Mater. Eng.*, 2019, **47**, 11–25.
56 R. A. Huggins, Lithium alloy negative electrodes, *J. Power Sources*, 1999, **81–82**, 13–19.
57 Y. Liu, J. Yang, N. Imanishi, A. Hirano, Y. Takeda and O. Yamamoto, Composite anode containing nano-SiO1.1 and Li2.6Co0.4N with solid PEO electrolytes for lithium-ion batteries, *J. Power Sources*, 2005, **146**, 376–379.
58 P. H. L. Notten, F. Roozeboom, R. A. H. Niessen and L. Baggetto, 3-D Integrated All-Solid-State Rechargeable Batteries, *Adv. Mater.*, 2007, **19**, 4564–4567.
59 Y. Kobayashi, S. Seki, Y. Mita, Y. Ohno, H. Miyashiro, P. Charest, A. Guerfi and K. Zaghib, High reversible capacities of graphite and SiO/graphite with solvent-free solid polymer electrolyte for lithium-ion batteries, *J. Power Sources*, 2008, **185**, 542–548.
60 J. Trevey, J. S. Jang, Y. S. Jung, C. R. Stoldt and S.-H. Lee, Glass–ceramic Li2S–P2S5 electrolytes prepared by a single

step ball billing process and their application for all-solid-state lithium–ion batteries, *Electrochem. Commun.*, 2009, **11**, 1830–1833.

61 J. W. Choi, J. McDonough, S. Jeong, J. S. Yoo, C. K. Chan and Y. Cui, Stepwise Nanopore Evolution in One-Dimensional Nanostructures, *Nano Lett.*, 2010, **10**, 1409–1413.

62 X. Liu, L. zhong, S. Huang, S. X. Mao, T. Zhu and J. Huang, size-dependent-fracture-of-silicon-nanoparticles-during-lithiation, *ACS Nano*, 2012, **6**, 1522–1531.

63 G. P. Pandey, S. A. Klankowski, Y. Li, X. S. Sun, J. Wu, R. A. Rojeski and J. Li, Effective Infiltration of Gel Polymer Electrolyte into Silicon-Coated Vertically Aligned Carbon Nanofibers as Anodes for Solid-State Lithium-Ion Batteries, *ACS Appl. Mater. Interfaces*, 2015, **7**, 20909–20918.

64 X. Li, P. Yan, B. W. Arey, W. Luo, X. Ji, C. Wang, J. Liu and J.-G. Zhang, A stable nanoporous silicon anode prepared by modified magnesiothermic reactions, *Nano Energy*, 2016, **20**, 68–75.

65 D. E. Galvez-Aranda, V. Ponce and J. M. Seminario, Molecular dynamics simulations of the first charge of a Li-ion—Si-anode nanobattery, *J. Mol. Model.*, 2017, **23**, 120.

66 F. Wang, L. Sun, W. Zi, B. Zhao and H. Du, Solution Synthesis of Porous Silicon Particles as an Anode Material for Lithium Ion Batteries, *Chem.–Eur. J.*, 2019, **25**, 9071–9077.

67 S. Cangaz, F. Hippauf, F. S. Reuter, S. Doerfler, T. Abendroth, H. Althues and S. Kaskel, Enabling High-Energy Solid-State Batteries with Stable Anode Interphase by the Use of Columnar Silicon Anodes, *Adv. Energy Mater.*, 2020, **10**, 2001320.

68 D. H. S. Tan, Y. Chen, H. Yang, W. Bao, B. Sreenarayanan, D. Jean-Marie, W. Li, B. Lu, S.-Y. Ham, B. Sayahpour, J. Scharf, E. A. Wu, G. Deysher, H. E. Han, H. J. Hah, H. Jeong, J. B. Lee, Z. Chen and Y. S. Meng, Carbon-free high-loading silicon anodes enabled by sulfide solid electrolytes, *Science*, 2021, **373**, 1494–1499.

69 M. Li, D. Xue, Z. Rong, R. Fang, B. Wang, Y. Liang, X. Zhang, Q. Huang, Z. Wang, L. Zhu, L. Zhang, Y. Tang, S. Zhang and J. Huang, Stack Pressure Enhanced Size Threshold of Si Anode Fracture in All-Solid-State Batteries, *Adv. Funct. Mater.*, 2024, **35**, 2415696.

70 X. Shen, Y. Wang, Z. Jiang, X. Liang, M. Demicoli, L. Mule Stagno, B. Sun, H. Sun, X. Hao, P. Zhang, Z. Wang, J. Deng, J. Wang and J. Song, Reversible Nano Crystalline-Phase Transformation in Si-Based Anode Enables Stable All-Solid-State Batteries, *Nano Lett.*, 2025, **25**, 10826–10833.

71 Y. Hamedi Jouybari, F. Berkemeier and G. Schmitz, High performance all-solid-state lithium battery: Assessment of the temperature dependence of Li diffusion, *J. Power Sources*, 2022, **517**, 230709.

72 S. Basak, V. Migunov, A. H. Tavabi, C. George, Q. Lee, P. Rosi, V. Arszelewska, S. Ganapathy, A. Vijay, F. Ooms, R. Schierholz, H. Tempel, H. Kungl, J. Mayer, R. E. Dunin-Borkowski, R.-A. Eichel, M. Wagemaker and E. M. Kelder, Operando Transmission Electron Microscopy Study of All-Solid-State Battery Interface: Redistribution of Lithium among Interconnected Particles, *ACS Appl. Energy Mater.*, 2020, **3**, 5101–5106.

73 P. Vadhva, A. M. Boyce, A. Hales, M.-C. Pang, A. N. Patel, P. R. Shearing, G. Offer and A. J. E. Rettie, Towards Optimised Cell Design of Thin Film Silicon-Based Solid-State Batteries via Modelling and Experimental Characterisation, *J. Electrochem. Soc.*, 2022, **169**, 100525.

74 P. Vadhva, A. M. Boyce, A. Patel, P. R. Shearing, G. Offer and A. J. E. Rettie, Silicon-Based Solid-State Batteries: Electrochemistry and Mechanics to Guide Design and Operation, *ACS Appl. Mater. Interfaces*, 2023, **15**, 42470–42480.

75 M. Otoyama, N. Terasaki, T. Takeuchi, T. Okumura and K. Kuratani, Visualization of Local Strain Distributions in All-Solid-State Batteries with Silicon Negative Electrodes Using Digital Image Correlation for Operando/In situ Microscopy Images, *ChemElectroChem*, 2025, **12**, e202400616.

76 Y. Sakka, M. Matsumoto, H. Yamashige, A. Takeuchi, M. Uesugi, K. Uesugi, C. Zhong, K. Shimoda, K.-i. Okazaki and Y. Orikasa, Investigating Plastic Deformation Between Silicon and Solid Electrolyte in All-Solid-State Batteries Using Operando X-ray Tomography, *J. Electrochem. Soc.*, 2024, **171**, 070536.

77 L. Guan, Y. Shi, C. Gao, T. Wang, J. Zhou and R. Cai, Interfacial contact loss and bending effects on electrochemical-mechanical modeling for all-solid-state Li-ion batteries, *Electrochim. Acta*, 2023, **440**, 141669.

78 D. L. Nelson, S. E. Sandoval, J. Pyo, D. Bistri, T. A. Thomas, K. A. Cavallaro, J. A. Lewis, A. S. Iyer, P. Shevchenko, C. V. Di Leo and M. T. McDowell, Fracture Dynamics in Silicon Anode Solid-State Batteries, *ACS Energy Lett.*, 2024, **9**, 6085–6095.

79 S. Y. Han, C. Lee, J. A. Lewis, D. Yeh, Y. Liu, H.-W. Lee and M. T. McDowell, Stress evolution during cycling of alloy-anode solid-state batteries, *Joule*, 2021, **5**, 2450–2465.

80 M. Yamamoto, Y. Terauchi, A. Sakuda, A. Kato and M. Takahashi, Effects of volume variations under different compressive pressures on the performance and microstructure of all-solid-state batteries, *J. Power Sources*, 2020, **473**, 228595.

81 Q. Wang, Y. Huang, J. Xu, X. Yu, H. Li and L. Chen, Interface and mechanical degradation mechanisms of the silicon anode in sulfide-based solid-state batteries at high temperatures, *Chin. Phys. B*, 2024, **33**, 088201.

82 K. Sun, G. Thorsteinsson, D. Zhao, C. Owen, A. Ponnekanti, Z. Herman, B. Parris, I. Kothari and D. A. Steingart, Chemo-mechanics and Morphological Dynamics of Si Electrodes in All-Solid-State Li-Ion Batteries, *ACS Energy Lett.*, 2025, **10**, 1229–1234.

83 H. Nagata and K. Kataoka, Influence of mechanochemical reactions between Si and solid electrolytes in the negative electrode on the performance of all-solid-state lithium-ion batteries, *J. Power Sources*, 2024, **623**, 235443.

84 S. Asano, J.-I. Hata, K. Watanabe, K. Shimizu, N. Matsui, N. L. Yamada, K. Suzuki, R. Kanno and M. Hirayama, Formation Processes of a Solid Electrolyte Interphase at

a Silicon/Sulfide Electrolyte Interface in a Model All-Solid-State Li-Ion Battery, *ACS Appl. Mater. Interfaces*, 2024, **16**, 7189–7199.

85 I. Na, H. Kim, S. Kunze, C. Nam, S. Jo, H. Choi, S. Oh, E. Choi, Y. B. Song, Y. S. Jung, Y. S. Lee and J. Lim, Monolithic 100% Silicon Wafer Anode for All-Solid-State Batteries Achieving High Areal Capacity at Room Temperature, *ACS Energy Lett.*, 2023, **8**, 1936–1943.

86 R. Matsuda, A. Tanaka, K. Yanagihara, Y. Sasaki, K. Hikima, H. Muto and A. Matsuda, Deterioration Analysis of Si Composite Anodes for All-Solid-State Batteries during Charge–Discharge by Auger Electron Spectroscopy and Scanning Electron Microscopy with Energy Dispersive Spectroscopy, *J. Phys. Chem. C*, 2023, **127**, 16508–16514.

87 Y. Rudel, M. Rana, J. Ruhl, C. Rosenbach, J. Müller, P. Michalowski, A. Kwade and W. G. Zeier, Investigating the Influence of the Effective Ionic Transport on the Electrochemical Performance of Si/C-Argyrodite Solid-State Composites, *Batteries Supercaps*, 2023, **6**, e202300211.

88 M. So, S. Yano, A. Permatasari, T. D. Pham, K. Park and G. Inoue, Mechanism of silicon fragmentation in all-solid-state battery evaluated by discrete element method, *J. Power Sources*, 2022, **546**, 231956.

89 X. Li, Z. Wang, H. Lin, Y. Liu, Y. Min and F. Pan, Composite electrolytes of pyrrolidone-derivatives-PEO enable to enhance performance of all solid state lithium-ion batteries, *Electrochim. Acta*, 2019, **293**, 25–29.

90 B. Deng, M.-x. Jing, R. Li, L.-x. Li, H. Yang, M.-q. Liu, J. Xiang, W.-y. Yuan and X.-q. Shen, Integrating high ionic conductive PDOL solid/gel composite electrolyte for enhancement of interface combination and lithium dentrite inhibition of solid-state lithium battery, *J. Colloid Interface Sci.*, 2022, **620**, 199–208.

91 H. Chen, P. He, M. Li, Y. Wen, Y. Wang, J. Qiu, G. Cao, P. Zhao, S. Zhang and H. Ming, Enabling Stable Cycling of 4.6 V High-Voltage LiCoO2 with an In Situ-Modified PEGDA-Based Quasi-Solid Electrolyte, *ACS Appl. Energy Mater.*, 2022, **5**, 5170–5181.

92 H. He, Y. Wang, M. Li, J. Qiu, Y. Wen and J. Chen, In situ cross-linked fluorinated gel polymer electrolyte based on PEGDA-enabled lithium-ion batteries with a wide temperature operating range, *Chem. Eng. J.*, 2023, **467**, 143311.

93 Y. Wang, T. Li, X. Yang, Q. Yin, S. Wang, H. Zhang and X. Li, 2D Solid-Electrolyte Interphase Built by High-Concentration Polymer Electrolyte for Highly Reversible Silicon Anodes, *Adv. Energy Mater.*, 2023, **14**, 2303189.

94 P. Qiu, M. Cui, H. Gan, L. Li, Y. Xia, J. Sun and W. Zhu, Hierarchically structured silicon–carbon anodes: Achieving high-performance all-solid-state Li-ion batteries via chemical pre-lithiation and in-situ polymerization, *Carbon*, 2025, **233**, 119905.

95 X. Rui, R. Hua, D. Ren, F. Qiu, Y. Wu, Y. Qiu, Y. Mao, Y. Guo, G. Zhu, X. Liu, Y. Gao, C. Zhao, X. Feng, L. Lu and M. Ouyang, In Situ Polymerization Facilitating Practical High-Safety Quasi-Solid-State Batteries, *Adv. Mater.*, 2024, **36**, 2402401.

96 S. He, S. Huang, X. Liu, X. Zeng, H. Chen, L. Zhao, H. Noor and X. Hou, Interfacial self-healing polymer electrolytes for Long-Cycle silicon anodes in High-Performance solid-state lithium batteries, *J. Colloid Interface Sci.*, 2024, **665**, 299–312.

97 E. Zhao, S. Luo, A. Hu, Z. Liao, C. Huang, O. Akihiro, P. Jiang and L. Yang, Rational design of an in-build quasi-solid-state electrolyte for high-performance lithium-ion batteries with the silicon-based anode, *Chem. Eng. J.*, 2023, **463**, 142306.

98 M. Göttlinger, S. Amrhein, C. Piesold, M. Weller, S. Peters and G. A. Giffin, Development of Silicon Polymer Electrodes with a Hybrid Polymer Electrolyte for All-Solid-State Lithium-Ion Batteries, *J. Electrochem. Soc.*, 2023, **170**, 030541.

99 P. Dong, Y. Cha, X. Zhang, J. Zamora and M.-K. Song, Poly(ethylene) Oxide Electrolytes for All-Solid-State Lithium Batteries Using Microsized Silicon/Carbon Anodes with Enhanced Rate Capability and Cyclability, *ACS Appl. Mater. Interfaces*, 2024, **16**, 41018–41026.

100 M. Li, B. Liu, Y. Wu, Y. Ren, P. Qin, J. Qian and X. Ding, SiO with ZSM-5 to regulate interfacial stability for fast-charging lithium-ion batteries, *J. Electroanal. Chem.*, 2024, **968**, 118500.

101 D. Zhang, P. Yu, Y. Zhang, X. Zhao and J. Yu, Vertical Graphene Sheet-Encapsulated Silicon Nanoparticles for Anodes of Polymer-Based All-Solid-State Batteries, *ACS Appl. Energy Mater.*, 2023, **7**, 726–734.

102 Y. Wu, Y. Liu, X. Feng, Z. Ma, X. Xu, D. Ren, X. Han, Y. Li, L. Lu, L. Wang, X. He and M. Ouyang, Smart Solid-State Interphases Enable High-Safety and High-Energy Practical Lithium Batteries, *Adv. Sci.*, 2024, **11**, 2400600.

103 X. Meng, Y. Liu, Z. Wang, Y. Zhang, X. Wang and J. Qiu, A quasi-solid-state rechargeable cell with high energy and superior safety enabled by stable redox chemistry of Li2S in gel electrolyte, *Energy Environ. Sci.*, 2021, **14**, 2278–2290.

104 H. M. Bintang, S. Lee, J. T. Kim, H.-G. Jung and H.-D. Lim, Self-Constructed Intimate Interface on a Silicon Anode Enabled by a Phase-Convertible Electrolyte for Lithium-Ion Batteries, *ACS Appl. Mater. Interfaces*, 2022, **14**, 805–813.

105 H. Ueda, F. Mizuno, M. Forsyth and P. C. Howlett, Tailoring Silicon Composite Anodes with Li+-Containing Organic Ionic Plastic Crystals for Solid-State Batteries, *J. Electrochem. Soc.*, 2024, **171**, 020556.

106 C. Chae, W. Choi, S. Ji, S. S. Lee, J.-K. Kim, S. Choi, Y. Kang, Y. Choi, D. Y. Kim and S. Jeong, Electrostatically Assembled Silicon–Carbon Composites Employing Amine-Functionalized Carbon Intra-interconnections for Lithium-Ion Battery Anodes, *ACS Appl. Energy Mater.*, 2019, **2**, 1868–1875.

107 Y. Zhang, L. Zhang, Z. Zhao, Y. Zhang, J. Cui, C. Liu, D. Mu, Y. Su, B. Wu and F. Wu, Lithiophilic Li-Si alloy-solid electrolyte interface enabled by high-concentration dual salt-reinforced quasi-solid-state electrolyte, *J. Energy Chem.*, 2024, **95**, 216–230.

108 M. Balaish, J. C. Gonzalez-Rosillo, K. J. Kim, Y. Zhu, Z. D. Hood and J. L. M. Rupp, Processing thin but robust

electrolytes for solid-state batteries, *Nat. Energy*, 2021, **6**, 227–239.

109 J. B. Goodenough, H. Y. P. Hong and J. A. Kafalas, Fast Na+-ion transport in skeleton structures, *Mater. Res. Bull.*, 1976, **11**, 203–220.

110 H. Aono, E. Sugimoto, Y. Sadaoka, N. Imanaka and G. Adachi, Ionic conductivity of solid electrolytes based on lithium titanium phosphate, *J. Electrochem. Soc.*, 1990, **137**, 1023–1027.

111 H. Aono, E. Sugimoto, Y. Sadaoka, N. Imanaka and G.-y. Adachi, Electrical Properties and Sinterability for Lithium Germanium Phosphate Li1+xMxGe2−x(PO4)3, M = Al, Cr, Ga, Fe, Sc, and In Systems, *Bull. Chem. Soc. Jpn.*, 2006, **65**, 2200–2204.

112 J. B. Bates, N. J. Dudney, G. R. Gruzalski, R. A. Zuhr, A. Choudhury, C. F. Luck and J. D. Robertson, Electrical properties of amorphous lithium electrolyte thin films, *Solid State Ionics*, 1992, **53–56**, 647–654.

113 Y. Inaguma, C. Liquan, M. Itoh, T. Nakamura, T. Uchida, H. Ikuta and M. Wakihara, High ionic conductivity in lithium lanthanum titanate, *Solid State Commun.*, 1993, **86**, 689–693.

114 V. Thangadurai, H. Kaack and W. J. F. Weppner, Novel fast lithium ion conduction in garnet-type Li5La3M2O12 (M = Nb, Ta), *J. Am. Ceram. Soc.*, 2003, **86**, 437–440.

115 R. Murugan, V. Thangadurai and W. Weppner, Fast Lithium Ion Conduction in Garnet-Type Li7La3Zr2O12, *Angew. Chem., Int. Ed.*, 2007, **46**, 7778–7781.

116 K. Marumoto, K. Nakano, Y. Kondo, M. Inaba and T. Doi, Tailored Design of a Nanoporous Structure Suitable for Thick Si Electrodes on a Stiff Oxide-Based Solid Electrolyte, *ACS Appl. Mater. Interfaces*, 2024, **16**, 62274–62281.

117 R. Sugimoto, K. Marumoto, M. Haruta, M. Inaba and T. Doi, Quantitative Evaluation and Improvement of Interfacial Li+ Transfer Between SiOx Electrode and Garnet-Type Ta-Doped Li7La3Zr2O12 Electrolyte, *ChemElectroChem*, 2022, **9**, e202200491.

118 P. Srivastava, Y. K. Liao, K. Iputera, S. F. Hu and R. S. Liu, Robust and Intimate Interface Enabled by Silicon Carbide as an Additive to Anodes for Lithium Metal Solid-State Batteries, *ChemSusChem*, 2023, **16**, e202300504.

119 W. Ping, C. Yang, Y. Bao, C. Wang, H. Xie, E. Hitz, J. Cheng, T. Li and L. Hu, A silicon anode for garnet-based all-solid-state batteries: Interfaces and nanomechanics, *Energy Storage Mater.*, 2019, **21**, 246–252.

120 B. Ke, C. Zhang, S. Cheng, W. Li, R. Deng, H. Zhang, J. Lin, Q. Xie, B. Qu, D. L. Peng and X. Wang, Tape-casting electrode architecture permits low-temperature manufacturing of all-solid-state thin-film microbatteries, *Interdiscip. Mater.*, 2024, **3**, 621–631.

121 P. Liang, Z. Huang, L. Chen, G. Shao, H. Wang, H. Sun and C. Wang, Highly elastic and low resistance deformable current collectors for safe and high-performance silicon and metallic lithium anodes, *J. Power Sources*, 2021, **511**, 230418.

122 S. Sau, M. R. Panda, G. Barik, M. Gautam, M. Adil, S. N. Jha and S. Mitra, Unravelling redox phenomenon and electrochemical stability of Li1.6Al0.5Ge1.5P2.9Si0.1O12 solid electrolyte against Li metal and silicon anodes for advanced solid-state batteries, *Mater. Today Energy*, 2023, **38**, 101445.

123 Y. Qiao, S. Yang, Z. Ma, Y. Yang, X. Hong and Z. Fu, Solid-state corrosion of lithium for prelithiation of SiOx-C composite anode with carbon-incorporated lithium phosphorus oxynitride, *Nano Res.*, 2022, **16**, 8394–8404.

124 H. Nagata and J. Akimoto, High areal capacity LiNi1/3Co1/3Mn1/3O2 positive composite electrode employing an oxide solid electrolyte for an all-solid-state lithium-ion battery, *Solid State Ionics*, 2022, **379**, 115905.

125 Q. Feng, C. Xu, X. Xie and N. Liao, Enabling high performance all-solid-state thin films microbatteries with silicon oxycarbide/lithium-metal composites anodes, *Surf. Interfaces*, 2024, **44**, 103759.

126 C. Xu, J. Tu, D. Yang, W. Xue and N. Liao, Highly functional LiXPON (X=Al, Si, C, Sn, Y, Ta) electrolytes for silicon/silicon oxycarbide composite all-solid-state batteries: First-principles design and experimental validation, *Surf. Interfaces*, 2025, **59**, 105981.

127 G. Ferraresi, M. El Kazzi, L. Czornomaz, C.-L. Tsai, S. Uhlenbruck and C. Villevieille, Electrochemical Performance of All-Solid-State Li-Ion Batteries Based on Garnet Electrolyte Using Silicon as a Model Electrode, *ACS Energy Lett.*, 2018, **3**, 1006–1012.

128 X. Li, Y. Zhou, J. Tang, S. Zhao, J. Zhang, X. Huang and B. Tian, Optimizing Li1.3Al0.3Ti1.7(PO4)3 Particle Sizes toward High Ionic Conductivity, *ACS Appl. Mater. Interfaces*, 2023, **15**, 36289–36300.

129 P. Wu, W. Zhou, X. Su, J. Li, M. Su, X. Zhou, B. W. Sheldon and W. Lu, Recent Advances in Conduction Mechanisms, Synthesis Methods, and Improvement Strategies for Li1+xAlxTi2−x(PO4)3 Solid Electrolyte for All-Solid-State Lithium Batteries, *Adv. Energy Mater.*, 2022, **13**, 2203440.

130 J.-H. Yin, H. Zhu, S.-J. Yu, Y.-B. Dong, Q.-Y. Wei, G.-Q. Xu, Y. Xiong and Y. Qian, Recent Advances of LATP and Their NASICON Structure as a Solid-State Electrolyte for Lithium-Ion Batteries, *Adv. Eng. Mater.*, 2023, **25**, 2300566.

131 K. Yang, L. Chen, J. Ma, Y. B. He and F. Kang, Progress and perspective of Li1 + xAlxTi2-x(PO4)3 ceramic electrolyte in lithium batteries, *InfoMat*, 2021, **3**, 1195–1217.

132 L. Liu, Q. Wang, Z. Jie, J. Ma, X. Cui, G. Xu, C. Gu, L. Ma and Y. Liu, Stable interface between anode materials and Li1.3Al0.3Ti1.7(PO4)3-based solid-state electrolyte facilitated by graphene coating, *Electrochim. Acta*, 2022, **431**, 141136.

133 C. A. Augustine, D. Panoth and A. Paravannoor, High Performance Li-ion battery Anodes based on Si Nano core in an LATP Matrix with better Electrolyte Compatibility and Temperature Resistance, *ChemistrySelect*, 2019, **4**, 7090–7095.

134 X. Xu, Z. Wen, X. Wu, X. Yang and Z. Gu, Lithium Ion-Conducting Glass–Ceramics of Li1.5Al0.5Ge1.5(PO4)3–xLi2O (x=0.0–0.20) with Good Electrical and

Electrochemical Properties, *J. Am. Ceram. Soc.*, 2007, **90**, 2802–2806.

135 J. Fu, Fast Li+ ion conducting glass-ceramics in the system Li_2O–Al_2O_3–GeO_2–P_2O_5, *Solid State Ionics*, 1997, **104**, 191–194.

136 M. Cretin and P. Fabry, Comparative study of lithium ion conductors in the system Li1+xAlxA2−xIV (PO4)3 with AIV=Ti or Ge and 0≤x≤0·7 for use as Li+ sensitive membranes, *J. Eur. Ceram. Soc.*, 1999, **19**, 2931–2940.

137 L. Han, C. Hsieh, B. Chandra Mallick, J. Li and Y. Ashraf Gandomi, Recent progress and future prospects of atomic layer deposition to prepare/modify solid-state electrolytes and interfaces between electrodes for next-generation lithium batteries, *Nanoscale Adv.*, 2021, **3**, 2728–2740.

138 W. Dai, Y. Qiao, Z. Ma, T. Wang and Z. Fu, All-solid-state thin-film batteries based on lithium phosphorus oxynitrides, *Future Mater.*, 2022, **1**, 032101.

139 Q. Feng, X. Xie, B. Zheng and N. Liao, Superior Effect of Si Doping on Interfacial Reaction of LiPON Solid Electrolyte for the Silicon-Rich Oxide (SiO1/2) Anode in All-Solid-State Batteries: A First-Principles Prediction, *ACS Appl. Energy Mater.*, 2023, **6**, 2698–2706.

140 L. Li, Y. Deng and G. Chen, Status and prospect of garnet/polymer solid composite electrolytes for all-solid-state lithium batteries, *J. Energy Chem.*, 2020, **50**, 154–177.

141 Y. Zhao, L. Chen, Y. Su, H. Jin and C. Wang, Review of garnet-type Li7La3Zr2O12 solid electrolyte: materials and interface issues, *J. Mater. Sci.*, 2024, **60**, 629–661.

142 H. Nagata and J. Akimoto, Room-temperature Operation of Lithium Sulfide Positive and Silicon Negative Composite Electrodes Employing Oxide Solid Electrolytes for All-solid-state Battery, *Electrochemistry*, 2022, **90**, 017006.

143 R. Mercier, J. P. Malugani, B. Fahys and G. Robert, Superionic conduction in Li2S-P2S5-LiI-glasses, *Solid State Ionics*, 1981, **5**, 663–666.

144 R. Kanno and M. Murayama, Lithium Ionic Conductor Thio-LISICON The Li_2S GeS_2 P_2S_5 System, *J. Electrochem. Soc.*, 2001, **148**, A742–A746.

145 F. Mizuno, A. Hayashi, K. Tadanaga and M. Tatsumisago, New, highly ion-conductive crystals precipitated from Li2S-P2S5 glasses, *Adv. Mater.*, 2005, **17**, 918–921.

146 F. Mizuno, A. Hayashi, K. Tadanaga and M. Tatsumisago, New lithium-ion conducting crystal obtained by crystallization of the Li2S-P2S5 glasses, *Electrochem. Solid-State Lett.*, 2005, **8**, A603–A606.

147 A. Hayashi, T. Konishi, K. Tadanaga, T. Minami and M. Tatsumisago, All-solid-state lithium secondary batteries with SnS-P_2S_5 negative electrodes and Li_2S-P_2S_5 solid electrolytes, *J. Power Sources*, 2005, **146**, 496–500.

148 F. Mizuno, A. Hayashi, K. Tadanaga and M. Tatsumisago, Design of composite positive electrode in all-solid-state secondary batteries with Li2S-P2S5 glass-ceramic electrolytes, *J. Power Sources*, 2005, **146**, 711–714.

149 T. Ohtomo, F. Mizuno, A. Hayashi, K. Tadanaga and M. Tatsumisago, Mechanochemical synthesis of lithium ion conducting glasses and glass-ceramics in the system Li2S-P-S, *Solid State Ionics*, 2005, **176**, 2349–2353.

150 H. J. Deiseroth, S. T. Kong, H. Eckert, J. Vannahme, C. Reiner, T. Zaiß and M. Schlosser, Li6PS5X: A Class of Crystalline Li-Rich Solids With an Unusually High Li+ Mobility, *Angew. Chem., Int. Ed.*, 2008, **47**, 755–758.

151 Y. Kato, S. Hori, T. Saito, K. Suzuki, M. Hirayama, A. Mitsui, M. Yonemura, H. Iba and R. Kanno, High-power all-solid-state batteries using sulfide superionic conductors, *Nat. Energy*, 2016, **1**, 16030–16036.

152 Y. Li, S. Song, H. Kim, K. Nomoto, H. Kim, X. Sun, S. Hori, K. Suzuki, N. Matsui, M. Hirayama, T. Mizoguchi, T. Saito, T. Kamiyama and R. Kanno, A lithium superionic conductor for millimeter-thick battery electrode, *Science*, 2023, **381**, 50–53.

153 N. A. Dunlap, J. Kim, H. Guthery, C.-S. Jiang, I. Morrissey, C. R. Stoldt, K. H. Oh, M. Al-Jassim and S.-H. Lee, Towards the Commercialization of the All-Solid-State Li-ion Battery: Local Bonding Structure and the Reversibility of Sheet-Style Si-PAN Anodes, *J. Electrochem. Soc.*, 2020, **167**, 060522.

154 R. Okuno, M. Yamamoto, A. Kato and M. Takahashi, Stable Cyclability Caused by Highly Dispersed Nanoporous Si Composite Anodes with Sulfide-based Solid Electrolyte, *J. Electrochem. Soc.*, 2020, **167**, 140522.

155 M. Branchi, G. Maresca, A. Tsurumaki, N. Suzuki, F. Croce, S. Panero, J. Voje, Y. Aihara and M. A. Navarra, Silicon-Based Composite Anodes for All-Solid-State Lithium-Ion Batteries Conceived by a Mixture Design Approach, *ChemSusChem*, 2023, **16**, e202202235.

156 K. Nam, D. Kim, Y. Lee, S. C. Han, J. Choi, Y. Ha and C. Park, Silicon disulfide for high-performance Li-ion batteries and solid-state electrolytes, *J. Mater. Chem. A*, 2023, **11**, 4987–5000.

157 M. Chiku, N. Kitade, C. Hotehama, H. Kowada, A. Sakuda, E. Higuchi, A. Hayashi and H. Inoue, Si particle size blends to improve cycling performance as negative electrode for all-solid-state lithium-ion battery, *Electrochim. Acta*, 2024, **505**, 144963.

158 J. Kim, C. Kim, I. Jang, J. Park, J. Kim, U. Paik and T. Song, Si nanoparticles embedded in carbon nanofiber sheathed with Li6PS5Cl as an anode material for all-solid-state batteries, *J. Power Sources*, 2021, **510**, 230425.

159 L. Hu, X. Yan, Z. Fu, J. Zhang, Y. Xia, W. Zhang, Y. Gan, X. He and H. Huang, A "Reinforced Concrete" Structure of Silicon Embedded into an In Situ Grown Carbon Nanotube Scaffold as a High-Performance Anode for Sulfide-Based All-Solid-State Batteries, *ACS Appl. Energy Mater.*, 2022, **5**, 14353–14360.

160 N. Ishii, N. Kakinuma and H. Morimoto, Properties of Carbon-coated SiO-C Pelletized Negative Electrodes for All-solid-state Batteries, *Electrochemistry*, 2024, **92**, 017006.

161 J. Sakabe, N. Ohta, T. Ohnishi, K. Mitsuishi and K. Takada, Porous amorphous silicon film anodes for high-capacity and stable all-solid-state lithium batteries, *Commun. Chem.*, 2018, **1**, 24.

162 R. Okuno, M. Yamamoto, A. Kato and M. Takahashi, Performance improvement of nanoporous Si composite anodes in all-solid-state lithium-ion batteries by using

acetylene black as a conductive additive, *Electrochem. Commun.*, 2022, **138**, 107288.

163 F. Sun, Z. Ma, S. Xin, Y. Fu, P. Li, J. Li, Q. Wan and X. Qu, Performance Degradation Mechanism of the Si@N, S-Doped Carbon Anode in Sulfide-Based All-Solid-State Batteries, *Small*, 2024, **21**, 2407284.

164 S. Poetke, S. Cangaz, F. Hippauf, S. Haufe, S. Dörfler, H. Althues and S. Kaskel, Partially Lithiated Microscale Silicon Particles as Anode Material for High-Energy Solid-State Lithium-Ion Batteries, *Energy Technol.*, 2023, **11**, 2201330.

165 E. Sánchez-Ahijón, A. Pendashteh and J. J. Vilatela, Paper-Like 100% Si Nanowires Electrodes Integrated with Argyrodite Li6PS5Cl Solid Electrolyte, *Batteries Supercaps*, 2024, **7**, e202400292.

166 S. Ham, E. Sebti, A. Cronk, T. Pennebaker, G. Deysher, Y. Chen, J. A. S. Oh, J. B. Lee, M. S. Song, P. Ridley, D. H. S. Tan, R. J. Clément, J. Jang and Y. S. Meng, Overcoming low initial coulombic efficiencies of Si anodes through prelithiation in all-solid-state batteries, *Nat. Commun.*, 2024, **15**, 2991.

167 K.-B. Kim, N. A. Dunlap, S. S. Han, J. J. Jeong, S. C. Kim, K. H. Oh and S.-H. Lee, Nanostructured Si/C Fibers as a Highly Reversible Anode Material for All-Solid-State Lithium-Ion Batteries, *J. Electrochem. Soc.*, 2018, **165**, A1903–A1908.

168 M. Yamamoto, M. Takatsu, R. Okuno, A. Kato and M. Takahashi, Nanoporous silicon fiber networks in a composite anode for all-solid-state batteries with superior cycling performance, *Sci. Rep.*, 2023, **13**, 17051.

169 X. Xu, Q. Sun, Y. Li, F. Ji, J. Cheng, H. Zhang, Z. Zeng, Y. Rao, H. Liu, D. Li and L. Ci, Nano Silicon Anode without Electrolyte Adding for Sulfide-Based All-Solid-State Lithium-Ion Batteries, *Small*, 2023, **19**, 2302934.

170 R. Okuno, M. Yamamoto, A. Kato, Y. Terauchi and M. Takahashi, Microstructures of nanoporous-Si composite anodes in sulfide-based all-solid-state lithium-ion batteries, *IOP Conf. Ser.: Mater. Sci. Eng.*, 2019, **625**, 012012.

171 M. Grandjean, M. Pichardo, Y. Biecher, C. Haon and P. Chenevier, Matching silicon-based anodes with sulfide-based solid-state electrolytes for Li-ion batteries, *J. Power Sources*, 2023, **580**, 233386.

172 D. Cao, X. Sun, Y. Li, A. Anderson, W. Lu and H. Zhu, Long-Cycling Sulfide-Based All-Solid-State Batteries Enabled by Electrochemo-Mechanically Stable Electrodes, *Adv. Mater.*, 2022, **34**, 2200401.

173 X. Xu, J. Cheng, Y. Li, X. Nie, L. Dai and L. Ci, Li metal-free rechargeable all-solid-state Li2S/Si battery based on Li7P3S11 electrolyte, *J. Solid State Electrochem.*, 2019, **23**, 3145–3151.

174 N. Chen, H. Li, Y. Zou, Z. Ao, P. Li, Y. Lao and Y. Wan, Li7P3S11 double-layer electrolyte for silicon-based all-solid-state batteries: Interface SiS2-doping, *Mater. Res. Bull.*, 2025, **182**, 113179.

175 Z. Wang, X. Shen, S. Chen, R. Qiao, B. Sun, J. Deng and J. Song, Large-Scale Fabrication of Stable Silicon Anode in Air for Sulfide Solid State Batteries via Ionic-Electronic Dual Conductive Binder, *Adv. Mater.*, 2024, **36**, 2405025.

176 Z. Fan, B. Ding, Z. Li, Z. Chang, B. Hu, C. Xu, X. Zhang, H. Dou and X. Zhang, In-situ prelithiation of electrolyte-free silicon anode for sulfide all-solid-state batteries, *eTransportation*, 2023, **18**, 100277.

177 R. Huang, R. Li, S. Li, W. Yang, Y. Bai, Z. Wang and K. Sun, In-situ constructing 3D nanocarbon conduction conformal network on silicon anodes for high-performance sulfide-based all-solid-state batteries, *Chem. Eng. J.*, 2025, **503**, 158154.

178 J. Jeong, K. Lee, C. Carpenter, S. Shrestha, J. Kim, H.-S. Chung, J. Moon, K. H. Oh, J.-Y. Sun and S.-H. Lee, Improved Cycle Properties of All-Solid-State Li-Ion Batteries with Al2O3 Coating on the Silicon-Based Anode, *J. Energy Eng.*, 2024, **150**, 04024003.

179 S. Jing, Y. Lu, Y. Huang, H. Liu, Y. Shen, W. Kuang, H. Shen, S. Liu, Z. Zhang and F. Liu, High-Performance Sheet-Type Sulfide All-Solid-State Batteries Enabled by Dual-Function Li4.4Si Alloy-Modified Nano Silicon Anodes, *Adv. Mater.*, 2024, **36**, 2312305.

180 Y. H. Jo, Y. J. Lee and D. W. Kim, Exploring the Optimal Binder Content in Composite Electrodes for Sulfide-Based All-Solid-State Lithium-Ion Batteries, *J. Electrochem. Soc.*, 2024, **171**, 100525.

181 Y. T. Chen, J. Jang, J. A. S. Oh, S. Y. Ham, H. Yang, D. J. Lee, M. Vicencio, J. B. Lee, D. H. S. Tan, M. Chouchane, A. Cronk, M. S. Song, Y. Yin, J. Qian, Z. Chen and Y. S. Meng, Enabling Uniform and Accurate Control of Cycling Pressure for All-Solid-State Batteries, *Adv. Energy Mater.*, 2024, **14**, 2304327.

182 S. An, Y. Ma, S. Payandeh, A. Mazilkin, R. Zhang, J. Janek, A. Kondrakov and T. Brezesinski, Comparative Analysis of Aqueous and Nonaqueous Polymer Binders for the Silicon Anode in All-Solid-State Batteries, *Adv. Energy Sustainability Res.*, 2023, **4**, 2300092.

183 D. Cao, X. Sun, Y. Wang and H. Zhu, Bipolar stackings high voltage and high cell level energy density sulfide based all-solid-state batteries, *Energy Storage Mater.*, 2022, **48**, 458–465.

184 R. Okuno, M. Yamamoto, Y. Terauchi and M. Takahashi, Stable cyclability of porous Si anode applied for sulfide-based all-solid-state batteries, *Energy Procedia*, 2019, **156**, 183–186.

185 M. Yamamoto, Y. Terauchi, A. Sakuda and M. Takahashi, Slurry mixing for fabricating silicon-composite electrodes in all-solid-state batteries with high areal capacity and cycling stability, *J. Power Sources*, 2018, **402**, 506–512.

186 Ö. U. Kudu, T. Famprikis, B. Fleutot, M.-D. Braida, T. Le Mercier, M. S. Islam and C. Masquelier, A review of structural properties and synthesis methods of solid electrolyte materials in the Li2S – P2S5 binary system, *J. Power Sources*, 2018, **407**, 31–43.

187 Y. S. Oh, M. Kim, S. Kang, J.-Y. Park and H.-T. Lim, Redox activity of Li2S–P2S5 electrolyte inducing chemo-mechanical failure in all-solid-state batteries comprising

sulfur composite cathode and Li–Si alloy anode, *Chem. Eng. J.*, 2022, **442**, 136229.

188 R. Ohta, T. Hiraoka, Y. Shibano, H. Kawamura, K. Kawamoto, T. Tanaka, A. Takeuchi, M. Dougakiuchi, K. Fukuda and M. Kambara, Influence of structural characteristics of a Si nanoparticulate anode on all-solid-state Li-ion batteries, *J. Phys. D: Appl. Phys.*, 2024, **57**, 255501.

189 J. Zhou, P. Chen, W. Wang and X. Zhang, Li7P3S11 electrolyte for all-solid-state lithium-ion batteries: structure, synthesis, and applications, *Chem. Eng. J.*, 2022, **446**, 137041.

190 N. D. Lepley and N. A. W. Holzwarth, Computer Modeling of Crystalline Electrolytes: Lithium Thiophosphates and Phosphates, *J. Electrochem. Soc.*, 2012, **159**, A538.

191 J. Fan, W. Sun, Y. Fu and W. Guo, Activation of Li_2S Cathode by an Organoselenide Salt Mediator for All-Solid-State Lithium–Sulfur Batteries, *Adv. Funct. Mater.*, 2024, **34**, 2407166.

192 M. Xu, J. Ding and E. Ma, One-dimensional stringlike cooperative migration of lithium ions in an ultrafast ionic conductor, *Appl. Phys. Lett.*, 2012, **101**, 031901.

193 S. Poetke, F. Hippauf, A. Baasner, S. Dörfler, H. Althues and S. Kaskel, Nanostructured Si—C Composites As High-Capacity Anode Material For All-Solid-State Lithium-Ion Batteries, *Batteries Supercaps*, 2021, **4**, 1323–1334.

194 T. Neumann, L. Alexander Dold, A. Thomas Cerny, E. Tröster, M. Günthel, A. Fischer, K. Peter Birke, I. Krossing and D. Biro, Towards Sustainable Sulfide-Based All-Solid-State-Batteries: An Experimental Investigation of the Challenges and Opportunities Using Solid Electrolyte Free Silicon Anodes, *Batteries Supercaps*, 2024, **8**, e202400412.

195 G. Chen, L. Guan, Y. Chen, H. Xu, J. Zhou and R. Cai, Optimization Effect on the Interfacial Impedance and Contact Stress of the ASSLB with Porous Polymer Buffer Layer, *J. Phys. Chem. C*, 2024, **128**, 20407–20422.

196 W. Weppner and R. A. Huggins, Ionic Conductivity of Solid and Liquid LiAlCl4, *J. Electrochem. Soc.*, 1977, **124**, 35.

197 R. Xu, Y. Wu, Z. Dong, R. Zheng, Z. Song, Z. Wang, H. Sun, Y. Liu and L. Zhang, Halide solid electrolytes in all-solid-state batteries: Ion transport kinetics, failure mechanisms and improvement strategies, *Nano Energy*, 2024, **132**, 110435.

198 X. Shi, Z. Zeng, H. Zhang, Y. Huang, C. H. Yan and Y. Du, Encapsulating and Operating a Stable Li3ErBr6-Based Solid Li–SeS2 Battery at Room Temperature, *Adv. Funct. Mater.*, 2023, **33**, 2213638–2213644.

199 X. Li, J. T. Kim, J. Luo, C. Zhao, Y. Xu, T. Mei, R. Li, J. Liang and X. Sun, Structural regulation of halide superionic conductors for all-solid-state lithium batteries, *Nat. Commun.*, 2024, **15**, 53.

200 T. Asano, A. Sakai, S. Ouchi, M. Sakaida, A. Miyazaki and S. Hasegawa, Solid Halide Electrolytes with High Lithium-Ion Conductivity for Application in 4 V Class Bulk-Type All-Solid-State Batteries, *Adv. Mater.*, 2018, **30**, 1803075.

201 Y. Li, Z. Zhang, P. Su, L. Luo, C. Lan, S. Xu, X. Han, W. Huang and S. Chen, Enhancing conductivity of Si anode enabled by selecting Si particle size for interface stabilized all-solid-state batteries, *Ionics*, 2024, **30**, 3789–3798.

202 R. Miyazaki and T. Hihara, All-solid-state half-cell of Li/a-Si film using guest Li+ conductor 15NaI·LiBH4 as a solid electrolyte, *J. Solid State Electrochem.*, 2020, **24**, 1687–1693.

203 A. K. Sharma, K. Sharma, F. Guo, K. Shrivastava, M. K. Gupta, T. Ichikawa, A. Jain and S. Agarwal, Electrochemical reaction mechanism of silicon nitride as negative electrode for all-solid-state Li-ion battery, *J. Mater. Sci.: Mater. Electron.*, 2024, **35**, 914.

204 A. K. Sharma, K. Sharma, M. K. Gupta, F. Guo, T. Ichikawa, A. Jain and S. Agarwal, Si3N4 as an Alternative of Silicon for the Anode Application in All-Solid-State Li-Ion Batteries, *Energy Storage*, 2024, **6**, e70010.

205 Y. Huang, B. Shao, Y. Wang and F. Han, Solid-state silicon anode with extremely high initial coulombic efficiency, *Energy Environ. Sci.*, 2023, **16**, 1569–1580.

206 X. Li, L. Zhang, Y. Fan, S. Lin, Y. Lin, Y. Ying, M. Hu, H. Gao, X. Xu, Z. Xia, X. Lin, J. Lu and X. Han, Carbon interconnected microsized Si film toward high energy room temperature solid-state lithium-ion batteries, *Chin. Chem. Lett.*, 2025, **36**, 109776.

207 X. Han, L. Gu, Z. Sun, M. Chen, Y. Zhang, L. Luo, M. Xu, S. Chen, H. Liu, J. Wan, Y.-B. He, J. Chen and Q. Zhang, Manipulating charge-transfer kinetics and a flow-domain LiF-rich interphase to enable high-performance microsized silicon–silver–carbon composite anodes for solid-state batteries, *Energy Environ. Sci.*, 2023, **16**, 5395–5408.

208 X. Han, M. Xu, L. Gu, C. Lan, M. Chen, J. Lu, B. Sheng, P. Wang, S. Chen and J. Chen, Monothetic and conductive network and mechanical stress releasing layer on micron-silicon anode enabling high-energy solid-state battery, *Rare Met.*, 2023, **43**, 1017–1029.

209 X. Han, W. Zhou, M. Chen, J. Chen, G. Wang, B. Liu, L. Luo, S. Chen, Q. Zhang, S. Shi and C.-P. Wong, Interfacial nitrogen engineering of robust silicon/MXene anode toward high energy solid-state lithium-ion batteries, *J. Energy Chem.*, 2022, **67**, 727–735.

210 L. Gu, J. Han, M. Chen, W. Zhou, X. Wang, M. Xu, H. Lin, H. Liu, H. Chen, J. Chen, Q. Zhang and X. Han, Enabling robust structural and interfacial stability of micron-Si anode toward high-performance liquid and solid-state lithium-ion batteries, *Energy Storage Mater.*, 2022, **52**, 547–561.

211 L. Zhang, Y. Lin, X. Peng, M. Wu and T. Zhao, A High-Capacity Polyethylene Oxide-Based All-Solid-State Battery Using a Metal–Organic Framework Hosted Silicon Anode, *ACS Appl. Mater. Interfaces*, 2022, **14**, 24798–24805.

212 H. Huo, J. Sun, C. Chen, X. Meng, M. He, N. Zhao and X. Guo, Flexible interfaces between Si anodes and composite electrolytes consisting of poly(propylene carbonates) and garnets for solid-state batteries, *J. Power Sources*, 2018, **383**, 150–156.

213 J. Pan, H. Peng, Y. Yan, Y. Bai, J. Yang, N. Wang, S. Dou and F. Huang, Solid-state batteries designed with high ion conductive composite polymer electrolyte and silicon anode, *Energy Storage Mater.*, 2021, **43**, 165–171.

214 K. Tian, W. Zhang, J. Zeng, Y. Gao, X. Guang, H. Luo, M. Lu and X. Li, In Situ Reconstruction and Anion Blocking Interphase Strategy for High-Performance Silicon-Based Anodes in Liquid and Solid-State Batteries, *Adv. Funct. Mater.*, 2025, **35**, 2424137.

215 X. Wang, S. He, Z. Hu, H. Xu, L. Pan and J. Li, Grafting strategy achieving self-healing polymer/sulfide electrolyte for high-performance solid-state lithium–silicon batteries, *Rare Met.*, 2025, **44**, 7159–7172.